The Role of the Diamine Oxidase AOC1 in Polyamine Homeostasis and Kidney Injury

Inaugural-Dissertation

to obtain the academic degree
Doctor rerum naturalium (Dr. rer. nat.)

submitted to the Department of Biology, Chemistry, Pharmacy
of Freie Universität Berlin

by

Tobias Sieckmann

Berlin, 2023

The doctoral thesis was performed under the supervision of Dr. Karin Kirschner at the Institute for Translational Physiology at the Charité - Universitätsmedizin Berlin - between May 2019 and April 2023.

1st reviewer: Dr. Karin Kirschner

2nd reviewer: Prof. Dr. Christian Freund

Date of defense: 03. August 2023

Acknowledgements

I would like to express my sincere gratitude to the individuals who supported and contributed to this work, without whom it would not have been possible.

First I want to thank Karin Kirschner for giving me the opportunity to research this exciting topic. Both the expert supervision and time spent on discussions is well acknowledged. It has really been a great journey, starting from initial qPCR data and culminating in three *in vivo* experiments. I appreciate her constant support and encouragement over the years, while allowing me the freedom to develop my own ideas. Thank you for being there all the time and supporting me!

Second I want to thank Holger Scholz for his whole support and guidance. His frequent discussions and feedback on data and experiments contributed significantly to the success of this project.

Special thanks also to Ulrike Neumann for technical support and general help with many experiments. Ulrike was always there to help and her expertise was instrumental in ensuring the smooth progression of this work.

In addition I would like to express my gratitude to several colleagues who have contributed to the success of this project. I want to thank Simon Kelterborn and Falk Lichtenberger for valuable input, discussion and support throughout this project. In addition I want to thank our former students Neslihan Ögel and Sophie Hänle for the valuable discoveries concerning *Aoc1* splice variants and regulation of expression.

I am also grateful to the staff of the animal facility for their excellent care of the animals and support during the *in vivo* experiments. I want to extend my appreciation to Felix Boivin and Gabriele N'diaye for great help with the ischemia reperfusion model.

Furthermore, I want to acknowledge all those who supported this study with material from the different injury models. Their contributions were crucial to the success of this project.

Finally I want to thank my family and all friends for their constant support.

Hierdurch versichere ich, dass ich meine Dissertation selbstständig verfasst und keine anderen als die von mir angegeben Quellen und Hilfsmittel verwendet habe. Diese Arbeit hat in gleicher oder ähnlicher Form noch keiner anderen Prüfungsbehörde vorgelegen und wurde bisher nicht veröffentlicht.

Contents

List of Figures

List of Tables

List of Abbreviations

αSMA α smooth muscle actin

***Act*β** Gene encoding βActin

Arg1 Gene encoding Arginase 1

Ccl2 Gene encoding CC-chemokine ligand 2

Ccr5 Gene encoding C-C motif chemocine receptor 5

Cldn10 Gene encoding Claudin 10

F4/80 Gene encoding EGF-like module-containing mucin-like hormone receptor-like 1

LacZ Gene encoding β-galactosidase

Lcn2 Gene encoding Lipocalin 2

Lrp2 Gene encoding LDL receptor related protein 2

Mrc1 Gene encoding Mannose receptor C-type 1

Neo Gene encoding Amino 3'-glycosyl phosphotransferase

Nos2 Gene encoding Nitric oxide synthase 2

Slc12a3 Gene encoding Solute carrier family 12 member 3

Umod Gene encoding Uromodulin

2K1C Two kidney, one clip

5'UTR Five prime untranslated region

AA Amino acids

AKI Acute kidney injury

AKT Gene encoding protein kinase B

ANOVA Analysis of variance

AOC1 Amine oxidase copper-containing 1

APS Ammonium persulfate

AQP1 Aquaporin 1

AQP2 Aquaporin 2

ATP Adenosine triphosphate

BCA Bicinchoninic acid

BF Bright field/ transmitted light

BSA Bovine serum albumin

Cas9 Gene encoding CRISPR-associated protein 9

CD Collecting duct

CKD Chronic kidney disease

CMV Cytomegalovirus

CRISPR Clustered regularly interspaced short palindromic repeats

CsA Cyclosporine A

Ct Cycle threshold

d.p.c. Days post contraception

DAPI 4',6-diamidino-2-phenylindole

dcSAM Decarboxylated S-adenosylmethionine

DCT Distal convoluted tubule

DMEM Dulbecco's modified Eagle medium

DNA Deoxyribonucleic acid

DTT Dithiothreitol

EDTA Ethylenediaminetetraacetic acid

eGFP Enhanced green fluorescent protein

eIF5A Eukaryotic initiation factor 5A

ER Endoplasmatic reticulum

EtOH Ethanol

FACS Fluorescence activated cell sorting

FBS Fetal bovine serum

FRT Flip recognition target

GAPDH Glyceraldehyde-3-phosphate dehydrogenase

GFP Green fluorescent protein

GFR Glomerular filtration rate

HBSS Hanks' balanced salt solution

HE Hematoxylin eosin

HEPES 4-(2-hydroxyethyl)-1-piperazineethanesulfonic acid

HRP Horseradish peroxidase

IL10 Interleukin 10

IL1β Interleukin 1β

IRI Ischemia reperfusion injury

JAK Janus kinase

KI67 Antigen KI-67

KIM1 Kidney injury molecule 1

LoxP Locus of x(cross)-over in P1

MGT Masson-Goldner trichrome

MTA 5'-Methyladenosine

NFAT5 Nuclear factor of activated T-cells 5

NGAL Neutrophil gelatinase-associated lipocalin

NLRP3 NLR family pyrin domain containing 3

ODC1 Ornithine decarboxylase 1

ORF Open reading frame

PAGE Polyacrylamide gel electrophoresis

PAOX Polyamine oxidase

PAS Periodic acid Schiff reagent

PCR Polymerase chain reaction

PCT Proximal convoluted tubule

PST Proximal straight tubule

PVDF Polyvinylidene fluoride

RNA Ribonucleic acid

RPMI Roswell Park Memorial Institute

s*Xbp1* Spliced X-box binding protein 1 transcript

SAT1 Spermidine/spermine N^1-acetyltransferase 1

SDS Sodium dodecyl sulfate

siRNA Small interfering RNA

SMOX Spermine oxidase

SMS Spermine synthase

SNAP S-nitroso-N-Acetylpenicillamine

SP Signal peptide

SRM Spermidine synthase

STAT3 Signal transducer and activator of transcription proteins 3

TAL Thick ascending limb

TDL Thick descending limb

TEMED Tetramethylethylenediamine

TGFβ Transforming growth factor β

TNFα Tumor necrosis factor α

TRP Transient receptor potential

TSS Transcription start site

TUNEL TdT-mediated dUTP-biotin nick end labeling

us*Xbp1* Unspliced X-box binding protein 1 transcript

UUO Unilateral ureter obstruction

VIM Vimentin

WT Wild-type

Abstract

The complex structural and functional organization of the kidneys as well as the heterogeneity of underlying etiologies of kidney disease complicate therapy. Treatment might benefit from the identification of common disease mechanisms that are shared by various kidney pathologies. The polyamine system is a highly conserved network consisting of the biogenic polyamines putrescine, spermidine, and spermine. Polyamines are organic polycationic molecules with several amino groups. Because of their positive charge, polyamines can bind to proteins and nucleic acids, thereby influencing a plethora of cellular processes. The polyamine homeostasis is frequently dysregulated in acute and chronic renal pathologies. As polyamines are involved in injury and repair in different organs, the hypothesis is tested that different forms of renal injury lead to a similar dysregulation of the polyamine system and that changing polyamine levels have an influence on the severity of renal injury. Eleven different animal models of acute and chronic kidney injury with various etiologies were used. Among these models, a similar pattern of polyamine dysregulation was observed. While the polyamine synthesizing genes *Odc1*, *Srm* and *Sms* are downregulated, polyamine catabolism by *Aoc1*, *Smox* or *Sat1* is upregulated after injury. Here, ODC1 and AOC1, which can synthesize and degrade putrescine respectively show the most prominent changes. While *Odc1* is strongly expressed in healthy kidneys, *Aoc1* shows little expression. After injury however the expression shifts with *Aoc1* strongly increasing and *Odc1* being reduced. Within the injured kidney, AOC1 is necessary for degradation of putrescine and ablation of *Aoc1* increases renal putrescine levels after injury. Different stimuli, leading to increased *Aoc1* expression were assessed and hyperosmolarity was found as a strong stimulus. Hyperosmolarity stimulates transcription of *Aoc1* involving NFAT5 and also stabilizes *Aoc1* mRNA.The transcriptional activation is initiated at a promoter element of a certain isoform, containing additional N-terminal amino acids, leading to increased secretion. Using a germline deletion of *Aoc1* in mice, it was tested whether ablation of *Aoc1* changes the outcome of kidney injury. Here, only mild improvements were detected, including the reduction of intratubular casts after ischemia-reperfusion injury. These data show that various types of acute and chronic kidney injury result in a similar dysregulation of the polyamine system with inhibition of polyamine synthesis and activation of polyamine breakdown. Furthermore, it is shown that polyamine homeostasis influences regeneration after renal injury.

Zusammenfassung

Die komplexe strukturelle und funktionelle Organisation der Nieren, sowie die Heterogenität der zugrundeliegenden Ursachen von Nierenerkrankungen, erschweren die Therapie. Die Behandlung von Nierenerkrankungen könnte von der Identifizierung übergreifender Mechanismen profitieren. Das Polyaminsystem ist ein stark konserviertes Netzwerk, das aus den biogenen Polyaminen Putrescin, Spermidin, und Spermin besteht. Polyamine sind organische, polykationische Verbindungen mit mehreren Aminogruppen. Aufgrund ihrer positiven Ladung können Polyamine an Proteine und Nukleinsäuren binden und dadurch eine Vielzahl von zellulären Prozessen beeinflussen. Die Polyamin-Homöostase ist bei akuten und chronischen Nierenerkrankungen häufig gestört. Da Polyamine in verschiedenen Organen an Schädigung und Reparatur beteiligt sind, wird die Hypothese geprüft, dass verschiedene Formen der Nierenschädigung zu einer ähnlichen Dysregulation des Polyaminsystems führen und dass veränderte Polyaminspiegel einen Einfluss auf die Schwere der Nierenschädigung haben. Es wurden elf verschiedene Nierenschädigungsmodelle verwendet darunter Modelle für akute und chronische Nierenschädigungen unterschiedlicher Ätiologie. Innerhalb dieser Modelle wurde ein ähnliches Muster der Dysregulation beobachtet. Während die Polyamin-synthetisierenden Gene *Odc1*, *Srm* und *Sms* vermindert exprimiert werden, wird der Polyaminabbau durch Expression von *Aoc1*, *Smox* oder *Sat1* nach der Schädigung verstärkt. Hier zeigen ODC1 und AOC1, die Putrescin synthetisieren beziehungsweise abbauen können, die auffälligsten Veränderungen. Während *Odc1* in der gesunden Niere stark exprimiert wird, zeigt *Aoc1* nur eine geringe Expression. Nach der Schädigung verschiebt sich jedoch die Expression, wobei die mRNA der *Aoc1* stark zunimmt und *Odc1* reduziert wird. In der geschädigten Niere ist AOC1 für den Abbau von Putrescin notwendig, und die Deletion von *Aoc1* erhöht den Putrescinspiegel in der geschädigten Niere. Verschiedene Stressoren wurden untersucht, ob diese zu einer erhöhten *Aoc1*-Expression führen. Hier erwies sich Hyperosmolarität als starker Stimulus. Hyperosmolarität kann die *Aoc1* Expression über den Transkriptionsfaktor NFAT5 transkriptionell aktivieren, aber auch die *Aoc1*-mRNA stabilisieren. Die transkriptionelle Aktivierung wird an einem Promotorelement einer bestimmten Isoform initiiert, welche zusätzliche N-terminale Aminosäuren enthält, was zu einer verstärkten Sezernierung führt. Durch eine Keimbahndeletion von *Aoc1* in Mäusen wurde getestet, ob diese das Ergebnis einer Nierenschädigung verändert. Hier wurden lediglich leichte Verbesserungen der Nierenmorphologie festgestellt, einschließlich der Verringerung von intratubulären Ablagerungen nach Ischämie-Reperfusionsschädigung. Diese Daten zeigen, dass das renale Polyaminsystem mit Hemmung der Polyaminsynthese und Aktivierung des Abbaus auf Nierenschädigungen reagiert und dass die Polyamin-Homöostase die Regeneration nach Nierenschädigungen beeinflusst.

1 Introduction

1.1 Structural and functional organization of the kidney

The kidney is a paired organ in the retroperitoneal space, which is best known for its excretory function. Additional tasks include the regulation of extracellular volume, arterial blood pressure, acid-base homeostasis, and erythropoiesis. Each kidney has its own blood supply from the *Arteria renalis* and drains into the systemic circulation via the *Vena renalis*. A single kidney is built up from more than one million nephrons representing the smallest functional units. The nephron is composed of the renal corpuscle (the glomerulus within Bowman's capsule) to filter the blood and the tubular system (the proximal tubule, the loop of Henle, the distal tubule, and the collecting duct) to reabsorb all indispensable molecules (figure 1a). Incoming blood is filtered within the glomerulus through the glomerular capillaries. Here, the hydrostatic pressure drives fluid and filtratable solutes from the blood across the glomerular filtration barrier into Bowman's space. This barrier consists of a negatively charged surface, repelling most plasma proteins while retaining high permeability to small molecules with radii smaller than 40 Å including water, glucose, amino acids, and electrolytes [1, 2]. The flow rate of filtered fluid, or glomerular filtration rate (GFR), is highly dependent on the hydrostatic pressure exercised by the intrarenal blood pressure. To prevent that changes in the systemic blood pressure have a direct effect on the intrarenal blood pressure and thus the GFR, the kidneys are able to intrinsically regulate their own blood flow [3]. The renal blood flow is almost constant in the range between 80 and 170 mmHg systemic blood pressure [4]. The combined GFR of both kidneys amounts to around 180 L per day. As the resulting ultra-filtrate (primary urine) is identical to the volume of filtered plasma, the kidneys must counteract the imminent volume depletion. Therefore, the kidneys reabsorb most of the water and many filtered compounds while retaining waste products in the tubular fluid. Reabsorption is achieved by the different tubular segments of the nephron (figure 1a).

While the proximal tubules reabsorb most of filtered solutes including vast amounts of electrolytes, glucose, amino acids, and water, the distal segments control adjustment of osmoregulation by precise salt and water reabsorption. The luminal surface of the proximal convoluted tubule contains a dense brush border membrane (figure 1b). Reabsorption in the proximal tubules is mainly dependent on cotransport with sodium. The reabsorption of sodium from the urine is driven by the activity of a basolateral Na^+/K^+-ATPase, which transports sodium ions into the interstitium. ATP for Na^+/K^+-ATPase activity is generated in mitochondria by oxidative phosphorylation of free fatty acids. Within the kidney, mitochondria are densely packed in the proximal tubular epithelium.

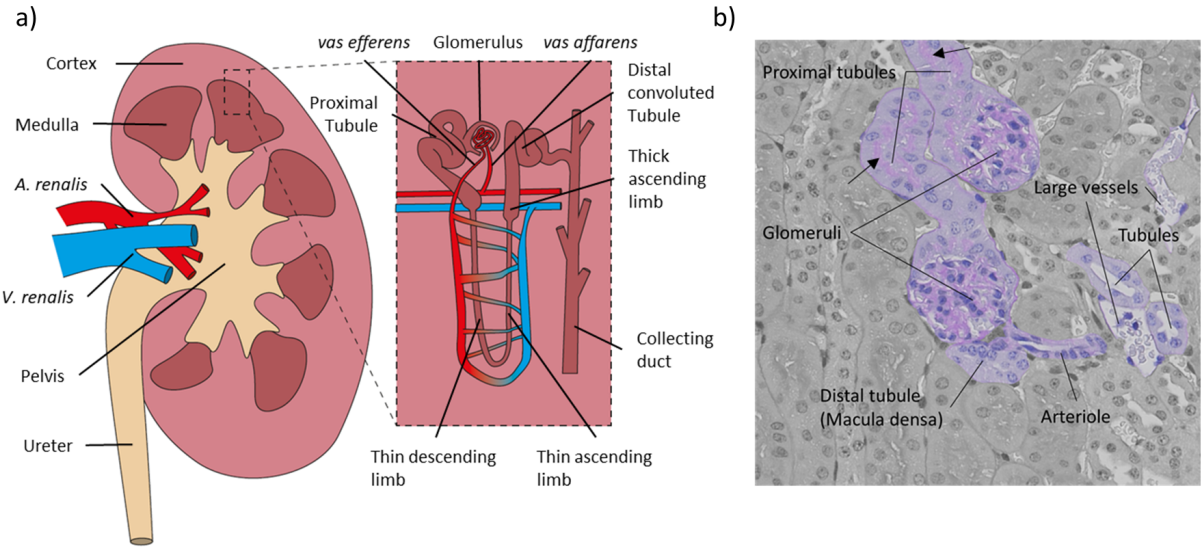

Figure 1: Anatomy of the kidney and the nephron.
a) Schematic illustration showing a multipapillary kidney with the connecting renal artery, vein, and the ureter. The magnification shows a schematic nephron. **b)** Representative PAS staining within the murine cortex. Selected structures of the nephron are shown in original colors, everything else in greyscale. Arrows indicate brush border membrane.

After passing the proximal tubule, the primary urine enters the loop of Henle. The main function of this nephron segment is the establishment of a cortico-medullary osmotic gradient which is used in a counter current multiplier system for urine concentration. The descending limb of Henle's loop is water permeable through its aquaporin 1 (AQP1) channels, whereas the whole ascending limb of Henle's loop is resistant to transepithelial water flux. The thick ascending limb pumps NaCl from the tubular fluid into the interstitium, but water cannot follow. Water is therefore reabsorbed from the thin descending limb as it follows the osmotic gradient established by the NaCl transport activity of the thick ascending limb. The osmolality within the descending limb and the interstitium are therefore equal and increase from the kidney cortex towards the medulla. However, the osmolarity in the tubular fluid decreases along the thick ascending limb due to net NaCl reabsorption and water retention. The distal convoluted tubule continues to reabsorb more ions including sodium, chloride, and calcium. Under the influence of vasopressin, the collecting duct is water permeable through the incorporation of aquaporin 2 (AQP2) channels. Following the cortico-medullary osmotic gradient, the osmolality in the tubular fluid steadily increases until finally reaching osmolality of up to 1300 mOsm/kg under complete vasopressin mediated antidiuresis. The urine is drained from the renal pelvis through the ureter into the urinary bladder.

Tubular reabsorption and concentration of urine demands a specialized vascular architecture. The arteriole reaching the glomerulus (*vas afferens*) branches into the glomerular capillary bed and leaves it again in form of the *vas efferens*. The *vas efferens* is not a vein but an artery that further supplies the cortical tubular cells through the peritubular capillary bed.

The renal circulation is therefore arranged in series, supplying first the glomerular capillary bed for filtration and afterwards the peritubular capillary bed to provide energy to the tubular epithelium and returning reabsorbed molecules into circulation. While a fifth of the cardiac output perfuses the kidneys, its oxygen consumption is relatively low with an arteriovenous oxygen difference of only around 10-15% [5, 6]. The cortex is receiving roughly 90% of the renal blood flow, whereas the inner medulla receives only 1-2% [7]. The proximal tubules reabsorb many compounds including around 60% of filtered water [8, 9] and around 50% of total NaCl [10]. Its Na^+/K^+-ATPase dependent transport processes are energetically expensive, and the high perfusion rate is necessary for maintaining filtration and reabsorption. Therefore, renal oxygen consumption is based on Na^+/K^+-ATPase activity and not on the kidney's metabolic needs. With a decreasing renal blood flow and less filtration, there is a reduction in reabsorption together with decreasing Na^+/K^+-ATPase activity and therefore a decreasing oxygen consumption. The kidney is unique, as renal blood flow regulates the renal oxygen consumption. In other organs such as the brain or heart, the metabolic needs i.e., the oxygen consumption of the tissue is regulating the blood flow. This makes the kidney extremely sensitive to ischemic periods.

1.2 Renal pathophysiology

Renal pathologies are generally classified in two major categories, acute kidney injury (AKI) and chronic kidney disease (CKD). AKI is defined by an abrupt reduction in GFR [11]. This decrease in GFR is usually associated with an increase in serum creatinine and a reduction of urine excretion (oliguria) or both. CKD is defined as "abnormalities of kidney structure or function, present for >3 months, with implications for health" [12]. Kidney disease in general is a global health burden. CKD of any stage exhibits a global prevalence of 13.4% [13]. In high-income countries, hospital-acquired AKI is most common with 21.6% of hospitalized adults and 33.7% of children developing AKI [14, 15]. Notably, AKI can progress to CKD and is considered to be a risk factor for CKD [16], the following paragraphs focus therefore on the classical classification of AKI etiologies.

AKI etiologies can be grouped into prerenal, renal and postrenal causes. Prerenal AKI results from a critical reduction of blood supply to the kidneys leading to a decrease in GFR. Typical insults include volume depletion, severe arterial hypotension, heart failure and renal artery stenosis [17]. Pathophysiological, prerenal AKI is caused by an imbalance between the delivery of oxygen and nutrients and the requirements of the nephron [18–20]. A common feature of prerenal kidney injury is therefore hypoperfusion leading to reduced tissue oxygenation and thus hypoxia [17]. This can result in ATP depletion [21] with consecutive metabolic changes causing alterations of the tubular epithelium and other cell types [22]. The kidneys are the organ with the second highest abundancy of mitochondria [23] and require a constant supply with oxygen for normal function. Especially the mitochondria-rich proximal tubules are therefore at risk of energy shortage due to hypoxic episodes and other reasons.

Renal forms of AKI are caused by injury of the major structures of the kidney, i.e., the tubules, glomeruli, interstitium and blood vessels. Tubular damage and necrosis can occur during prolonged hypoxic episodes, when the energy consumption of the kidneys exceeds the supply with oxygen and nutrients. Exogenic nephrotoxic drugs such as aminoglycosides or cisplatin can directly damage the tubules. But also endogenous molecules such as myoglobin, which is released upon massive muscle injury (rhabdomyolysis) can damage the tubules [24]. Glomerulonephritis, i.e., the inflammatory infiltration of the filtering units of the kidney, is a cause of glomerular injury. Interstitial damage can result from allergic reactions or infections. Vascular injury is observed in malignant hypertension, where elevated blood pressure results in necrosis of the arterial wall. Postrenal injury is commonly caused by a blockage in the urinary tract leading to increasing intratubular pressure and consequently a reduction in GFR. Causes of postrenal AKI include intrarenal obstruction of urinary flow by kidney stones and blood clots, or extrarenal ureteral obstruction by prostate hypertrophy, cancers, or other reasons.

1.3 Molecular and histopathological changes in the regenerating kidney

Many molecular and histopathological changes occur in a dynamic fashion after kidney injury. This is partly due to the heterogeneity of the underlying etiologies, but also because of the kidneys' intrinsic ability for self-repair. Furthermore, different etiologies lead to different patterns of injury. While ischemia reperfusion injury (IRI) damages mostly the proximal tubules [25, 26] , radiocontrast-induced nephropathy is associated with injury predominantly of the thick ascending limbs [27].

Damage to the nephron is often accompanied by visible histological alterations. A typical hallmark seen during prolonged ischemia is tubular necrosis. While appearing dilated, damaged tubules present flattened epithelia with a loss of the brush border membrane. The luminal space is frequently filled with casts consisting of detached tubular cells that obstruct the tubular lumen [26]. Tubular damage is caused mainly by necrosis, necroptosis and apoptosis [28] starting as early as six hours after IRI [29]. Injured epithelial cells, which do not become necrotic, undergo diverse adaptive processes. One of the early adaptations is the upregulation of neutrophil gelatinase-associated lipocalin (NGAL), which can already be detected three hours after IRI [30]. NGAL mediates antiapoptotic and antioxidant effects, preserving the tubular epithelium [31]. These surviving epithelial cells are reprogrammed and start to regenerate the injured tubule [32]. During this process, these cells lose their polarity and show cytoskeletal changes [33]. A common marker of their dedifferentiation is the intermediate filament vimentin (VIM), which is normally restricted to mesenchymal cells [34]. One of the most striking changes in regenerating tubular epithelial cells, however, is the induction of kidney injury molecule-1 (KIM1). KIM1 is expressed in dedifferentiated, regenerating tubular cells where it promotes migration and proliferation [35].

However, renal cells can also fail to repair [32]. These cells become arrested at the G_2/M cell cycle and produce transforming growth factor β1 (TGFβ), a cytokine that drives fibrosis [36]. Fibrosis is the scarring of tissue by substantial deposition of extracellular matrix components. Most fibrosis is observable within the interstitium, where pericytes are a major source for myofibroblasts [37]. Myofibroblasts are characterized by their neo-expression of α-smooth muscle actin (αSMA) and their ability to proliferate and deposit vast quantities of extracellular matrix [38].

Importantly, many inflammatory processes can take place after kidney injury. One of these is the increase in mononuclear phagocytes such as macrophages. While macrophages are known to contribute to AKI [39, 40], they are necessary for clearing of debris and tissue restoration in CKD [41]. Generally, mononuclear phagocytosis occurs after injury with macrophages secreting pro-inflammatory mediators like tumor necrosis factor alpha (TNFα) and interleukin 1 beta (IL1β) [42]. Later occurring M2 macrophages however start to secrete anti-inflammatory mediators like TGFβ or interleukin 10 (IL10), contributing to recovery [43].

In summary, the processes after injury are diverse and depend on the underlying etiology. However, there are conserved processes that can be used for discrimination of different cells and their fate in the injured kidney.

1.4 Experimental models of kidney injury

Preclinical models of AKI and CKD are an integral part in studying pathophysiological mechanisms and developing new therapeutics and interventions. Therefore, different acute and chronic kidney injury models were established over time, many of them using mice as a model organism. The following paragraphs give an overview of the experimental kidney injury models used in this study.

IRI and kidney transplantation are widely used as prerenal AKI models. In the unilateral IRI model, the *Arteria* and *Vena renalis* of one kidney are clamped. The depletion of energy [44], hypoxia [45] and the accumulation of toxic metabolites [46] leads to injury of the kidney. The contralateral kidney remains untouched and can be used as a control. This model ressembles allograft transplantation model in regard of the underlying pathology. However, ischemia of the allograft is established *ex vivo* and in cold conditions. The second difference is the immune reaction that occurs after allograft transplantation. Depending on the used mouse strains and alloantigens, survival and rejection times are variable [47, 48].

Chronic intra-renal models are often based on microvascular damage achieved by malignant hypertension or diabetes. Examples are the streptozotocin-induced diabetic nephropathy, the two kidney, one clip (2K1C) hypertension model and the angiotensin II hypertension model. Administration of streptozotocin destroys the insulin producing cells in the pancreas

and induces a pathology resembling human type I diabetes. This results in glomerular damage with thickening of the mesangium [49], fibrosis [50] and activation of reactive oxygen species [51], therefore reducing kidney function. In the 2K1C model, a clip is applied to the artery of one kidney, resulting in reduced perfusion. Subsequent activation of the renin-angiotensin-system causes systemic arterial hypertension. Another possibility to achieve chronic hypertension in animals is the direct administration of angiotensin II. The resulting elevated blood pressure leads to increased intraglomerular pressure and damages the vasculature. As consequence, kidney perfusion is reduced, and glomerular filtration rates decrease.

Other models of renal AKI and CKD target the tubulointerstitial cells. In the rhabdomyolysis model, rapid destruction of skeletal muscle tissue leads to a strong myoglobinaemia. Myoglobin can pass the glomerular filtration barrier and cause tubular injury and necrosis [52]. In contrast to the other acute models, namely IRI and transplantation, rhabdomyolysis-induced kidney injury progresses faster, exhibiting more necrosis [53]. Cyclosporine A (CsA) administration is considered as a model of CKD. CsA is an immunosuppressant given after organ transplantation. As an adverse effect, CsA can induce chronic nephrotoxicity associated with interstitial renal fibrosis. The excess production of extracellular matrix replaces injured cells without restoring their original function. Other chronic models such as the high-oxalate diet or adenine-induced nephropathy are characterized by their potential to injure tubules by deposition of crystals. A high-oxalate diet leads to formation of calcium-oxalate crystals within the tubular system. This induces tubular damage mainly by NLRP3-mediated inflammation [54]. Adenine-induced nephropathy by feeding of a special diet containing adenine results in deposition of the metabolite 2,8-dihydroxyadenine, therefore exhibiting toxic effects on the tubules [55].

The most common model for postrenal kidney injury uses unilateral ureteral obstruction. Here, one ureter is surgically ligated. As a consequence, backlog of urine increases the hydrostatic pressure in the tubular system [56] leading to hypoxia and fibrosis [57], immune cell infiltration [58] and apoptosis [47] in the kidney.

Altogether, the heterogeneous nature of AKI and CKD necessitates a variety of models to reproduce different human kidney pathologies. Even though most models share major pathophysiological mechanisms such as hypoxia or damage by reactive oxygen species, each model has unique mechanisms leading to the development of AKI or CKD.

1.5 The polyamine system

Polyamines are naturally occurring polycations with multiple functions. Polyamines are present ubiquitously in all living organisms. In eukaryotes, the biogenic polyamines are the diamine putrescine, the triamine spermidine and the tetraamine spermidine (figure 2a). Polyamines

are ingested by food [59], derived from the gut microbiota [60] and endogenously produced. The homeostasis of polyamines is tightly controlled by their rate of synthesis, interconversion, and degradation.

The synthesis, interconversion and degradation of polyamines are shown in figure 2b. The rate-limiting step in polyamine biosynthesis is the decarboxylation of ornithine to putrescine, which is catalyzed by ornithine decarboxylase 1 (ODC1). The next step is the formation of spermidine. Here, an aminopropyl group originating from decarboxylated S-adenosylmethionine (dcSAM) is added. This reaction is catalyzed by the aminopropyltransferase spermidine synthase (SRM). Afterwards, another aminopropyltransferase, namely the spermine synthase (SMS) catalyzes the addition of another aminopropyl group from dcSAM to spermidine, forming spermine. Spermine is degraded by the spermine oxidase (SMOX). Oxidation of spermine generates 3-aminopropanal, H_2O_2 and spermidine. Spermidine/spermine N^1-acetyltransferase (SAT1) is another degrading molecule. This enzyme catalyzes the transfer of an acetyl group from acetyl-coenzyme A to spermidine or spermine resulting in the formation of N^1-acetylspermidine and N^1-acetylspermine, respectively. These acetylated derivatives are either secreted [61] or interconverted by the polyamine oxidase (PAOX). PAOX can oxidize either N^1-acetylspermine forming spermidine and 3-acetamidopropanal or N^1-acetylspermine forming putrescine and 3-acetamidopropanal. In mammals, polyamines can be degraded by copper-containing oxidases such as the amine oxidase copper containing 1 (AOC1). Putrescine is broken-down by AOC1 into 4-aminobutanal, ammonia and hydrogen peroxide.

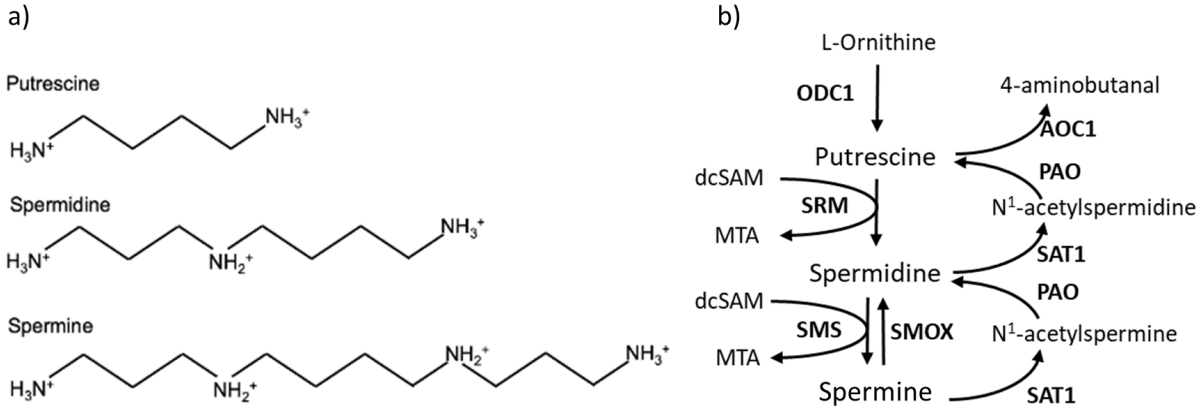

Figure 2: Structural representation of the polyamine system and schematic overview of polyamine metabolism.

a) Structures of the three biogenic polyamines putrescine, spermidine and spermine. **b)** Representation of the polyamine system; ODC1 = Ornithine decarboxylase 1, SRM = Spermidine synthase, SMS = Spermine synthase, SMOX = Spermine oxidase, SAT1 = Spermidine/spermine N^1-acetyltransferase 1, PAOX = Polyamine oxidase, AOC1 = Amine oxidase copper containing 1, dcSAM = decarboxylated S-adenosylmethionine, MTA = 5'-Methyladenosine.

The diverse functions of polyamines are mainly based on their ability to strongly interact with anions such as nucleic acids and phospholipids [62]. Polyamines can regulate transcription and translation by alterations of DNA conformation [63], chromatin structure [64], DNA stability [65], and increasing ribosome activity [66, 67]. By these processes, polyamines can influence elemental cellular processes such as cell growth [68], cell cycle regulation [69], proliferation [70] and apoptosis [71]. Polyamines play further a pivotal role in transcription initiation by the eukaryotic initiation factor 5A (eIF5A). eIF5A is the only protein containing the unique amino acid hypusine, formed from spermidine. This posttranslational addition transforms the inactive eIF5A into its active form, enabling proliferation [72] and escape from the G_1 phase [73]. Besides these processes, polyamines influence cellular signaling [74, 75], cell-cell interactions [76, 77] and ion channel activities [78–82]. Through these mechanisms, polyamines are necessary for many physiologic processes. These include the normal development of the embryo [83] and the central nervous system [84], intestinal epithelial barrier function [85], angiogenesis [86], fertility [87] and functions of the immune system [88–92].

Because of their multifarious modes of action, polyamines are also involved in pathophysiological processes. On one side, early studies suggested that the polyamines spermidine and spermine are toxic, resulting in effects like nephrotoxicity [93] and systemic hypothermia [94]. On the other hand, polyamine depletion can also have deleterious consequences. For example, inactivation of the putrescine synthesizing enzyme ODC1 is embryonic lethal [95] and loss of function of SMS and therefore the inability to produce spermine, results in Snyder-Robinson Syndrome. Snyder-Robinson syndrome is characterized by intellectual disability, osteoporosis, seizures and kyphoscoliosis [96]. These, however, are both extreme situations with organisms being challenged with too many or too little polyamines.

Pathophysiological, polyamines are associated with diverse traits. These include cerebral disorders such as neurodegeneration [97, 98] and behavioral changes [99]. Increased synthesis of polyamines and upregulation of ODC1 can be detected in different forms of cancer such as skin cancer [100], lung mesothelioma [101] and prostate cancer [102]. Alterations in polyamine metabolism were further shown in different injuries such as wounded skin [103], ischemia reperfusion injury of the heart and kidney [104, 105], cerebral ischemia [106] and transplanted liver [107]. Because of their dysregulation in various pathologies, polyamines have been suggested as biomarkers in different cancers [108–110], Parkinson disease [111] and lupus erythematosus [112].

1.6 Polyamines and the kidney

The glomerular basement membrane is the selective filtration barrier of the kidneys. Larger molecules above 70 kDa [113] and anionic molecules are retained in the blood, whereas polyamines as small cationic molecules are freely filtrated. While more than 80% of filtered spermidine and spermine are thereafter reabsorbed from the tubular fluid, over 70% of filtered putrescine is excreted in the urine [114]. This rate of excretion and reabsorption, however, is disturbed in different kidney pathologies, leading to impaired polyamine homeostasis.

Patients with CKD often show increased levels of putrescine in their blood [115, 116], probably due to reduced filtration. Spermidine and spermine are reduced in the blood of these patients [115, 116], likely due to reduced reabsorption by the injured kidneys. Patients developing AKI after cardiac surgery show increased spermidine levels in the urine [117]. In a rat model of cisplatin-induced nephropathy, urinary excretion of spermidine and putrescine was enhanced [118]. These findings indicate that reduced tubular reabsorption capacity for polyamines plays a major role in the decrease of blood polyamines upon kidney injury. However, a recent study linked elevated serum spermidine levels to a decline of estimated GFR in CKD patients [119], which might indicate that reduced filtration of spermidine is not always compensated by reduced reabsorption. The levels of circulating spermidine and spermine in the blood can be influenced not only by excretion but also by synthesis and degradation. The renal expression of the catabolic enzymes SAT1 and SMOX is increased in different models of kidney injury such as IRI, cisplatin treatment and folic acid nephropathy [104, 120, 121]. Increased plasma AOC1 was also detected in patients with CKD [122]. Besides the increased catabolism, the interconverting enzyme PAOX is increased in plasma of CKD patients [115], leading to a shift in favor of smaller polyamines.

Dysregulation of polyamine homeostasis promoting their degradation is considered to be damaging. Polyamine breakdown produces reactive hydrogen species and other toxic byproducts. Reactive oxygen species generated by SMOX and PAOX cause oxidative DNA damage in lung epithelial cells [123]. Another byproduct of polyamine catabolism by SMOX and PAOX is acrolein, which is increased in the plasma of CKD patients [115, 116]. Consistently, inhibition of *Paox* protects against renal IRI [124]. Overexpression of polyamine degrading *Sat1* in kidney cells resulted in oxidative stress, decreased proliferation, reduced cell attachment, mitochondrial damage, DNA damage with subsequent G_2 arrest and apoptosis [104, 125, 126]. In line with this, inactivation of *Sat1* in proximal tubules of mice attenuates the severity of renal IRI outcomes [124, 127].

Kidney damage can be enhanced by degradation of polyamines and by polyamine depletion. Inhibition of ODC1 results in exacerbated kidney injury by nitrative and oxidative stress as well as plasma membrane disruption after IRI [128, 129]. These effects were alleviated by pre-surgical administration of spermidine [128, 129]. Spermidine was further shown to induce

autophagy in proximal tubular cells and podocytes, exhibiting protective effects [128, 130]. The administration of exogenous spermine alleviates kidney injury by type 1 diabetes and IRI through promotion of autophagy and reduction of apoptosis [131, 132].

Overall, dysregulation of polyamines is a hallmark of different kidney pathologies. Enhanced breakdown of polyamines exacerbates kidney injury either by the increase in toxic byproducts or by lowering the renoprotective capacity provided by spermidine and spermine.

1.7 Amine Oxidase Copper Containing 1 (AOC1)

The amine oxidase copper containing 1 (AOC1) is an 85 kDa large, secreted protein that catalyzes the oxidative deamination of amines to the corresponding aldehyde under production of hydrogen peroxide and ammonia. AOC1 exhibits highest affinity to the diamines histamine and putrescine [133] and is expressed most strongly in the human intestine, kidney and placenta, i.e. at the sites of histamine/ putrescine uptake and excretion [133].

AOC1 plays a major role in histamine degradation, and decreased serum AOC1 is common in patients with histamine intolerance [134]. Increased plasma histamine as well as decreased AOC1 activity is linked to migraine [135–137]. Oral administration of AOC1 can reduce headache in these patients [138] and improves symptoms in patients with histamine intolerance [139].

AOC1 levels are frequently altered in different pathologies. Decreased gut mucosa AOC1 activity was observed in Crohn's disease [140] and, consistently, increased plasma AOC1 has been used as a marker for intestinal mucosal injury [141, 142]. Increased expression of *Aoc1* was also observed in other pathologies such as AKI [143], during cardiopulmonary bypass [144] and in different forms of cancer [145–148]. Increased *Aoc1* in cancer cells promotes tumor progression and epithelial to mesenchymal transition [149], whereas a decrease of AOC1 reduces tumor growth [150].

Besides AOC1's role in polyamine and histamine homeostasis and its dysregulation in different pathologies, little is known about its function and regulation.

1.8 Aims and hypothesis

Due to renal injury of different etiologies, alterations in polyamine content in serum, urine, and renal tissue are frequently detected together with alterations in mRNA levels of polyamine regulating enzymes. These alterations are described in patients as well as in murine injury models, underlining the conserved disposition of the polyamine system. Previous studies demonstrated the possibility to influence polyamine homeostasis and therefore the severity of renal injury. The main scope of this thesis is to evaluate genes regulating polyamine homeostasis as targets for renoprotection.

To evaluate this, the aim of this thesis is to (I) characterize changes in genes regulating polyamine homeostasis across a broad range of kidney injury models. The next aim is to (II) evaluate potential stimuli leading to this dysregulation and to gain insights into *cis*- and *trans*-acting factors regulating expression changes. Finally, the aim is to (III) gain insights into potential mechanisms that follow the altered gene expression and if they are renoprotective or aggravating kidney injury.

2 Material and Methods

2.1 Murine kidney injury models

Total RNA of the following murine kidney injury models was obtained from the authors of the corresponding publications. The generation of the samples is published in detail. A brief description of experimental procedures, summarized from the original publication is provided here for each model.

In the unilateral ischemia reperfusion model [151] male C57Bl/6N mice were used at the age of 9 to 10 weeks. The left renal pedicle was clipped for 25 min and kidneys were harvested after (n=4), 24 hours (n=3), 48 hours (n=6), 7 days (n=6), and 21 days (n=6) of reperfusion.

For allograft transplantation of the kidney [152] male C57Bl/6 mice, weighing 24-28 g were used. Following left nephrectomy of the recipient, the donor kidney was implanted. The times of cold and warm ischemia of the graft were maintained at 40 min and 30 min, respectively. The contralateral native kidney was removed 24 hours before the allograft harvest. RNA was isolated from kidneys harvested 3 days (n=3), 5 days (n=5) and 7 days (n=5) after transplantation.

In rhabdomyolysis induced AKI [53], mice of both sexes (24-31 g body weight) with the genetic modification Pax8 rtTA x VHLfl/fl mice, but without doxycycline injection, were used. Therefore, these mice are considered to display a wildtype phenotype. To induce AKI, 50% glycerol (0.05 ml per 10 g body weight) was injected intramuscularly into the left hind limb. Drinking water was withdrawn between 20 hours before and 24 hours after glycerol injection. The kidneys were harvested 24 hours after glycerol injection. Here, 5 animals with rhabdomyolysis and 3 untreated controls were used.

For CKD by cyclosporine A injection [153] 10- to 12-week-old mice with the genetic modification Pax8 rtTA x VHLfl/fl mice but without doxycycline injection, therefore to be considered to have a wildtype phenotype, were used. Animals had free access to distilled water and low sodium chow (0.05% sodium content). Mice received for six weeks a daily subcutaneous 60 mg/kg CsA injection or the CsA solvent cremophore only as controls. Here, 5 animals with cyclosporine A injection and 5 control mice were used.

Induction of diabetes by streptozotocin injection [154] was performed by a single intraperitoneal injection of 200 mg/kg streptozotocin (n=6) dissolved in 0.1 M sodium citrate buffer (pH 4.5) or solvent only as control (n=9). Wild type mice of a mixed C57Bl/6/129Sv background were used. Diabetic and control mice were followed for six weeks.

Hypertension was achieved by angiotensin II injection [155]. Male C57Bl/6 mice at 11-13 weeks of age had a subcutaneous implantation of osmotic mini-pumps delivering either isotonic saline (n=5) or angiotensin II (n=7) at a rate of 3.0 mg/kg per min for 28 days. The upper pole of the left kidney was snap frozen in liquid nitrogen for isolation of mRNA.

For inducing renovascular hypertension [156] the two-kidney, one-clip method was used in male Sprague Dawley rats weighing 150-170 g by placing a silver clip of 0.2 mm internal diameter around the left renal artery (n=6). Control animals underwent sham operation without placement of the clip (n=6). Five weeks after clipping of the renal artery kidneys were harvested.

For oxalate nephropathy [157] mice were fed a synthetic mouse diet with high oxalate (0.67% sodium oxalate; n=14) or control (0% oxalate; n=4) for 21 days. Studies were performed on 12- to 16-week-old male C57Bl/6N wild-type mice. Mice were obtained from Charles River Laboratory.

Unilateral ureter obstruction [158] was performed on male C57Bl/6 mice. Mice contain the genetic modification Tie2-Cre x Hif-1αfl/fl and only cre negative animals were used. These mice are considered to display the wildtype phenotype. Under isoflurane anesthesia, the right ureter was twice ligated and cut (n=5). Untreated mice were used as control (n=5). Kidneys were harvested after 7 days.

Conditional deletion of claudin 10 (*Cldn10*) in the thick ascending limb [159] was used as a model for nephrocalcinosis. For generation of knockout animals loxP sites were introduced flanking exons 2 and 3 of the *Cldn10* gene, resulting in a premature stop codon in all *Cldn10* isoforms (*Cldn10fl/fl*). These mice were bred to mice expressing Cre recombinase under control of the cadherin 16 promoter (*Ksp-cre*) resulting in a thick ascending limb specific knockout. *Cldn10* knockout animals (n=4) or their control littermates (n=6) were used.

2.1.1 Generation of *Aoc1* knockout mice

Heterozygous C57Bl6/N Aoc1$^{tm1a(EUCOMM)Hmgu}$ mice were provided by the European Mouse Mutant Archive, Munich, Germany and backcrossed into the C57Bl/6J background. The C57Bl/6J Aoc1$^{tm1a(EUCOMM)Hmgu}$ mice were bred at the Forschungseinrichtungen für Experimentelle Medizin, Charité Universitätsmedizin Berlin, in accordance with local rules and regulations. Ear punches of resulting C57Bl/6J Aoc1$^{tm1a(EUCOMM)Hmgu}$ mice were used for genomic DNA extraction (2.7.1) and genotyped by PCR using primers 5' TCAGCGCCTTCTGAGGTTGCTC 3' and 5' GGGCAAGAACATAAAGTGACCCTCC 3' for detection of knockout alleles and 5' GGTTGCTCGGTGTGTTTCATGGAT 3' and 5' GCTGTGCTCTGAAACATTTTCTGTGGTC 3' for detection of wild-type alleles. Animals

homozygous for the knockout allele are designated as *Aoc1*$^{-/-}$ while the homozygous wild-type allele is designated as WT.

2.1.2 Renal unilateral ischemia reperfusion injury

Renal unilateral ischemia reperfusion injury was induced surgically in *Aoc1*$^{-/-}$ and WT mice aged 9-10 weeks. The procedures were carried out by Dr. Felix Boivin under permission number G0180/18 at the Max-Delbrück-Centrum, Berlin, Germany. Briefly, animals were anesthesized using 2.3% isoflurane and analgised using 0.05-0.1 mg/kg body weight buprenorphine. The left renal pedicle was clamped for 25 minutes. After 21 days of reperfusion, spontaneous urine was collected and animals sacrifized by cervical dislocation. Whole blood was collected from the aorta and kidneys were excised. Serum was prepared according to (2.2.1) and kidneys were frozen in liquid nitrogen for RNA extraction (2.7.4) and polyamine measurements (2.2.2) or immersion fixed for histology (2.3.1).

2.1.3 Adenine nephropathy

Tubulointerstitial nephritis was induced in 13- to 26-week-old *Aoc1*$^{-/-}$ and WT animals by feeding an adenine enriched diet (0.2% w/w (ssniff-Spezialdiäten, Soest, Germany)) or control chow for 14 days. The study was permitted under the number G0085/22 and conducted according to local rules. Spontaneous urine was collected one day prior to adenine feeding and 8 and 15 days after. Animals were sacrificed under isoflurane anesthesia by cervical dislocation. Quickly after, whole blood was drained from the heart through cardiac puncture and kidneys were excised. Serum was prepared according to (2.2.1) and kidneys were frozen in liquid nitrogen for RNA extraction (2.7.4) and polyamine measurements (2.2.2) or immersion fixed for histology (2.3.1).

2.2 Clinical chemistry

2.2.1 Preparation of serum

Serum was prepared from whole blood through clotting at room temperature for 10 minutes and subsequent centrifugation at 10℃ and 2500 xg for 10 minutes.

2.2.2 Measurement of metabolites

Measurement of creatinine, albumine and urea in urine and serum samples was performed by the department for clinical chemistry at the Max-Delbrück-Centrum, Berlin, Germany. Determination of polyamines in urine, serum and tissue was performed by Lipidomix, Berlin, Germany. The used method for determination of polyamines is described in detail elsewhere [160].

2.2.3 Measurement of osmolality

Osmolality of cell culture supernatants was measured using the osmomat 3000 basic freezing point osmometer (Gonotec Meß- und Regeltechnik, Berlin, Germany).

2.2.4 Determination of total urinary protein

Total urinary protein was detected using a BCA assay (Thermo Fisher, Waltham, USA) according to the manufacturer's protocol using spot urine 1:100 diluted in dH_2O.

2.3 Histology

2.3.1 Preparation of formalin fixed, paraffin embedded kidney slices

The kidneys were immersion fixed for at least one week in Roti Histofix (Carl Roth, Karlsruhe, Germany). Kidneys were embedded in Paraplast Plus (Leica, Wetzlar, Germany) using an automated Leica TP1020 tissue processer (Leica, Wetzlar, Germany). Here, samples were dehydrated and paraffinized by incubation for 1.5 hours in each step of an descending ethanol dilution series (70% EtOH, 80% EtOH, 96% EtOH, 99% EtOH) followed by two incubations in xylene and a 50℃ 1:1 mixture of xylene and Paraplast Plus (Leica, Wetzlar, Germany) and finally in 50℃ Paraplast Plus (Leica, Wetzlar, Germany). The embedded kidneys were sectioned into 1.5 µm slices using an automated HM355S microtome (Epredia, Michigan, USA). Sections were mounted on SuperFrost Plus microscope slides (Thermo Fisher, Waltham, USA) and stored at 4℃. Before use, sections were deparafinized by incubation over night at 60℃ and subsequent dissolving of paraffin using two 10 minute washes in Neo-Clear (Sigma-Aldrich, St. Louis, USA).

2.3.2 Histochemical stainings and histomorphologic evaluation

Staining of renal sections using periodic acid Schiff reagent (PAS), hematoxylin and eosin (HE) and Masson-Goldner trichrome (MGT) was performed by the institute for pathology at the Charité – Universitätsmedizin Berlin, Germany, Berlin. Histomorphologic evaluation was performed by acquiring four to five non-overlapping images from the renal cortex, each representing 0.79 mm^2, using a widefield Ti2 microscope (Nikon, Minato, Japan). Tubular casts and mononuclear cells were manually counted. Determination of total healthy area was performed using scans of kidney sections stained with MGT and by dividing the healthy cortical area by the total cortical area. Determination of the relative fibrotic area was performed using color thresholding in ImageJ version 1.53.

2.3.3 RNAScope *in situ* hybridization

RNAScope chromogen *in situ* hybridization on deparafinized kidney slices was performed using the RNAScope 2.5 HD Assay Brown (Advanced Cell Diagnostics, Hayward, USA)

Kit according to the manufacturer's instructions with minor changes. A food steamer (Braun, Kronberg im Taunus, Germany) was used for target retrieval for 15 minutes. AMP5 hybridization was prolonged to one hour. Counterstaining was performed using hematoxylin solution, Gill No.1 (Sigma-Aldrich, St. Louis, USA) for 5 seconds and subsequent washes in tap water. Slides were mounted using Aquatex (Sigma-Aldrich, St. Louis, USA). For fluorescent staining, the RNAScope Multiplex Fluorescent V2 Assay (Advanced Cell Diagnostics, Hayward, USA) was used according to manufacturer's instructions. A food steamer (Braun, Kronberg im Taunus, Germany) was used for target retrieval for 15 minutes. Labeling was performed using Opal dyes (Akoya Biosciences, Marlborough, USA) at a dilution of 1:750. Slides were mounted using Vectashield H1000 mounting medium for fluorescence (Vector Laboratories, Newark, USA). Used probes are listed in table 2.1.

Table 2.1: Probes used for RNAScope Assays 2.5 HD Brown and Multiplex Fluorescent V2. Table adapted from Sieckmann *et al.* [161].

Target	Product number	Channel
Odc1	417721	C1
Srm	559411	C1
Sms	559421	C1
Aoc1	524481	C1
Sat1	423361	C1
Paox	559401	C1
Smox	559431	C1
Lrp2	425881-C3	C3
Aqp1	504741-C2	C2
Umod	476301-C2	C2
Slc12a3	476311-C3	C3
Aqp2	452411-C3	C3
Odc1	417721-C2	C2

2.3.4 Immunohistochemistry

Deparafinized slides were rehydrated using an ascending ethanol dilution series. Here, slides were incubated two times in 100% ethanol for 5 minutes. Afterwards, in 96% ethanol and 70% ethanol for 5 minutes and rehydrated by incubation in dH_2O twice for 5 minutes. For target retrieval, the slides were boiled in target retrieval solution (Dako, Carpinteria, USA) for 30 minutes using a food steamer (Braun, Kronberg im Taunus, Germany). Samples were blocked for 1 hour using serum free protein block (Dako, Carpinteria, USA). For detection of target proteins, 50 µL of specific primary antibody dilution (table 2.2) was added to each slide. Incubation of primary antibodies was carried out over night at 4℃ in a humidified chamber. Afterwards, slides were washed three times for 10 minutes in TBST before addition of the appropriate secondary antibody (table 2.2). After incubation for 1 hour in a dark humidified

chamber at room temperature, slides were washed two times for 5 minutes with TBST before staining of nuclei with DAPI (10 µg/mL, 10 min). After washing in TBST for 5 minutes, the slides were mounted using Vectashield H1000 mounting medium for fluorescence (Vector Laboratories, Newark, USA).

Table 2.2: Antibodies used for immunohistochemistry. Specified dilution refers to dilution in antibody diluent reagent solution (Life Technologies, Carlsbad, USA) if not otherwise stated. Table adapted from Sieckmann *et al.* [161].

Antigen	Name	Supplier	Product number	Lot number	Final conc.
AOC1	Rabbit anti AOC1, polyclonal	LSBio (Seattle, USA)	LS-C294123	171827	5 µg/mL
KI-67	Rat anti Ki-67, monoclonal (SolA15)	Invitrogen (Waltham, USA)	14-5698-82	2196796	5 µg/mL
KIM1	Goat anti KIM1, polyclonal	R&D Systems (Minneapolis, USA)	AF1817	KCA0319011	4 µg/mL
Vimentin	Rabbit anti Vimentin, Monoclonal (ERP3776)	Abcam (Cambridge, UK)	ab92547	3179947	1 µg/mL
Rabbit IgG (H+L)	Donkey anti rabbit Cy3	Jackson (Bar Harbor, USA)	711-165-152	109623	7.5 µg/mL
Rat IgG (H+L)	Goat anti rat Cy2	Jackson (Bar Harbor, USA)	112-226-003	62775	7.25 µg/mL
Goat IgG (H+L)	Donkey anti goat A488	Jackson (Bar Harbor, USA)	705-545-003	113181	7.5 µg/mL

2.3.5 Immunohistochemistry combined with RNAScope *in situ* hybridization

RNAScope *in situ* hybridization was performed according to the manufacturer's instructions using the Multiplex Fluorescent V2 Assay (Advanced Cell Diagnostics, Hayward, USA). The protocol was continued up to the HRP blocking step. Therefore, the target retrieval, hybridization of probes, amplifiers and fluorophore is completed. After the HRP blocking step, slices were incubated for one hour at room temperature in serum free protein blocking solution (Dako, Carpinteria, USA). Afterwards, immunohistochemistry protocol was performed as described earlier (see 2.3.4).

2.3.6 TUNEL assay combined with immunohistochemistry

For the detection of necrotic and apoptotic cells, TUNEL assay was performed using the *in situ* cell death detection kit (Roche, Basel, Switzerland). The deparafinized kidney slices were rehydrated as described in the immunohistochemistry protocol (see 2.3.4). Afterwards, the slices were blocked using serum free protein block (Dako, Carpinteria, USA) for 1 hour at room temperature. The primary AOC1 antibody (table 2.2) was diluted at 5 µg/mL in the Kits TUNEL solution and incubated on the slices for 1 hour at 37℃. The slides were washed two times for 5 minutes in TBST and nuclei stained using DAPI (10 µg/mL) for 10 minutes. After a

5 minute wash in TBST, slides were mounted using Vectashield H1000 mounting medium for fluorescence (Vector Laboratories, Newark, USA).

2.3.7 Immunohistochemistry on whole mount specimens

Immunohistochemistry was performed on embryonic kidneys cultivated for one day in either isosmotic or hyperosmotic (DMEM (Gibco, Carlsbad, USA), 10% FBS (Sigma-Aldrich, St. Louis, USA), 0.2 M sucrose) conditions (see 2.6.2). After cultivation, the kidneys were immersion fixed using Roti Histofix (Carl Roth, Karlsruhe, Germany) for 20 minutes. Fixation was stopped by washing and subsequent incubation in 50 nM ammonium chloride in PBS (Gibco, Carlsbad, USA) for 30 minutes at room temperature. The kidneys were washed and incubated over night at 4℃ in blocking solution (0.2% BSA and 0.05% Triton X100 in PBS (Gibco, Carlsbad, USA)). The blocking solution was removed and the kidneys were incubated using an antibody directed against AOC1 (LSBio, Seattle, USA (LS-C294123)) in blocking solution at 2.5 µg/mL over night at 4℃. The kidneys were rinsed two times with blocking solution and washed for 7 hours at 4℃ in blocking solution with a change of the blocking solution every 2 hours. The secondary antibody (table 2.2) was incubated over night at 4℃. This step was performed at a dilution of 1:100 in blocking solution with the addition of DAPI (10 µg/mL). Finally, the kidneys were rinsed two times with blocking solution before washing for 2 hours in blocking solution at 4℃. The kidneys were mounted using Vectashield H1000 mounting medium for fluorescence (Vector Laboratories, Newark, USA).

2.4 Molecular cloning and generation of knockout cells

2.4.1 *Aoc1* expression construct

Overexpression construct for *Aoc1* was generated using primers for amplification containing *Hin*dIII and *Not*I restictions sites (underlined) in addition to the complementary sequence (5' CGTAAGCTTGACGGAGCAGAGCACACAG 3', 5' CGTGCGGCCGCCTTCAGAGGCTGGGGTCAGA 3'). cDNA from C57Bl/6J duodenum was used as a template and amplification was performed using the Expand Long Template PCR System (Roche, Basel, Switzerland) according to the manufacturer's instructions. The amplicon was cloned into the pcDNA3 vector using *Hin*dIII and *Not*I. Correct sequence and insertion into the plasmid was verified by Sanger sequencing (LGC, Teddington, UK) from 5' and 3' ends inward using primers 5' TAATACGACTCACTATAGGG 3' and 5' CTATTTAGGTGACACTATAG 3'.

2.4.2 Promoter construct generation

Promoter constructs were amplified using primers from table 2.3, which contain restriction sites for *Mlu*I and *Bgl*II respectively in addition to the complementary sequence. The -2000 bp to -1 bp (relative to transcription start site (TSS)) fragment was amplified from genomic DNA

(see 2.7.1) of C57Bl/6 mice using the Expand Long Template PCR System (Roche, Basel, Switzerland) according to the manufacturer's instruction. Smaller fragments were amplified using proof-reading Phusion DNA polymerase (NEB, Ipswich, USA). The plasmid containing the -2000 to -1 bp fragment was used as a template. The amplicons were cloned into the pGL3-basic vector (Promega, Madison, USA) using *Mlu*I and *Bgl*II.

Table 2.3: Primer used for amplification of *Aoc1* promoter fragments. Restriction sites for *Mlu*I and *Bgl*II are underlined. Minuscule letters indicate mutation of NFAT5 binding site.

5' – 3' Forward Sequence	5' – 3' Reverse Sequence	Position rel. to TSS
CGTACGCGTTCACTAGTCTCCTGGGTAAACCTT	CGTAGATCTTGAGCAGTGGAAAATTACAGAACC	-2000 to -1
CGTACGCGTATGCTTATTAGCCTGATGGCCT	CGTAGATCTTGAGCAGTGGAAAATTACAGAACC	-1494 to -1
CGTACGCGTCAGCATGACCTTTCTTCTCAGT	CGTAGATCTTGAGCAGTGGAAAATTACAGAACC	-1003 to -1
CGTACGCGTCTAGATGGCCTGGGGTCCTATT	CGTAGATCTTGAGCAGTGGAAAATTACAGAACC	-499 to -1
CGTACGCGTCTTTCTCCAATAAGGGGCTTTA	CGTAGATCTTGAGCAGTGGAAAATTACAGAACC	-372 to -1
CGTACGCGTCAAGATGAATGGGCAGGGAGCA	CGTAGATCTTGAGCAGTGGAAAATTACAGAACC	-248 to -1
CGTACGCGTAGAGTGGGTGAGCTCTGTCCAA	CGTAGATCTTGAGCAGTGGAAAATTACAGAACC	-124 to -1
CGTACGCGTAGAGTGGGTGAGCTCTGTCCAA	CGTAGATCTTGAGCAGTtGccAATTACAGAACC	-124 to -1

2.4.3 eGFP-construct generation

eGFP fusion-protein constructs were generated by amplification of M15 cells cDNA for the N-terminal AOC1 signal peptide and the signal peptide plus 22 additional amino acids of *Aoc1*-205 using primers displayed in table 2.4. Amplification was performed using proof-reading Phusion DNA polymerase (NEB, Ipswich, USA) according to manufacturer's instructions. The amplicons were cloned into the peGFP-N1 (Clontech Laboratories, Kyoto, Japan) vector using *Hin*dIII and *Bam*HI. Correct insertion and sequence was confirmed by sequencing (LGC, Teddington, UK) using 5' GCAAATGGGCGGTAGGCGT 3' primer.

Table 2.4: Primer used for amplification of *Aoc1* signal peptide sequence. Underlined bases indicate *Hin*dIII and *Bam*HI restriction sites.

Construct	5' – 3' Forward Sequence	5' – 3' Reverse Sequence
AOC1-SP	CGTAAGCTTATGAGGCTGGCACAGATGAG	CGTGGATCCACAGCAGATGCTGTGTCTG
AOC1-SP+22AA	CGTAAGCTTATGGATCAGTGGTCTGCTGC	CGTGGATCCACAGCAGATGCTGTGTCTG

2.4.4 CRISPR-Cas9 guide RNA expression construct

For generation of the *Aoc1* targeting CRISPR/Cas9 construct, oligonucleotides (5' CACCGGTCTTCCAGAGCCATGAGGC 3' and 5' AAACGCCTCATGGCTCTGGAAGACC 3') were ligated into *Bbs*I cutted pSpCas9(BB)-2A-GFP vector by Feng Zhang (Addgene plasmid # 48138 http://n2t.net/addgene:48138 ; RRID:Addgene_48138).

2.5 Cell culture techniques

2.5.1 General cell culture

The mouse mesonephros derived cell line M15 [162] and the human embryonic kidney cell line HEK293 (DSMZ, ACC 305) were cultivated in DMEM (Gibco, Carlsbad, USA) with the addition of 10% FBS (Sigma-Aldrich, St. Louis, USA). The mouse distal convoluted tubule cell line 209/MDCT (ATCC, Manassas, USA (CRL-3250)) was cultivated using RPMI 1640 (Gibco, Carlsbad, USA) with the addition of 10% FBS (Sigma-Aldrich, St. Louis, USA). All used cell lines were cultivated at 37℃ in a humified atmosphere under 95% air and 5% CO_2. All cell lines were routinely subcultured before reaching 90% confluence.

2.5.2 Transfection

Transient transfection of cells was carried out using the FuGene 6 HD transfection (Promega, Madison, USA) reagent according to manufacturer's instructions. For expression of constructs, 0.22 µg plasmid and 0.88 µL FuGene 6HD transfection reagent were used per cm^2 cell culture surface. For dual luciferase assay, 0.45 µg plasmid containing the promoter fragment together with 0.05 µg of the phRL-TK renilla luciferase plasmid (Promega, Madison, USA) was transfected.

2.5.3 Selection of plasmid expressing cells

For stable transfection, transfected cells were treated with the antibiotic G418 solution (Roche, Basel, Switzerland) at 400 µg/mL for M15 and 209/MDCT cells and at 600 µg/mL for HEK293 cells.

2.5.4 CRISPR/Cas9 mediated *Aoc1* deletion

Aoc1-deficient M15 cells were generated using CRISPR/Cas9 based gene editing as described elsewhere [163]. Briefly, M15 cells were transfected with either the empty pSpCas9(BB)-2A-GFP vector or the *Aoc1* targeting CRISPR/Cas9 construct 2.4.4. GFP positive cells were sorted as singe cells individually into wells of a 96 well plate using a FACS Aria III (Becton Dickinson, Franklin Lakes, USA). Expanded clones were screened by amplification of the genomic guide RNA target site from genomic DNA (see 2.7.1) using primer 5' CGTGAGCTCGCGTCAGGAACCATGAGTGA 3' and 5' CGTAAGCTTGGGGCTCAGGTCTGCAAATA 3'. The resulting amplicon was digested using *Bst*XI. Double strand break of *Aoc1* induced by the Cas9 and following repair by nonhomologous end joining leads to destruction of *Bst*XI restriction site. Therefore, clones with amplicons un-digested by *Bst*XI were validated for homozygous mutation of *Aoc1* by Sanger sequencing (LGC, Teddington, UK). The resulting clones exhibited deletions on both alleles, leading to frame shifts in the protein coding sequence. A detailed view of the deletions and flanking sequences is given in table 2.5.

Table 2.5: Genomic *Aoc1* reference sequence and sequencing of *Aoc1* knockout clones.

Origin	Sequence 5‘ - 3‘
Reference	...CTGACTTTGGCCAAGAACTCCGTGTTTCTCATTGAGATGCTACTGCCAAAAAAGAAGAATGTGC...
Clone 1, Allele 1	...CTGACTTT**********ATTGAGATGCTACTGCCAAAAAAGAAGAATGTGC...
Clone 1, Allele 2	...CTGACTTTGGCC*AGAACTCCGTGTTTCTCATTGAGATGCTACTGCCAAAAAAGAAGAATGTGC...
Clone 2, Allele 1	...CTGACTTTGGCC**********TGTTTCTCATTGAGATGCTACTGCCAAAAAAGAAGAATGTGC...
Clone 2, Allele 2	...C**********C...

2.5.5 NFAT5 Knockdown

NFAT5 knockdown was performed in M15 cells using ON-TARGETplus siRNA against mouse *Nfat5* (Horizon Discovery Group, Waterbeach, UK (L-058868-01)) or ON-TARGETplus Non-targeting Control Pool (Horizon Discovery Group, Waterbeach, UK (D-001810-10)). Knockdown was performed by transfection of 25 nM siRNA using Dharmafect1 (Horizon Discovery Group, Waterbeach, UK) according to the manufacturer's protocol. After 24 hours, the medium was changed. After another 24 hours, the medium was changed again to medium with or without addition of 0.2 M sucrose. The cells were cultivated for 24 hours and total RNA and protein were isolated.

2.5.6 Scratch assay

Cells were seeded at a density of 8000 cells/cm^2. After attachment of the cells and formation of a confluent cell layer, a scratch was made using a P200 pipette tip to remove the cells. Scratch closure was monitored using a phase contrast using a Ti2 eclipse widefield microscope (Nikon, Minato, Japan). The same field was imaged at every 3 hours for 9 hours. Images were evaluated for scratch closure as described in section 2.9.1.

2.5.7 Proliferation assay

Cells were seeded at a density of 5200 cells/cm² on several 9.6 cm^2 wells. Every 24 hours, one well was trypsinized. Dead cells were stained using 0.5% trypan blue and excluded from the measurement. Living cells were counted using a TC20 automated cell counter (Bio-Rad Laboratories, Hercules, USA).

2.6 Primary cell and organ culture

2.6.1 Primary proximal tubule culture

C57Bl/6 mice were anesthetized by isoflurane inhalation using forene (AbbVie, North Chicago, USA) and sacrificed by cervical dislocation. Dissection and prepration of the kidneys were performed under sterile conditions and ice-cold conditions if not mentioned otherwise. The abdomen was opened and the kidneys were excised and transferred into cold dissection buffer.

The *capsula fibrosa* of the kidney was removed. The cortex was separated from the medulla and pelvis. The cortex was minced finely using a scalpel and transferred into dissection buffer containing 0.1% collagenase type 2 (Gibco, Carlsbad, USA). Digestion of the tissue fragments was carried out in a shaking water bath at 37℃ for 30 minutes. Digestion was stoped by addition of 10% FBS (Sigma-Aldrich, St. Louis, USA). The solution was filtered through a 250 µm mesh and the flow-through collected and filtered again using a 40 µm mesh. Here the tubule fragments are stuck on the filter while smaller debris as well as erythrocytes pass through. For collection of the tubules the filter was reversed and flushed using the proximal tubule cultivation medium (2.10). The suspension was centrifuged at 170 xg at 4℃ for 5 minutes and the pellet was resuspended in isosmotic medium (proximal tubule cultivation medium) or hyperosmotic medium (proximal tubule cultivation medium with 0.2 M sucrose). After 24 hours, tubules attached to the plate were collected in RLT buffer, originating from the RNeasy micro kit (Qiagen, Venlo, Netherlands), containing 0.1% β-mercaptoethanol for subsequent RNA extraction.

2.6.2 Embryonic organ culture

Timed pregnant C57Bl/6 mice were used to obtain embryos aged 12.5 days post contraception (d.p.c.). The mice were anesthized by isoflurane inhalation using forene (AbbVie, North Chicago, USA) and sacrificed by cervical dislocation. The abdomen was opened and the uterus containing the embryos was removed and transferred into ice-cold PBS (Gibco, Carlsbad, USA). The uterus was opened and the embryos removed. The embryonic abdominal cavity was opened and the kidneys were explanted. The explants were cultivated for 24 hours on transwell permeable supports (24 mm insert, 0.4 µm membrane)(Corning, Corning, USA) at the liquid/air interface. These filters were placed onto DMEM (Gibco, Carlsbad, USA) containing, unless otherwise stated 10% FBS (Sigma-Aldrich, St. Louis, USA) with addition of 1x Penicillin/Streptomycin (Millipore, Burlington, USA (#TMS-AB2-C)) and were cultivated at 37℃ in a humidified atmosphere at 5% CO_2 and 95% air. Here, one kidney was used as an untreated control while the contralateral was treated. The treatments consisted of the addition of different stressors. These included cultivation in DMEM without FBS, DMEM without glucose (Gibco, Carlsbad, USA), DMEM with neither FBS nor glucose and DMEM without glutamine (Gibco, Carlsbad, USA). Other treatments consisted of addition of thapsigargin (2 µM) for induction of ER Stress, treatment with the NO-donor S-nitroso-N-acetylpenicillamine (SNAP (Cayman Chemical, Ann Arbor, USA); 100 µM), addition of H_2O_2 (0,1 µM, 1 µM or 100 µM), acidification of the medium using 10% CO_2, cultivation in 42℃, hypoxia (1% O_2), hyperosmotic conditions (DMEM with 0.2 M sucrose) and hypoosmotic conditions (DMEM, 25% H_2O), or addition of 100 µM putrescine (Sigma-Aldrich, St. Louis, USA). After 24 hours the kidneys were collected in 350 µL RLT buffer, originating from the RNeasy micro kit (Qiagen, Venlo, Netherlands) containing 0.1% β-mercaptoethanol for subsequent RNA extraction or in Roti Histofix (Carl Roth, Karlsruhe, Germany) for wholemount immunostaining.

2.7 Molecular biology techniques

2.7.1 Isolation of genomic DNA

Genomic DNA was isolated using the Dneasy Blood & Tissue Kit (Quiagen, Venlo, Netherlands) according to the manufacturer's instructions. Isolated DNA was measured spectrophotometrically using a NanoDrop 2000 (Thermo Fischer, Waltham, USA).

2.7.2 Protein extraction and precipitation

For protein extraction from adherent cultured cell, the cells were washed twice with ice-cold PBS (Gibco, Carlsbad, USA). SDS sample buffer (1.8 µl/cm^2) was added onto the cell culture dish for cell lysis. The cells were detached using a cell scraper. For protein extraction from embryonic kidneys, these were collected from the filter with a pipet tip placed into the SDS sample buffer. Cells and embryonic kidneys in SDS sample buffer were heated for 10 minutes at 95℃ and subsequently sonicated. Protein concentration was measured spectrophotometrically using a NanoDrop 2000 (Thermo Fischer, Waltham, USA) and calculated using the Warburg-Christian equation [164]. Proteins of cell culture supernatant was isolated by using a chloroform methanol precipitation method. One volume of supernatant was mixed with four volumes methanol. One volume of chloroform was added and the sample was shaken. Afterwards, three volumes of dH_2O were mixed in before the sample was centrifuged for one minute at 14000 xg. The aqueous layer was discarded and four volumes methanol were mixed in. The sample was centrifuged for two minutes at 14000 xg. Methanol was removed and the pellet was dried before reconstitution in SDS sample buffer.

2.7.3 SDS-PAGE and western blot

After protein extraction, 35 µg of total protein was used for SDS-PAGE and Western blotting. The samples were mixed with ¼ volume of 4x Roti Load 1 (Carl Roth, Karlsruhe, Germany) and adjusted to an equal volume by using SDS sample buffer. After heating for 5 minutes at 95℃, samples were loaded onto a SDS-Polyacrylamide gel consisting of a separation- and stacking gel. Depending on the mass of the detected protein, separation gels were used in percentages between 10% and 15%. The gel was placed in an electrophoresis chamber filled with 1x SDS running buffer and a voltage of 80 V was applied for 20 minutes. After this, the voltage was increased to 100 V and the run was continued until the running front reached the bottom of the separation gel. Afterwards, the gel was used for semi-dry blotting on a 0.45 µm pore size PVDF membrane (Carl Roth, Karlsruhe, Germany). Transfer was performed at 15 V for 45 minutes. After blotting, the membrane was blocked using 5% skim milk powder in TBST for 1 hour at room temperature. The primary antibody (table 2.6) was incubated on the membrane over night at 4℃ under slight agitation. The membrane was washed three times for 10 minutes in TBST before the secondary antibody (table 2.6) was incubated for 1 hour at room temperature. The membrane was washed three times and chemiluminescent

detection was performed using the westernbright chemiluminescence reagent (Advansta, San Jose, USA) according to the manufacturer's instructions. Blots were visualized using an ECL Chemo Star Imager System (INTAS, Göttingen, Germany).

Table 2.6: Antibodies used for Western Blot. Specified dilution refers to dilution in 2.5% skim milk powder in TBST.

Antigen	Name	Supplier	Product number	Lot number	Final conc.
AOC1	Rabbit anti AOC1	LSBio (Seattle, USA)	LS-C294123	171827	2.5 µg/mL
NFAT5	Rabbit anti NFAT5	Abcam (Cambridge, UK)	ab137407	GR209034-8	0.73 µg/mL
pan-actin	Mouse anti Aktin	Merck Millipore (Burlington, USA)	Mab1501R	1991258	0.1 µg/mL
GAPDH	Mouse anti-GAPDH	Merck Millipore (Burlington, USA)	Mab374	2606352	0.1 µg/mL
Rabbit IgG (H+L)	goat anti rabbit IgG HRP	Jackson (Bar Harbor, USA)	111-035-003	E1313	0.02 µg/mL
Mouse IgG (H+L)	goat anti mouse IgG HRP	Jackson (Bar Harbor, USA)	115-035-003	99630	0.02 µg/mL

2.7.4 RNA extraction

Total RNA was extracted using RNAStat-60 (Amsbio, Abingdon, UK) according to the manufacturer's instructions. For embryonic kidneys and primary proximal tubules, RNA was extracted using the RNeasy micro kit (Qiagen, Venlo, Netherlands) according to manufacturer's instructions. Here, RNA was eluted from the filter columns using 14.5 µL of nuclease free H_2O.

2.7.5 Reverse transcription

For cell lines and tissue specimens reverse transcription was performed with 2 µg of total RNA using oligo dT primer (Thermo Fisher, Waltham, USA) and superscript III DNA polymerase (Invitrogen, Waltham, USA) according to the manufacturer's instruction. For embryonic kidneys and primary proximal tubules 14 µl of extracted RNA (see 2.7.4) was used for reverse transcription using random hexamer primer (Thermo Fisher, Waltham, USA).

2.7.6 qPCR

For qPCR, cDNA was used at 1:10 dilution using FastStart Universal SYBR Green Master (Roche, Basel, Switzerland) according to manufacturer's instructions. Primers were used at 100 nM and are listed in table 2.7. qPCR was performed with an initial denaturation for 10 minutes, followed by 45 cycles of denaturation (95℃, 15 sec), annealing (60℃, 60 sec), elongation (77℃, 30 sec).

Table 2.7: Primer used for qPCR. Table adapted from Sieckmann *et al.* [161].

Transcript	Species	5' – 3' Forward Sequence	5' – 3' Reverse Sequence
Actb	mouse	CCGCGAGCACAGCTTCT	GGGTACTTCAGGGTCAGGAT
Odc1	mouse	CCTCAGTGTTAAGTTTGGTGC	CACTGGTGATCTCTTCAAATT
Sms	mouse	TATGGCAGCAGCAAGACACA	TGTTTGCCTTGCACATCACTG
Srm	mouse	TCCTCGTCTTCCGCAGTAAA	CATGCCAGGCAGGAACTCT
Aoc1	mouse	AGGCTGCATTCCGCTTTGGAC	GGATGTGCAGGAAGCCTACTG
Sat1	mouse	CCCCTGAAGGTTACAGTCTCT	ATACTGCTGCAAGCGACACTT
Paox	mouse	CGGAGAGTGACAGGAAACCC	GACTGCTCCACCTGTGAGTC
Smox	mouse	CGAGCCTTTGCGCTACAAC	TGTACCTCGTTTGGGCAGC
Lcn2	mouse	GACTTCCGGAGCGATCAGTT	GCGAACTGGTTGTAGTCCGT
Kim1	mouse	TTCACAGCAGATGCTTCAGGA	GCCCCTTTAAGTTGTACCGAC
Vim	mouse	GCCAGCAGTATGAAAGCGTG	GGTGACGAGCCATCTCTTCC
aSma	mouse	GCCAGTCGCTGTCAGGAACCC	TGCTCTTCAGGGGCCACACG
Il1b	mouse	GCCACCTTTTGACAGTGATGAG	AAGGTCCACGGGAAAGACAC
Tgfb	mouse/ rat	CGTCAGACATTCGGGAAGCA	TTCCGTCTCCTTGGTTCAGC
Tnfa	mouse	AAGAGGCACTCCCCCAAAAG	TTGCTACGACGTGGGCTACA
spliced *Xbp1*	mouse	CTGAGTCCGAATCAGGTGCAG	GTCCATGGGAAGATGTTCTGG
Xbp1	mouse	CAGCACTCAGACTATGTGCA	GTCCATGGGAAGATGTTCTGG
F4/80	mouse	AGTGCAGCTGTCTTAGAGGC	AGCTTCCGAGAGTGTTGTGG
Mrc1	mouse	GTCAGAACAGACTGCGTGGA	AGGGATCGCCTGTTTTCCAG
Arg1	mouse	TGTGAAGAACCCACGGTCTG	ACGTCTCGCAAGCCAATGTA
Ccl2	mouse	AGCCAACTCTCACTGAAGCC	GGACCCATTCCTTCTTGGGG
Nos2	mouse	GGGACTGAGCTGTTAGAGACAC	ATGCAGCTTGTCCAGGGATTC
Il10	mouse	CTTCCAGTCGGCCAGAG	CAGCTTCTCACCCAGGGA
Ccr5	mouse	AGACATCCGTTCCCCCTACA	GCAGCATAGTGAGCCCAGAA
Actb	rat	ATGGTGGGTATGGGTCAGAA	GGGGTGTTGAAGGTCTCAAA
Odc1	rat	TCCAGCCAGCCGCTTCCCT	CGTCTCCGAGGTCCGCAA
Sms	rat	TATGGCAGCAGCAAGGCACA	TGTTTGCCTTGCACATCACTG
Srm	rat	TCCTCGTCTTCCGCAGTA	TCCTCGTCTTCCGCAGTAAA
Aoc1	rat	AGGCTGCATTCCGCTTTGGAC	GGATGTGCAGGAAGCCTACTG
Sat1	rat	CAGTGACATCCTGCGACTGA	ATACTGCTGCAGCGACACTT
Paox	rat	CGGAGGGTGACAGGAAACCC	GACTGCTCCGCCTGTGAGTC
Smox	rat	CCTCTCTTGTCACAGGCTCCTA	TGATAGATAGGGTTCCCGTGG
Lcn2	rat	ACGTCACTTCCATCCTCGTC	TTCAGTTCATCGGACAGCCC
Kim1	rat	TGGCTCTATGTGAGCAAGGAC	GTCGTTGTGATTCCTCCACG
Vim	rat	CAGTCACTCACCTGCGAAGT	GAGTGGGTGTCAACCAGAGG
aSma	rat	CATCCGACCTTGCTAACGGA	AATAGCCACGCTCAGTCAGG
Il1b	rat	GCTATGGCAACTGTCCCTGA	CACACACTAGCAGGTCGTCA
Tnfa	rat	CTCATAGCTCGTCAGCTTGC	GCCAGGTAGTTGTATCCAGAA

2.8 Molecular assays

2.8.1 mRNA stability measurement

For induction of *Aoc1* expression, M15 cells were exposed to medium containing 0.2 M sucrose for 24 hours. Afterwards cells were cultivated in either isosmotic DMEM (Gibco, Carlsbad, USA) or hyperosmotic DMEM (Gibco, Carlsbad, USA) with addition of 0.2 M sucrose. To block *de novo* mRNA synthesis 5 µg/mL actinomycin D (Carl Roth, Karlsruhe, Germany) was added to inhibit the RNA polymerase. At the indicated timepoints the cells were harvested using RNAStat 60 (Amsbio, Abingdon, UK) and *Aoc1* expression was measured using RT-qPCR. Experimental procedures were conducted by Neslihan Ögel.

2.8.2 Dual luciferase reporter assay

M15 cells were seeded at a density of 13000 cells per cm^2 on 24 well plates. After 24 hours the medium was changed to either isosmotic DMEM (Gibco, Carlsbad, USA) or hyperosmotic DMEM (Gibco, Carlsbad, USA) with addition of 0.2 M sucrose. After 24 hours the cells were washed twice using ice-cold PBS (Gibco, Carlsbad, USA) and lysed using 50 µL passive lysis buffer (Promega, Madison, USA) for 2 hours in -20°C. For measurement of luciferase activity, 20 µl of lysate was mixed with 100 µL of firefly luciferase buffer. Firefly luciferase activity was measured using a FB 12 luminometer (Berthold Technologies, Bad Wildbad, Germany). Subsequently, 100 µL of renilla luciferase buffer was added to the same tube and the sample was measured again for renilla luciferase activity. Firefly luciferase activity was normalized compared to renilla luciferase activity. Changes were calculated relative to cells growing in medium without sucrose.

2.9 Image analysis and satistics

2.9.1 Image aquisition and processing

Images were acquired using a widefield Ti2 microscope (Nikon, Minato, Japan). Images of eGFP-construct transfected M15 cells were acquired using a scanning confocal A1Rsi+ microscope (Nikon, Minato, Japan). Images were processed using ImageJ version 1.53. If applicable, adjustments of the images were performed on the whole image. The makro used for scratch closure calculation is attached in the appendix. For counting of KIM1 positive tubules and TUNEL positive cells scans of a renal section were acquired and manually counted.

2.9.2 Statistics

Statistical analysis was performed using Prism version 9.3.1 (GraphPad Software, San Diego, USA). Used statistical tests, confidence intervals, and p-values are indicated in the figures and corresponding legends. If not mentioned otherwise, displayed error bars show the standard

deviation. Prior to analysis with the corresponding test, all data was tested for normal distribution. Hierarchical cluster analysis and generation of the heatmap and correlation matrix was performed in R version 4.0.5 (The R Foundation) using the heatmaply or corrplot package.

2.10 Solutions

Solutions used within this work are displayed in table 2.8.

Table 2.8: Solutions used within this work.

Solution	Ingredients
Dissection buffer	HBSS, 15 mM HEPES, 10 mM glucose, 5 mM glycine
Proximal tubule cultivation medium	DMEM/F-12, 10% FBS, 0.5 µM dexamethasone, 550 µM sodium pyruvate, 1x non-essential amino acids (Biochrom #K0293), 1x penicilin/streptomycin (Millipore #TMS-AB2-C), 1x insulin-transferrin-selenium (Gibco #51300-044), 10 ng/mL recombinant human epidermal growth factor
SDS sample buffer	50 mM Tris-HCl pH 6.8, 4 M Urea, 1% SDS, 6.25 mM DTT
SDS-polyacrylamide stacking gel	125 mM Tris-HCl pH 6.8, 0.1% SDS, 0.1% APS, 0.1% TEMED, 10% acrylamide/bisacrylamide
SDS-polyacrylamide separation gel	375 mM Tris-HCl pH 8.8, 0.1% SDS, 10 - 15% acrylamide/ bisacrylamide, 0.06% APS, 0.06% TEMED
TBST	2 mM Tris base, 13.7 mM NaCl, 0.1% Tween 20, adjusted to pH 7.6
SDS-PAGE running buffer	25 mM Tris base, 192 mM glycine, 0.1% SDS
Semi dry blotting buffer	10 mM e-amino caproic acid, 10% methanol
Firefly luciferase buffer	470 µM D-luciferine, 270 µM coenzyme A, 33.3 mM dithiothreitol, 530 µM ATP, 2.67 mM magnesium sulfate, 20 mM tricine, 0.1 mM EDTA disodium salt dihydrate, adjusted to pH 7.8
Renilla luciferase buffer	1.1 M sodium chloride, 2.2 mM EDTA disodium salt dihydrate, 0.22 M potassium phosphate, 0.44 mg/mL bovine serum albumin,1.3 mM sodium azide, 1.43 µM coelenterazine, adjusted to pH 5.0
DMEM	DMEM, 4.5 g/L D-Glucose, 0.59 g/L L-Glutamine (41965-039 (Gibco, Carlsbad, USA))
RPMI 1640	RPMI 1640, 0.44 g/L L-Alanyl-Glutamine (61870-010 (Gibco, Carlsbad, USA))

3 Results

3.1 The polyamine system shows a common pattern of dysregulation in various forms of kidney injury

Previous findings suggest that kidney injury can be associated with altered renal polyamine metabolism [115–117]. However, it is still unclear whether abnormal polyamine regulation in the kidney is detrimental or supportive to the recovery from injury. It is further unknown, whether disturbed polyamine homeostasis is restricted to specific subtypes of kidney injury or conserved among various renal pathologies. To evaluate, if this dysregulation follows a common pattern in acute and chronic kidney damage with different etiologies, expression changes of polyamine regulating enzymes were determined in eleven murine models of kidney injury. IRI [151], transplantation [152], unilateral ureter obstruction (UUO) [158] and rhabdomyolysis [53] are considered as acute models. Acute kidney injury can progress to chronic kidney failure [16]. Therefore, two of the acute models, IRI and transplantation, were performed as longitudinal studies. Cyclosporine A treatment [153], adenine nephropathy, oxalate treatment [157], and streptozotocin-induced diabetes [154] are considered as models of chronic kidney disease. The two chronic models of hypertension are the two kidney one clip [156] and angiotensin II models [155]. As a further model *Cldn10* KO mice were used as a model of monogenetic tubular calcinosis [159]. Transcript levels of enzymes involved in polyamine metabolism were measured by RT-qPCR. In addition, expression of lipocalin 2 (*Lcn2*), a biomarker of tubular injury, was analyzed. Renal expression of *Lcn2* correlates with CKD progression [165] and can therefore be used to estimate the severity of kidney damage. To gain insights how mRNA levels of polyamine metabolizing enzymes and *Lcn2* correlate among different models of kidney injury, a hierarchical cluster analysis was performed (figure 3). RT-qPCR data for this analysis were provided by Dr. Karin M. Kirschner.

The horizontal dendrogram in figure 3 displays the similarities between the regulation of expression of genes involved in polyamine homeostasis and *Lcn2* after kidney injury. Transcript levels of the kidney injury marker *Lcn2* are increased in all models. Most evident is the close correlation between *Lcn2* and enhanced *Aoc1* expression. Contrary to the observed increase in *Aoc1* and *Lcn2,* other genes of the polyamine system were predominantly downregulated. Most prominent is the strong downregulation of *Odc1* and *Sms* expression in all analyzed models. The spermidine synthesizing enzyme *Srm* is grouped together in close relationship to the enzymes *Paox, Smox* and *Sat1* as they exhibit a more heterogenous expression pattern. Common to all models except angiotensin II-induced hypertension are the increased transcript levels, coding for one enzyme in the polyamine catabolic pathway (*Smox*, *Sat1* or *Aoc1*) and decreased mRNA levels of the putrescine synthesizing enzyme *Odc1*.

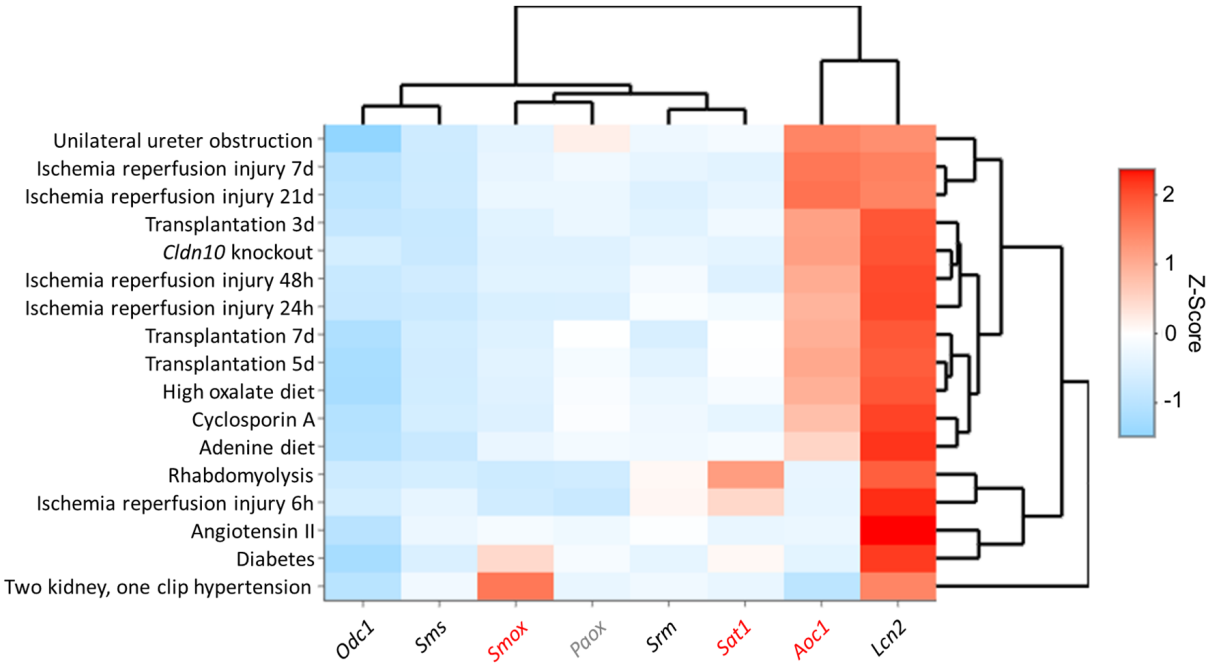

Figure 3: A conserved pattern of dysregulation within the polyamine system in eleven different kidney injury models.
Expression changes of polyamine regulating enzymes and the kidney injury marker *Lcn2* were analyzed in various models of kidney injury. Hierarchical cluster analysis of mean expression changes in the polyamine system and *Lcn2* in various models of kidney injury. Scaling of data was performed for each model; expression is displayed as Z-Scores (deviation from the mean value in units of standard deviation). Z-Scores are calculated from log2-fold change in comparison to their respective control. Increased expression is displayed in red; a decrease is displayed in blue color.

The vertical dendrogram in figure 3 clusters the different models. Here, two main clusters are visible. The bottom cluster consists mainly of the chronic models including both hypertensive models and diabetic nephropathy. Further it includes also two early acute models as rhabdomyolysis and 6 h after IRI. The upper cluster consists of models that are usually considered as AKI such as IRI, unilateral ureter obstruction, transplantation, and oxalate treatment. Interestingly, also more chronic models such as the tubular *Cldn10* knockout or CsA treatment are clustered together. Especially within the upper cluster, all models share the strong increase of *Aoc1* expression. There is no clear preference of polyamine regulating enzymes between the acute and chronic models. Although, the upregulation of *Aoc1* together with downregulation of *Odc1* is stronger in the acute kidney injury models.

To identify whether the observed changes in the polyamine system (figure 3) correlate with the severeness or certain processes of kidney injury, mRNA levels of each polyamine regulating enzyme were correlated with different kidney injury markers (figure 4).

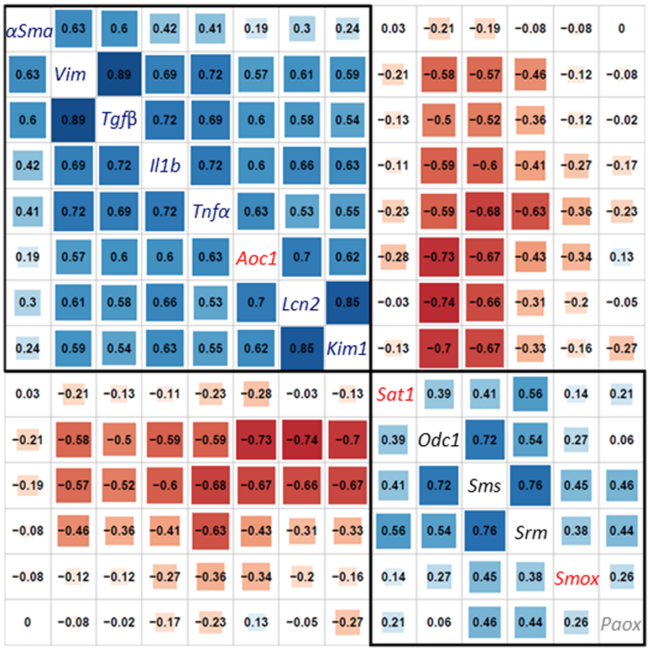

Figure 4: Correlation between relative expression changes of polyamine regulating enzymes and kidney injury markers after injury.
Transcript levels were measured by RT-qPCR relative to the housekeeping gene *Actb* and calculated as mean log2-fold change. Correlation matrix indicating Pearson correlation coefficient of different injury markers (blue text), and polyamine homeostatic genes (synthesis: black text; conversion: grey text; degradation: red text). Correlation of all transcripts was performed for all tested models of kidney injury. The size of red and blue boxes resembles the Pearson correlation coefficient (numbers within boxes), with blue color indicating positive and red color indicating negative correlation. Hierarchical cluster analysis was used for sorting of the genes. Black boxes indicate clusters of similar correlation. Adapted from Sieckmann *et al.* [161].

Here, different markers were used for tubular injury (*Lcn2* and *Kim1*), fibrosis (α*Sma*, *Vim*, *Tgf*β), pro-inflammatory mononuclear phagocytosis (*Il1*β, *Tnf*α) and correlated with expression of enzymes regulating polyamine metabolism after kidney injury. As the correlation matrix (figure 4) demonstrates, are all injury markers and most polyamine regulating genes positively correlated to each other respectively. *Aoc1* is the only gene positively correlated with all injury markers and clustered together with them. Especially the polyamine synthesizing enzymes *Odc1* and *Sms* exhibit a strong negative correlation to all measured injury markers. This is to a lesser extent true for *Srm* as well. The other polyamine metabolizing enzymes show weak mostly negative correlation with the measured markers of kidney injury.

Of all tested markers, *Lcn2* exhibits the strongest positive and negative correlation with *Aoc1* and *Odc1* respectively (figure 4). To illustrate the correlation for all analyzed models, changes in mRNA levels of polyamine regulating enzymes were correlated with the tubular injury marker *Lcn2* (figure 5). Here, *Odc1* exhibits the strongest negative correlation (r = -0.7668) with *Lcn2*. The synthesizing enzymes for the higher polyamines, *Srm* and *Sms*, correlate negatively (r = -0.1444 and r = -0.5624 respectively) with *Lcn2* expression but to a lesser extent.

Expression changes of the degrading enzymes are more ambiguous. While *Aoc1* expression shows a strong positive correlation (r = 0.7308) with *Lcn2* expression over all models, *Sat1* expression exhibits no correlation and *Smox* is slightly negatively (r = -0.1557) correlated. The interconverting enzyme *Paox* exhibits no correlation with *Lcn2* expression. In summary, these data indicate a negative correlation of all polyamine synthesizing enzymes and a positive correlation of the putrescine degrading enzyme *Aoc1* with different markers of kidney injury.

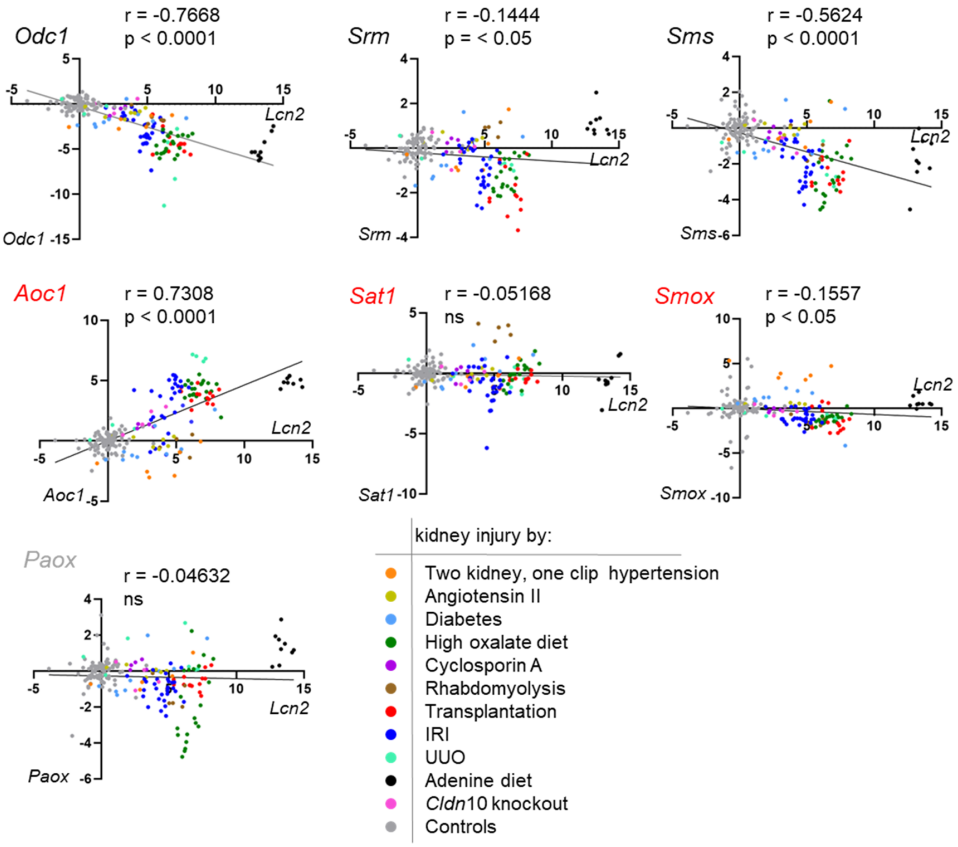

Figure 5: Relative expression changes of polyamine regulating enzymes correlate with expression of *Lcn2*.
Transcript levels were measured by RT-qPCR relative to the housekeeping gene *Actb* and calculated as mean log2-fold change. Correlation of *Lcn2* expression with expression levels of the polyamine regulating enzymes. For IRI samples, the contralateral kidney was used as a control and relative log2-fold changes are displayed. r indicates Spearman correlation coefficient. Previously published in Sieckmann *et al.* [161]

3.2 Expression changes of polyamine homeostasis affects renal and serum polyamine levels

Amounts of putrescine, spermidine and spermine were measured in renal tissue, serum and urine to determine how the changes in expression affect the metabolites (figure 6). While 21 days after unilateral IRI, renal putrescine and spermine levels were significantly decreased,

spermidine was increased (figure 6a). Serum levels of all polyamines were increased after unilateral IRI compared to untreated control animals (figure 6b). Polyamine levels in spot urine remained unchanged (figure 6c).

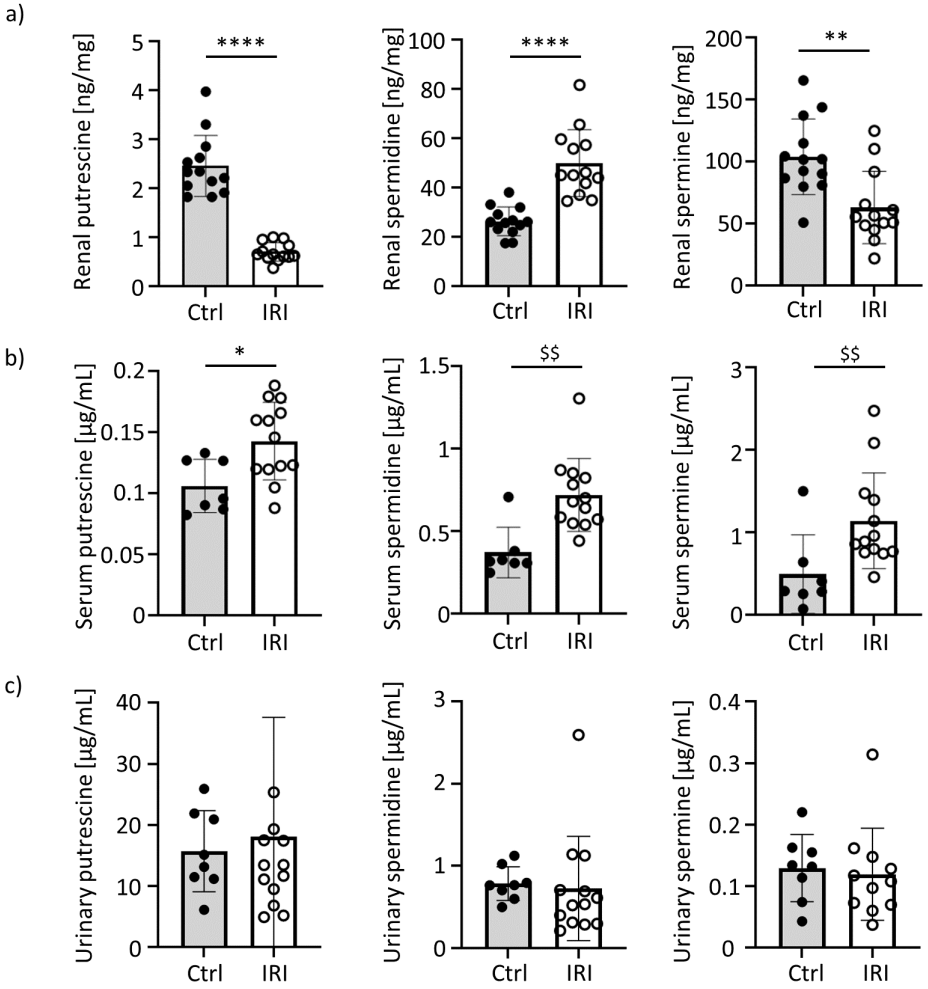

Figure 6: Concentrations of different polyamines are altered after kidney injury in renal tissue and serum.

Polyamines were measured in different specimens after kidney injury. **a)** Kidneys of untreated control mice and mice 21 days after unilateral IRI. **b)** Serum of untreated control mice and mice 21 days after unilateral IRI. **c)** Urine of untreated control mice and mice 21 days after unilateral IRI. Significances were calculated using unpaired t-test or Mann-Whitney test after testing for normal distribution using Shapiro-Wilk test. Significances for normal distributed data are indicated using asterisks (*p<0.05; **p<0.01; ***p<0.001; ****p<0.001) and for not normal distributed data by dollar signs ($^{\$}$p<0.05; $^{\$\$}$p<0.01). Adapted from Sieckmann *et al.* [161].

3.3 Expression changes of polyamine regulating enzymes after ischemia reperfusion injury occur mainly in the kidney cortex

To localize the expression changes (figure 3) to the histological structures of the kidney, RNAScope *in situ* hybridization of transcripts of the polyamine regulating enzymes was used

in healthy and injured kidneys (figure 7). As IRI was one of the models exhibiting the strongest expression changes in the polyamine system, analysis was performed seven days after IRI.

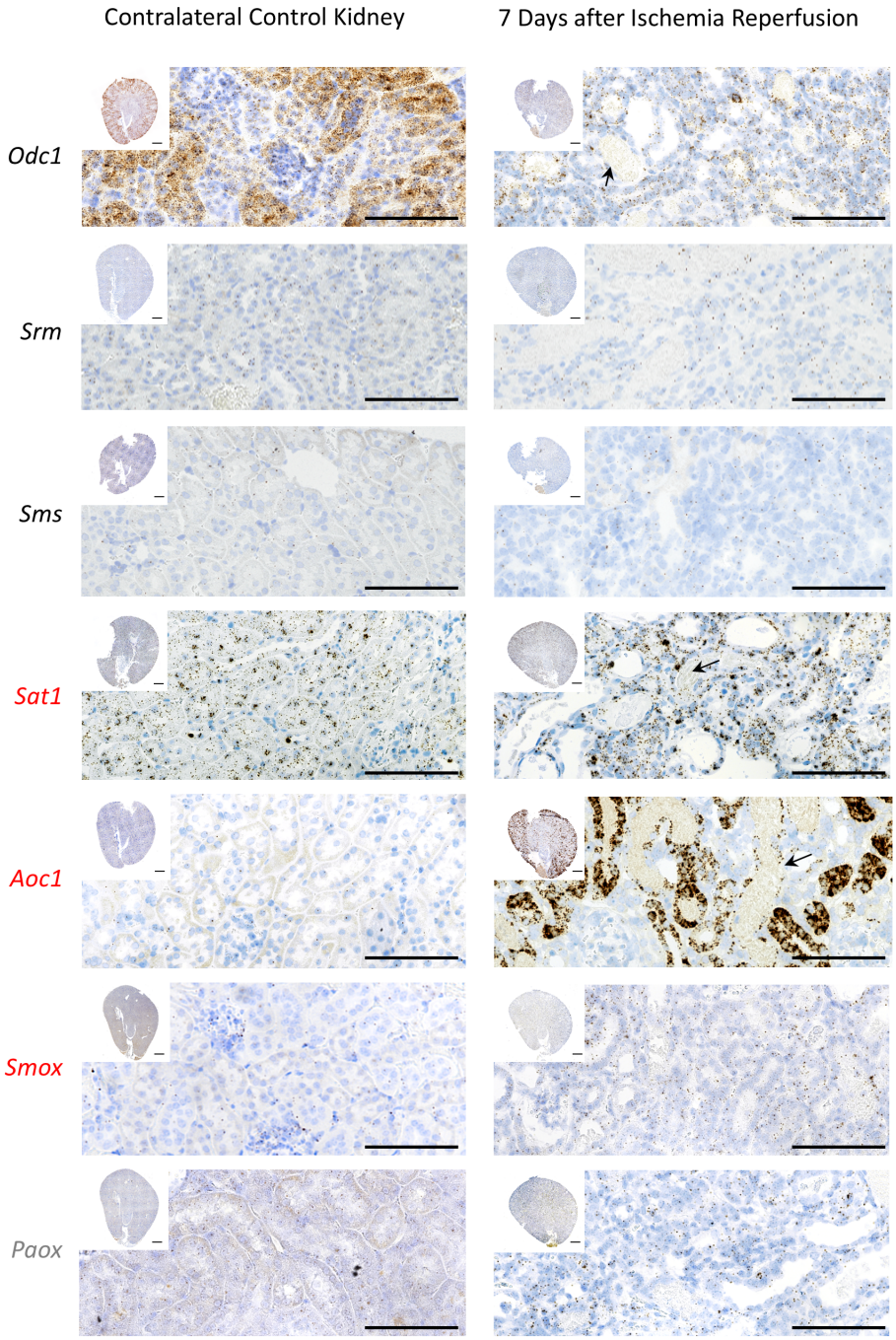

Figure 7: Visualization of transcripts of polyamine regulating enzymes by RNA *in situ* hybridization in kidneys seven days after ischemia reperfusion injury and their contralateral control kidneys.

Transcripts of enzymes involved in polyamine homeostasis were visualized by RNAScope chromogen *in situ* hybridization in kidneys seven days after ischemia reperfusion injury. The contralateral control kidney served as control. The high magnifications were obtained from the renal cortex. Scale bar equals 100 µm. An overview of scanned kidney sections is displayed in the upper left corner of each panel. Scale bar equals 1 mm. Arrows indicate atrophic tubules.

While the contralateral control kidneys appear normal, typical signs of acute kidney injury are seen seven days after IRI. These hallmarks include tubular atrophy with flattened epithelia and frequent intraluminal casts (see arrows in figure 7). Consistent with the RT-qPCR data (figure 3), *Odc1* and *Aoc1* show the most prominent changes. Within the contralateral control kidney, *Odc1* is expressed predominantly in tubules of the renal cortex. After IRI, the expression is strongly reduced and only a few cortical tubules retain *Odc1* transcripts. *Aoc1* mRNA is barely detected by RNAScope in intact kidneys, but clearly present in the renal cortex and the outer medullary stripe after kidney injury. *Aoc1* expression is limited to the epithelium of certain tubules. In accordance with the correlation shown in figure 5, all other genes show an ubiquitous downregulation over the whole kidney.

3.4 *Aoc1* expression peaks seven days after ischemia reperfusion injury in regenerating proximal tubules

Enhanced expression of the putrescine-degrading enzyme *Aoc1* is a striking feature after kidney injury. To gain additional insights into the possible role of *Aoc1* induction, the spatiotemporal expression changes were further assessed in kidneys after IRI.

3.4.1 Cortical *Aoc1* expression peaks seven days after ischemia reperfusion injury

The RNAScope *in situ* hybridizations at different time points and in different regions of the kidney (figure 8) demonstrate that *Aoc1* expression is visible 24 hours after IRI in some cortical and outer medullary tubules. Weaker hybridization signals are detected in tubules in the inner medulla (figure 8a). Tubular *Aoc1* expression peaks seven days after IRI. After 21 days, *Aoc1* transcripts are detected in cortical tubules as well as in some atrophic tubules with flattened epithelia in the outer medulla (arrows in figure 8a). At this time point, expression in the inner medulla decreases to similarly low levels as in the contralateral control kidney.

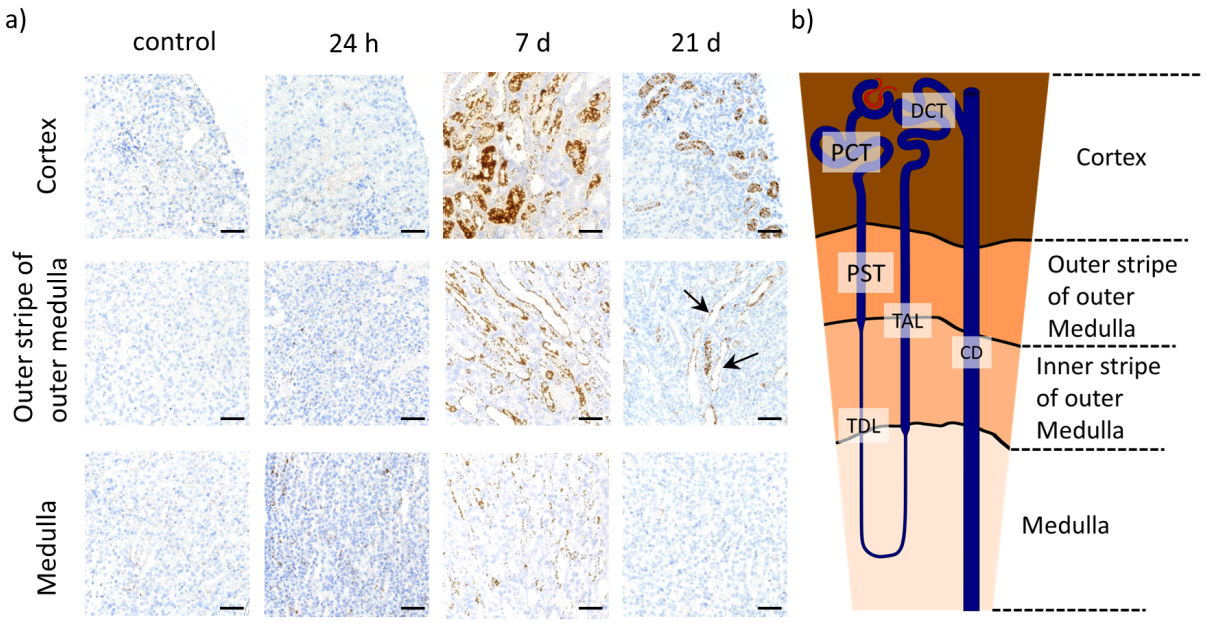

Figure 8: *Aoc1* expression in the tubular system varies over the total reperfusion period.
a) Transcripts of *Aoc1* were visualized using the chromogen RNAScope in situ hybridization technique. Kidneys from mice underwent ischemia reperfusion injury with reperfusion times of 24 hours, 7 and 21days. The contralateral control kidney 21 days after reperfusion served as control. Scale bar equals 50 µm. Arrows indicate atrophic tubules. **b)** Schematic representing the different renal zones in comparison to the nephrons segments. PCT: proximal convoluted tubule, PST: proximal straight tubule, TDL: thin descending limb, TAL: thick ascending limb, DCT: distal convoluted tubule, CD: collecting duct.

3.4.2 AOC1 protein and transcripts are co-localized in cortical tubular epithelia of injured kidney

Immunohistochemistry and immunoblotting were used to investigate whether AOC1 protein can be detected in injured kidneys (figure 9a-c). The contralateral control kidney (figure 9b) did not exhibit any tubular AOC1 protein, whereas seven days after IRI (figure 9a) a strong staining of the tubular epithelium in the cortex was visible. The overall increase in renal AOC1 is still visible 21 days post IRI as shown in figure 9c. Furthermore, a double *Aoc1*-AOC1 dual *in situ* hybridization/ immunohistochemistry approach demonstrated that the localization of *Aoc1* mRNA and AOC1 protein is congruent (figure 9d").

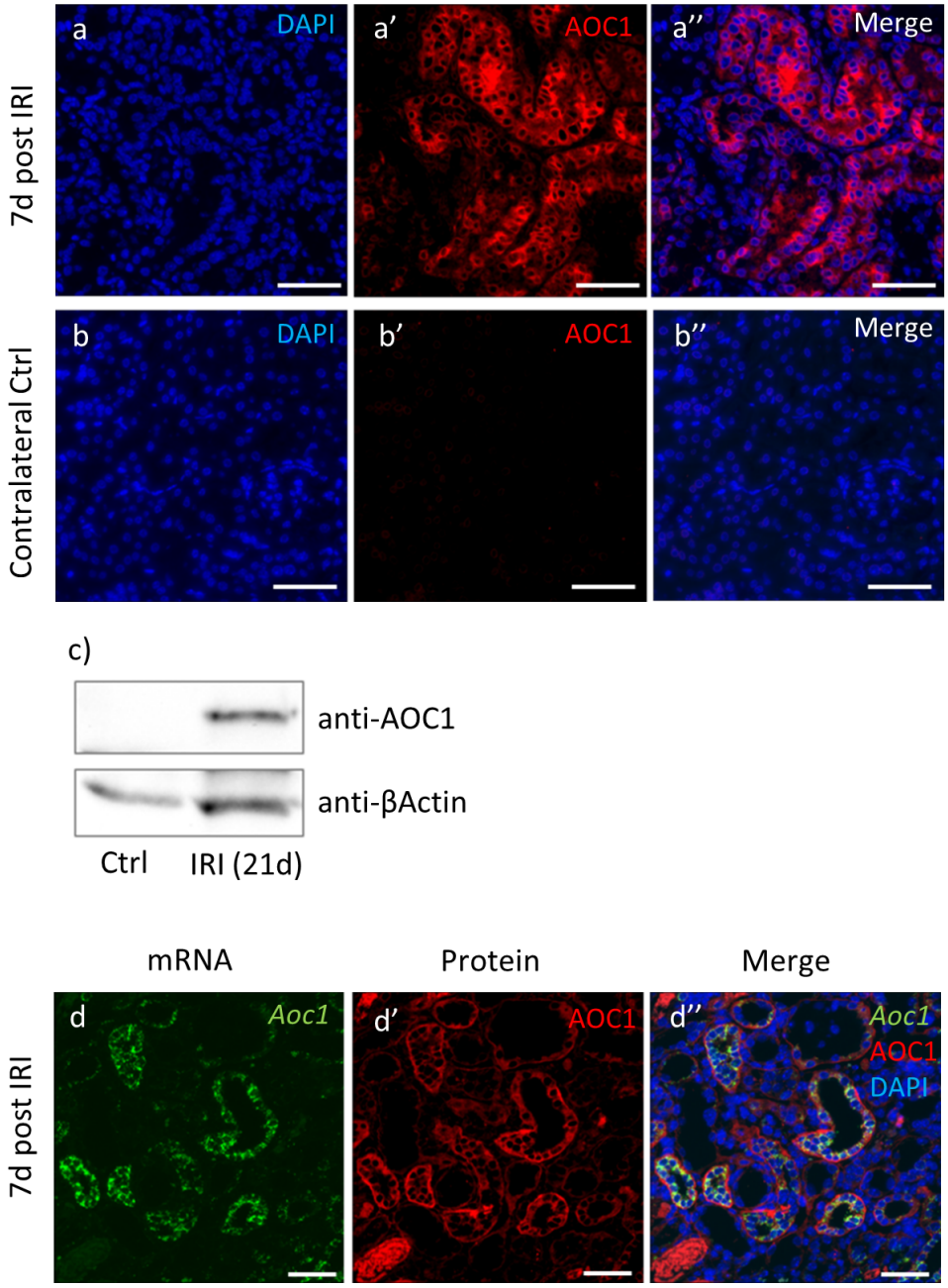

Figure 9: *Aoc1* mRNA and protein are co-localized in tubular epithelium of injured kidney.
a) AOC1 immunofluorescent staining of kidneys seven days after ischemia and **b)** their contralateral control. **c)** Immunoblotting of the contralateral control kidney (Ctrl) and 21 days after 25 min renal ischemia (IRI). Antibodies against AOC1 and βActin were used. **d)** Combined fluorescent RNAScope *in situ* hybridization using a probe directed against *Aoc1* mRNA (d) and immunofluorescence using an AOC1 antibody (d') in kidney seven days after ischemia reperfusion. Cell nuclei were visualized with DAPI (blue). Scale bar equals 50 µm. Adapted from Sieckmann *et al.* [161].

3.4.3 *Aoc1* expression is restricted to the proximal tubules and the descending limb of the loop of Henle

The nephrons' complex architecture with its specialized compartments makes it necessary to characterize the areas of *Aoc1* expression further. Figure 10a displays a schematic nephron showing expression of the used marker genes along the different nephron segments. LDL receptor related protein 2 (*Lrp2*) and aquaporin 1 (*Aqp1*) mark the proximal tubule. *Lrp2* shows strong expression in the proximal convoluted part, whereas *Aqp1* is most strongly expressed in the thick descending and the thin descending limb of the loop of Henle. Uromodulin (*Umod*) is a marker for the thick ascending limb of Henle's loop, while the sodium chloride cotransporter (*Slc12a3*) is expressed in the distal convoluted tubule. Aquaporin 2 (*Aqp2*) was used for staining of the collecting duct. To localize *Aoc1* transcripts along the nephron, a duplex RNAScope *in situ* hybridization approach was used. Seven days after IRI, *Aoc1* is co-expressed with *Lrp2* in the proximal tubule and with *Aqp1* identifying the thick and thin descending limb of Henle's loop as additional sites of *Aoc1* expression (figure 10b,c). After Injury, tubular cells start to dedifferentiate and alter their gene expression [32]. Therefore, not every single cell of an injured tubule is positive for *Aqp1* or *Lrp2*. Presence of stained cells in a tubular segment is however a clear indicator that these tubules are, or have been before the injury, the designated segment. For *Umod*, *Slc12a3* and *Aqp2* (figure 10d-f), there is no coexpression detectable.

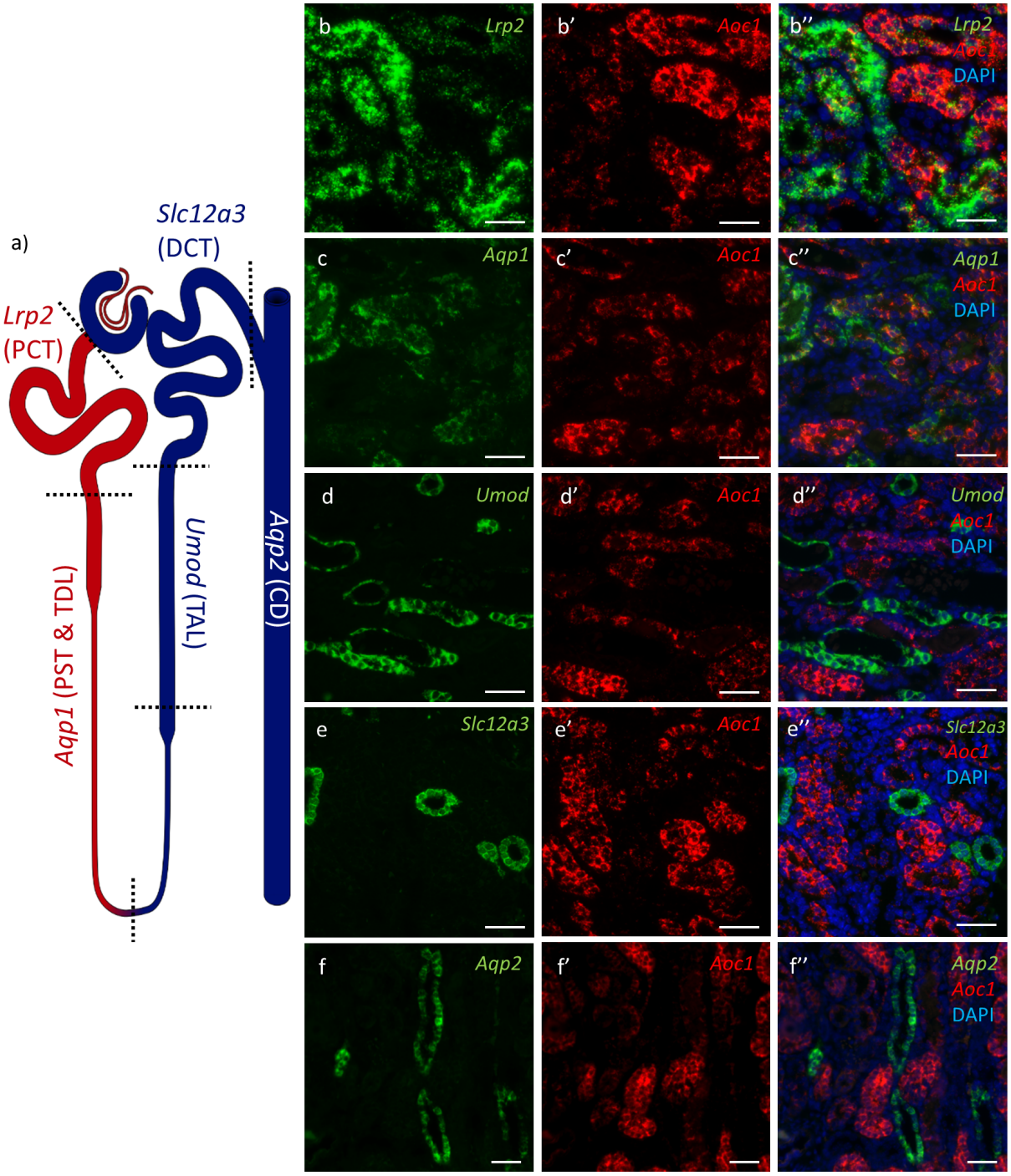

Figure 10: Coexpression with markers for the different nephron segments reveals *Aoc1* in the proximal tubule and descending limb of the loop of Henle.

a) Illustration showing expression of markers for the different nephron segments. **b-f)** Fluorescent duplex RNAScope in situ hybridization of *Aoc1* and several marker transcripts of the tubular system on kidneys seven days after IRI. *Lrp2* (b) is expressed in the proximal convoluted tubule (PCT), *Aqp1* (c) in the proximal straight tubule (PST) and the thin descending limb (TDL), *Umod* (d) in the thick ascending limb (TAL) and distal convoluted tubule (DCT), *Slc12a3* (e) within the distal convoluted tubule (DCT) and *Aqp2* (f) in the collecting duct (CD). Scale bar equals 50 µm. Previously published in Sieckmann *et al.* [161]

3.4.4 AOC1 is expressed in regenerating tubules

Damaged tubules can regenerate and replace injured or necrotic cells. After IRI, *Aoc1* is expressed in some, but not all proximal tubules (figure 10). To evaluate if expression of AOC1 is related to tubular injury and/ or regeneration, duplex staining for AOC1 and markers for proliferation, regeneration and cell death was performed in kidneys seven days after ischemia (figure 11).

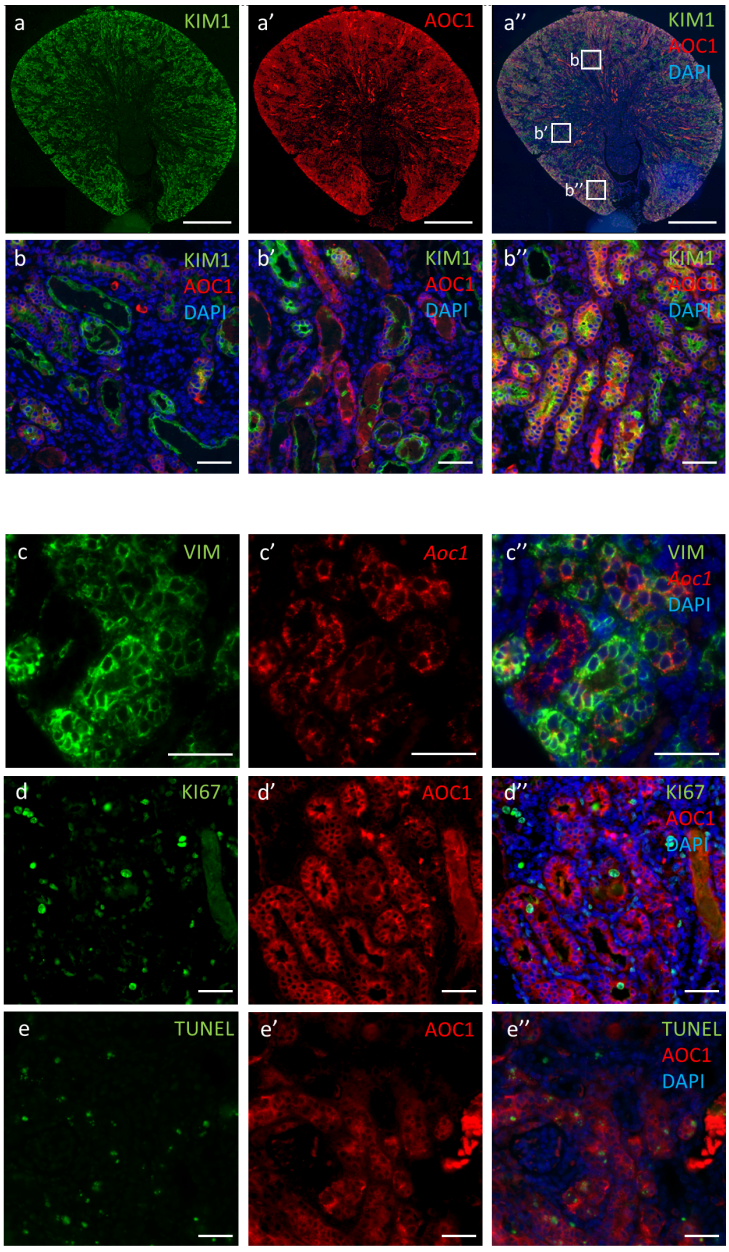

Figure 11: AOC1 is co-expressed with KIM1, a marker for regenerating tubules.
a,b) Immunofluorescent staining using antibodies against AOC1 and KIM1. Scale bars equal 1 mm (for a, a', a") and 50 µm (for b,b',b"). **c)** Immunofluorescent staining of mesenchymal marker vimentin (VIM) combined with RNAScope *in situ* hybridization of *Aoc1*. **d)** Immunofluorescent staining of AOC1 and cell cycle marker KI67. **e)** Immunofluorescent staining of AOC1 in combination with TUNEL assay to detect apoptosis and necrosis. Scale bars equal 50 µm. Previously published in Sieckmann *et al.* [161]

Kidney injury molecule 1 (KIM1) (figure 11a) and intermediate filament Vimentin (VIM) (figure 11c) were used as markers to visualize regenerating and scarring tubules. Proliferating cells were detected by KI67 immunostaining (figure 11d). TUNEL assay was performed for labeling of necrotic and apoptotic cells (figure 11e). Coexpression with KIM1 (figure 11a) localizes AOC1 in regenerating tubules after injury. AOC1 and KIM1 do not exhibit a complete coexpression over the whole kidney (figure 11, upper panels). In some regions, KIM1 expression dominates, whereas AOC1 is less abundant (figure 11b). As displayed in figure 11b', however, some tubules show the opposite staining pattern with higher AOC1 levels and less KIM1. The vast majority of tubules express both, KIM1 and AOC1 (figure11b"). Counting of all tubules in one kidney section (n = 1491) showed that a total of 1320 tubules are positive for both, AOC1 and KIM1 (88.5%). Ninety-five tubules (6.5%) showed only AOC1 staining and 76 (5%) only KIM1 labeling. The mesenchymal marker VIM, which is expressed in regenerating but scarring tubules, showed partial colocalization with AOC1 (figure 11c). Notably, this colocalization is not as strong as for KIM1. To investigate whether AOC1 expression correlates with proliferation or cell death, co-staining with proliferation marker KI67 and TUNEL assay were performed. Proliferating cells are detected in the injured kidneys by KI67 staining, but little overlap with AOC1 is seen (figure 11d). Combined AOC1 staining with TUNEL assay (figure 11e) shows only a partial overlap.

3.5 Cell stress is regulating transcription within the polyamine system

To assess which signals lead to the observed expression changes of polyamine metabolizing enzymes after kidney injury (figure 3 and 4), a screening approach for different stress stimuli was applied. *Ex-vivo* cultured embryonic mouse kidneys were used as a model (figure 12a). One kidney of each embryo served as untreated control, whereas the other one was exposed to different stress protocols.

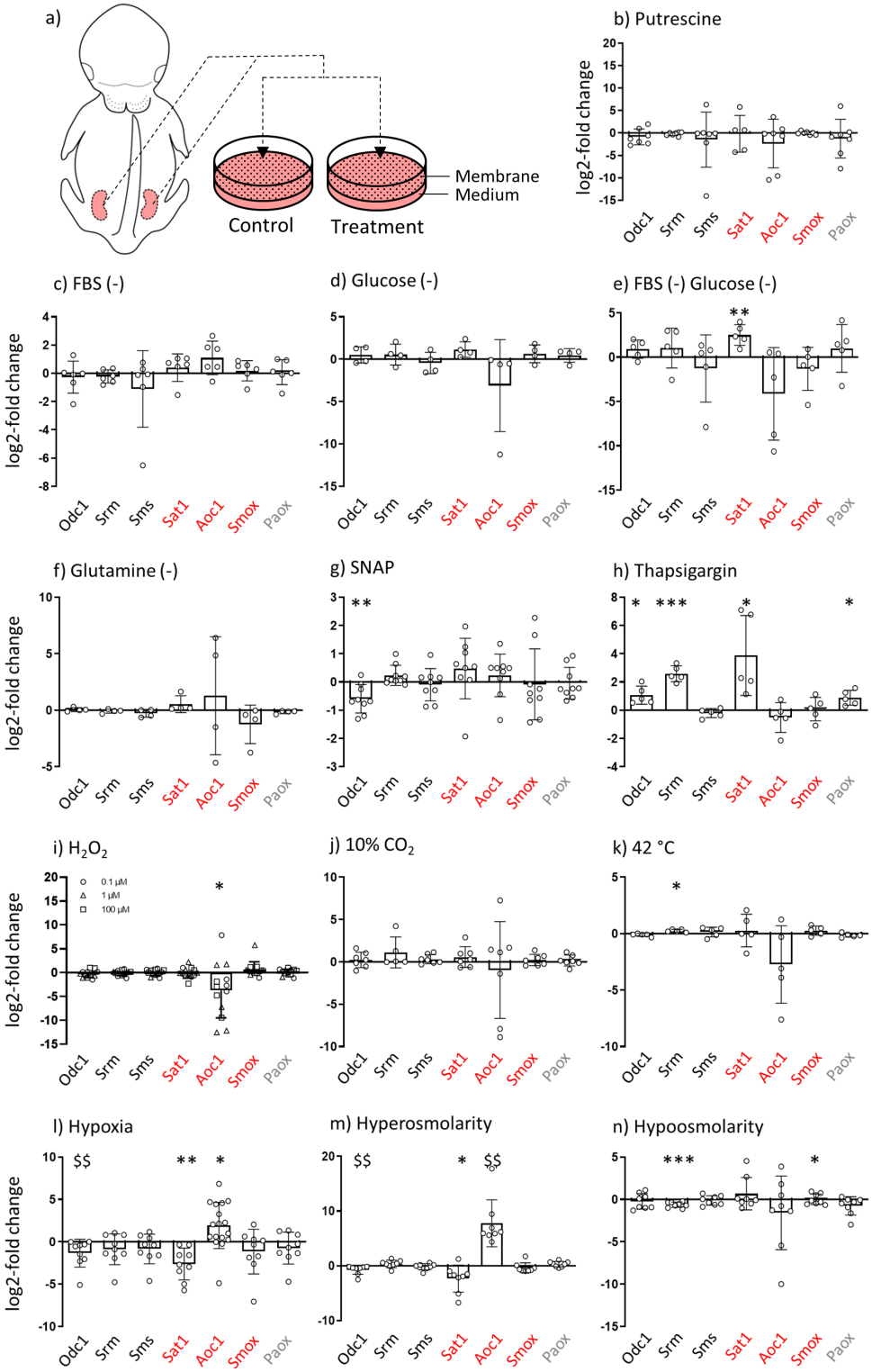

Figure 12: Screening for stress stimuli in embryonic kidney explant culture identifies hypoxia and hyperosmolarity as activators of *Aoc1* expression.

a) Schematic overview of the mouse embryonic kidney explant culture method. Different stimuli were applied to induce stress: **b)** addition of 100 µM putrescine, **c)** cultivation in medium without FBS, **d)** without glucose, **e)** with neither FBS nor glucose, **f)** without glutamine, **g)** with addition of the NO-donor S-nitroso-N-acetylpenicillamine (SNAP; 0.1 mM), **h)** with addition of the sarco/endoplasmic reticulum Ca^{2+}-ATPase inhibitor thapsigargin (2 µM) to induce ER-Stress, **i)** with addition of 0.1 µM (dots), 1 µM

(squares) or 100 µM (triangles) H_2O_2, **j)** acidification of medium by cultivation in a 10% CO_2 atmosphere, **k)** cultivation at 42°C, **l)** cultivation under hypoxic conditions (1% O_2), **m)** with addition of 0.2 M sucrose, **n)** dilution of the medium with 25% H_2O. Transcripts were measure by RT-qPCR and normalized to the housekeeping gene *Actb*. Single values are given as log2-fold change relative to the untreated control kidney. Significances were determined by paired t-test or Wilcoxon matched pairs-signed rank test after testing for normal distribution using Shapiro-Wilk test. Significances for normal distributed data is indicated using asterisks (*p<0.05; **p<0.01; ***p<0.001) and for not normal distributed data by dollar signs ($^{\$}$p<0.05; $^{\$\$}$p<0.01). Adapted from Sieckmann *et al.* [161].

The different stress stimuli shown in figure 12b-n were selected to mimic conditions related to kidney injury. As AOC1 and ODC1 are responsible for putrescine homeostasis, it was tested if elevated putrescine levels may account for the observed expression changes after kidney injury. As shown in figure 12b, addition of 100 µM putrescine does not lead to a change in expression genes involved in polyamine homeostasis. Energy depletion was simulated by cultivation without FBS (figure 12c), without glucose (figure 12d), with neither FBS nor glucose (figure 12e) or without glutamine (figure 12f). None of these protocols caused significant changes in mRNA levels of polyamine regulating enzymes as seen in the different kidney injury models (figure 3). The accumulation of noxious substances was simulated by addition of the NO-donor SNAP (100 µM) (figure 12g) and ER stress by thapsigargin (2 µM) (figure12h), by addition of H_2O_2 (0.1 µM, 1 µM, 100 µM) (figure 12i) and by cultivation under acidic conditions (10% CO_2) (figure 12j). Interestingly, addition of H_2O_2 leads to a 12.9 fold decrease of *Aoc1* transcripts. This is the only treatment resulting in a significant reduction of *Aoc1* mRNA levels. Heat stress (42°C) was used to mimic stimulation of the immune response and deployment of heat shock proteins after kidney injury (figure 12k). Both, accumulation of waste products and heat stress did not alter *Aoc1* and *Odc1* expression. One of the main driving forces behind ischemia reperfusion injury is hypoxia. Here, hypoxia was induced by cultivation under 1% O_2 leading to a decrease of *Odc1* and *Sat1* transcripts by 2.5 and 6.1 fold, respectively (figure 12l). *Aoc1* mRNA levels increase by 3.1 fold in 1% O_2. Hyperosmolarity by addition of 0.2 M sucrose to the culture medium also reduces *Odc1* and *Sat1* transcripts while increasing *Aoc1* mRNA levels (figure 12m). Here, *Odc1* and *Sat1* are downregulated by 1.6 and 5 fold, respectively, and *Aoc1* mRNA levels drastically increase by 219.7 fold. *Aoc1* transcript levels are not significantly affected in hypoosmolarity established by addition of 25% H_2O to the medium (figure 12n).

3.6 Hyperosmolarity is a general stimulus of *Aoc1* expression *in vitro*

Aoc1 showed the strongest increase in different kidney injury models (figure 3) with hypoxia and hyperosmolarity being potential inducers (figure 12l and 12m). Stimuli found in the embryonic kidney explant culture must not necessarily be reproducible in other models. To compensate for model-specific effects, the influence of hypersomolarity and hypoxia on *Aoc1* expression was tested in more cellular models (figure 13).

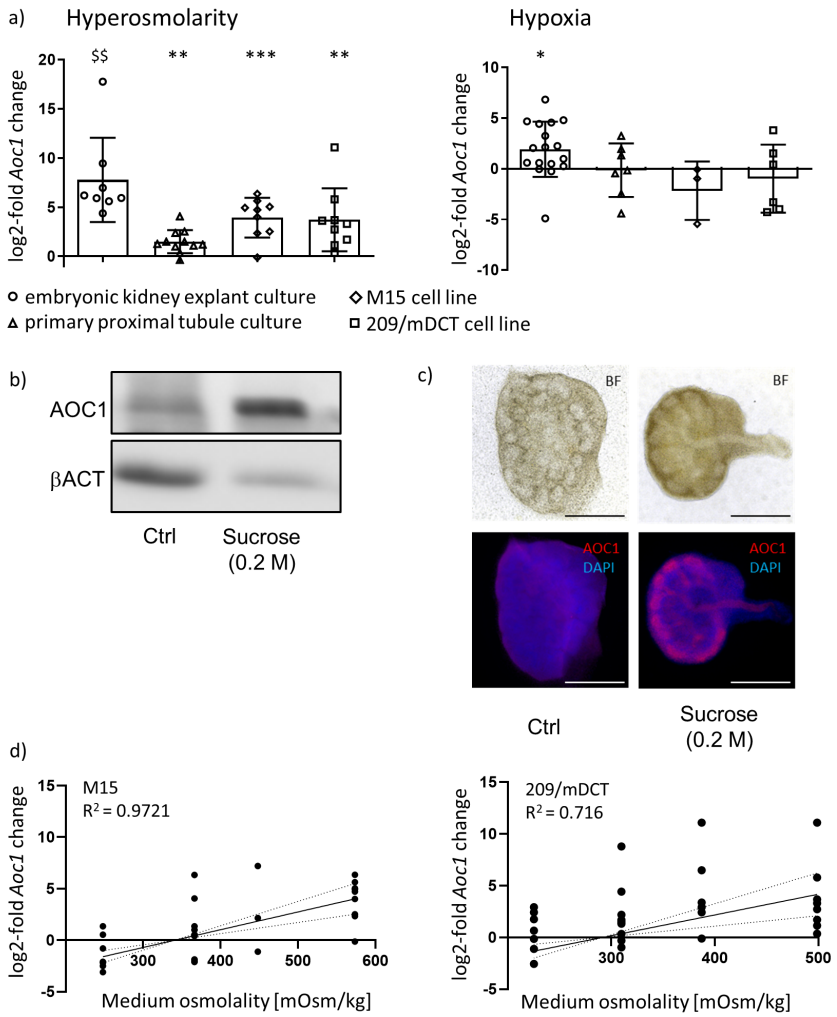

Figure 13: Hyperosmolarity is a stimulus of *Aoc1* expression *in vitro*.
a) *Aoc1* expression in hypoxia (1% O_2) and hyperosmolarity (0.2 M sucrose) in embryonic kidney explants, primary proximal tubules and the cell lines M15 and 209/MDCT. For better comparison, expression data of embryonic kidney explant culture are taken from figure 12l and 12m. Transcript levels are shown as log2-fold changes of *Aoc1* relative to *Actb* and the respective control conditions. Significances were determined by paired t-test or Wilcoxon matched pairs-signed rank test after testing for normal distribution using Shapiro-Wilk test. Significances for normal distributed data is indicated using asterisks (*p<0.05; **p<0.01; ***p<0.001) and for not normal distributed data by dollar signs ($^{\$}$p<0.05; $^{\$\$}$p<0.01). Embryonic kidney explants (12.5 d.p.c.) were cultured in medium containing 0.2 M sucrose and their controls were used for immunoblotting (b) and immunohistochemistry (c). **b)** For immunoblotting, antibodies directed against AOC1 and βACT were used. **c)** Immunohistochemistry of embryonic kidney explants (12.5 d.p.c.) was performed with an antibody against AOC1 and cell nuclei counterstained with DAPI. Respective transmitted light (BF) images are shown. Scale bars equal 500 µm. **d)** Changes of *Aoc1* expression in M15 and 209/MDCT cells cultured in medium with increasing osmolarity. Cells were treated with addition of either 25% H_2O to the medium (hypoosmolarity), 0.02 M sucrose, 0.1 M sucrose or 0.2 M sucrose. Correlation was calculated given Spearmans R^2. Linear regression is shown as solid line. Dotted lines indicate the framing 95% confidence interval. Parts a), b) and c) adapted from Sieckmann *et al.* [161].

Hypoxia as well as hyperosmolarity were evaluated further as potential stimuli of *Aoc1* induction using primary proximal tubule culture, the mesonephric M15 cell line and the distal convoluted tubule derived cell line 209/MDCT. As displayed in figure 13a, hypoxia stimulates *Aoc1* expression only in embryonic kidney explant cultures but not in the other models. On the contrary, hyperosmotic stress by addition of 0.2 M sucrose increases *Aoc1* mRNA levels in all models. In the primary proximal tubule culture, *Aoc1* is upregulated by 2.8 fold, in M15 and 209/MDCT cell lines *Aoc1* mRNA increases by 15.3 and 13 fold respectively. Hyperosmotic stress was confirmed as a stimulus of AOC1 expression by immunoblotting (figure 13b) and immunofluorescent whole-mount staining (figure 13c) Cultivation of embryonic kidney explant cultures in medium with 0.2 M sucrose leads to a strong increase in AOC1 protein levels in the tubules (figure 13b,c). Under isosmotic conditions, AOC1 is not detectable in embryonic kidney explants.

To test whether the changes of *Aoc1* expression under hyperosmotic conditions are dose-dependent, M15 and 209/MDCT cells were cultivated in increasing osmolarities (figure 13d). Here, hypoosmolarity by dilution of the medium with 25% H_2O and hyperosmolarity by addition of 0.02 M sucrose, 0.1 M sucrose or 0.2 M sucrose was used. In both cell lines, *Aoc1* expression correlates positively with increasing osmolarity.

3.7 *Aoc1* expression is transcriptionally activated by binding of NFAT5 to a *cis*-acting element

The increase in *Aoc1* mRNA expression in hyperosmotic conditions can result from promoter activation and/ or from stabilization of the mRNA. The *Aoc1* gene contains four coding isoforms. These isoforms are distinguishable by their unique 5'UTRs. Only one isoform contains an additional coding exon. To evaluate transcriptional activation, the putative promoter regions of the different *Aoc1* isoforms (ca. -2000 bp to transcription start site (TSS)) were cloned and ligated into the pGL3b reporter vector upstream of the firefly luciferase gene. A schematic drawing of different *Aoc1* isoforms and their respective promoter elements is shown in figure 14a.

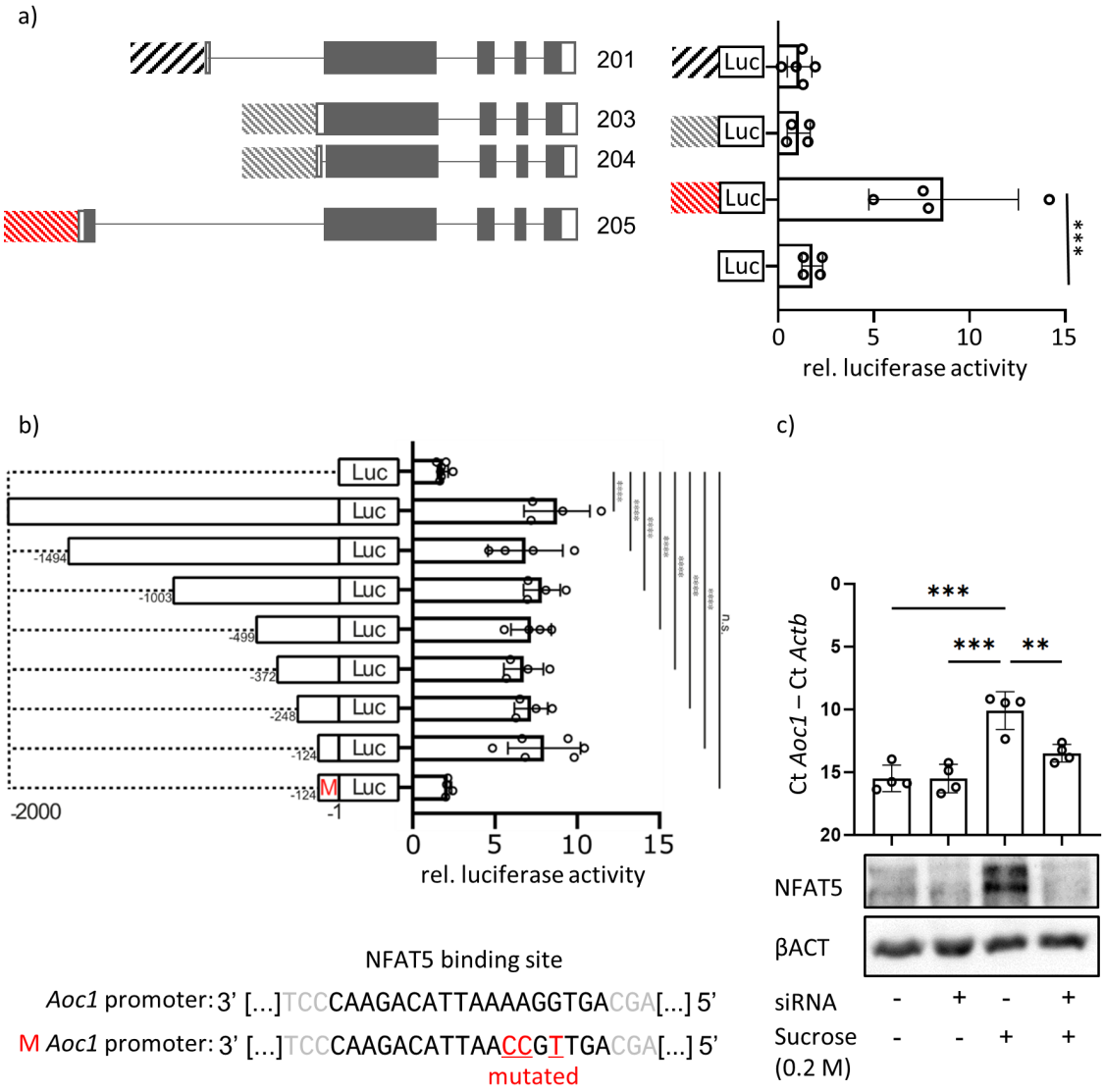

Figure 14: Expression of *Aoc1* is transcriptionally activated by NFAT5.

a) Illustration of the variable 5' region of the murine *Aoc1* gene and transcriptional activation of *Aoc1* isoforms. Numbering of *Aoc1* isoforms according to Ensembl gene database (ENSMUSG00000029811; Chromosome 6: 48,849,830-48,886,122 forward strand, GRCm39:CM000999.3). Dashed boxes indicate putative promoter regions, filled boxes coding exons and hollow boxes non-coding mRNA. Transcriptional activation was assessed by luciferase promoter assay in M15 cells transfected with the pGL3b plasmid (inserted with the different putative promoter regions) and subsequently treated with 0.2 M sucrose. Values are presented as fold changes in firefly luciferase activity, relative to renilla luciferase activity after hyperosmotic induction (0.2 M sucrose) compared to their isosmotic control. Experimental procedures conducted by N. Ögel and described in detail in Sieckmann *et al.* [161]. **b)** Promoter activity was measured using luciferase assay in M15 cells transfected with pGL3b plasmid containing 2 kb of the *Aoc1*-205 promoter region 5' of the firefly luciferase coding sequence. To characterize the promoter upstream of *Aoc1*-205 in depth, the initial sequence was shortened at the 5' end, creating fragments of the sizes 1494 bp, 1003 bp, 499 bp, 372 bp, 248 bp and 124 bp 5' upstream of the transcriptional start site. Values are shown as fold change in firefly luciferase activity, relative to co-transfected renilla luciferase activity after hyperosmotic (0.2 M sucrose) induction compared to their isosmotic control. Promoter labeled with "M" contains a mutated NFAT5 binding motif. The NFAT5 consensus binding sequence [166] within the 124 bp promoter fragment is displayed. With three mutations marked in red (A>C, A>C and G>T), a mutated NFAT5 binding site was created within

the 124 bp fragment. **c)** *Aoc1* expression changes after NFAT5 knockdown in M15 cells. For knockdown of NFAT5, M15 cells were treated with either siRNA directed against *Nfat5* or unspecific siRNA. Subsequently, cells were cultivated in isosmotic or hyperosmotic (0.2 M sucrose) conditions to stimulate NFAT5 expression. To confirm NFAT5 expression and knockdown, immunoblotting was performed with an antibody against NFAT5. Detection of βACT served as loading control. Expression changes of *Aoc1* mRNA after induction with 0.2 M sucrose were determined by RT-qPCR and are displayed as Ct values of *Aoc1* minus Ct of *Actb*. Significances were calculated using one-way ANOVA (a) or two-way ANOVA (c) after testing for normal distribution using Shapiro-Wilk test (*p<0.05; **p<0.01; ***p<0.001; ****p<0.0001). Parts a) and c) adapted from Sieckmann *et al.* [161].

Cultivation of M15 cells in hyperosmotic conditions resulted in an 8-fold activation of the putative *Aoc1*-205 promoter (figure 14a). The promoters of the *Aoc1* variants 201 and 202/3 were not activated by hyperosmolarity. To identify the specific hyperosmolarity response element in the promoter region of *Aoc1*-205, shorter promoter fragments were cloned and tested in the luciferase reporter gene assay. All shorter fragments showed activation under hyperosmotic conditions as well (figure 14b) with 6.7 to 8.7 fold changes of luciferase activity after induction with 0.2 M sucrose. In comparison, the empty pGL3b vector exhibits an activation of 1.8 fold. A potential binding site for the hypertonicity-induced transcription factor NFAT5 [166] was detected on the reverse strand of the 124 bp fragment (figure 14b). Mutation of the predicted NFAT5 binding site resulted in loss of activation of the 124 bp *Aoc1*-205 promoter by hyperosmolarity (figure 14b). siRNA mediated knockdown of NFAT5 was performed in M15 cells to confirm transcriptional activation of *Aoc1* by NFAT5 (figure 14c). Strong induction of NFAT5 in cells grown under hyperosmotic conditions is revealed by immunoblotting. Transfection with *Nfat5* siRNA effectively reduces NFAT5 to basal levels. Notably, *Aoc1* transcripts correlate with NFAT5 levels in M15 cells. *Aoc1* mRNA increases by 5.4 cycles (42.22 fold) in the presence of 0.2 M sucrose, while simultaneous silencing of *Nfat5* significantly reduces this effect to 2 cycles (4 fold).

3.8 *Aoc1* mRNA is stabilized by hyperosmolarity

In addition to transcriptional activation, mRNA stabilization may contribute to increased *Aoc1* mRNA levels in hyperosmotic conditions. This was assessed by growing M15 cells in the presence of 0.2 M sucrose to induce *Aoc1* expression. After induction, the cells were transferred into either isosmotic or hyperosmotic medium and *de novo* RNA synthesis was blocked by addition of the RNA polymerase inhibitor actinomycin D (5 µg/µL).

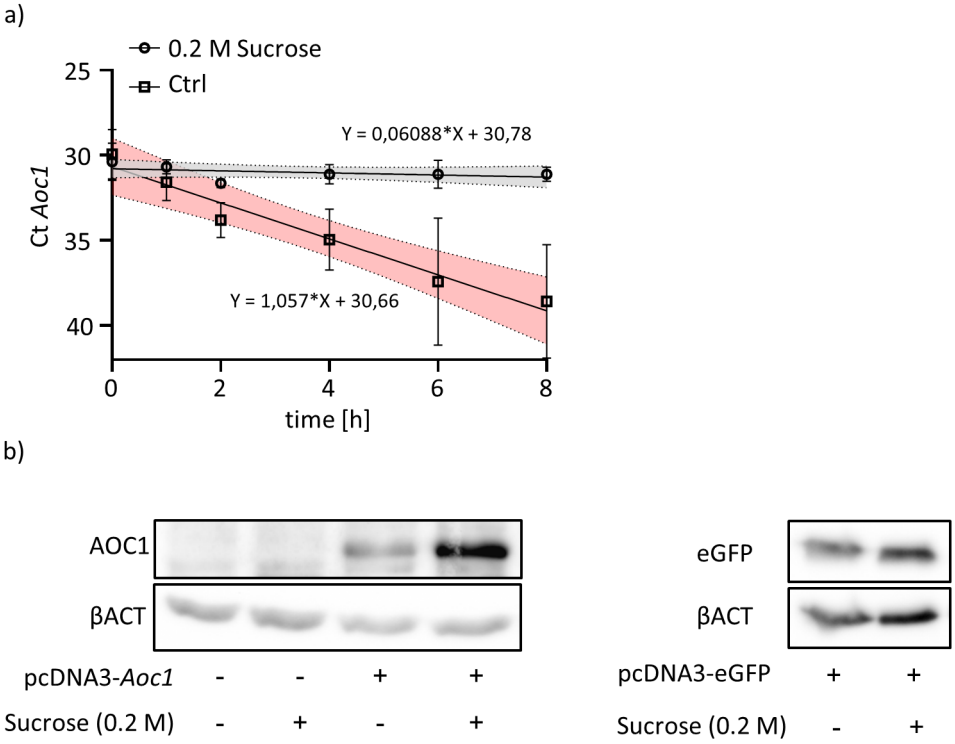

Figure 15: Expression of *Aoc1* mRNA is stabilized under hyperosmotic conditions.
a) Kinetics of *Aoc1* mRNA under iso- and hyperosmotic (0.2 M sucrose) conditions during inhibition of *de novo* RNA synthesis with actinomycin D. Data are shown as Ct values with an increase by one cycle corresponding to a 50% reduction of mRNA levels. Solid lines indicate the best fitting linear regression including its equation. Dashed lines and colored area frame the 95% confidence interval. Adapted from Sieckmann *et al.* [161]. **b)** Immunoblot showing increased AOC1 protein under hyperosmotic conditions. Cells were transfected either with the empty pcDNA3 vector or pcDNA3 containing the *Aoc1* coding sequence and then cultivated under isosmotic or hyperosmotic (0.2 M Sucrose) conditions. As a control for possible induction of the pcDNA3 vector, cells were transfected with pcDNA3-eGFP (provided by Holger Scholz) and cultivated in isoosmotic or hyperosmotic (0.2 M sucrose) conditions. Immunoblotting was performed using antibodies directed against βACT and eGFP.

Under isosmotic conditions, *Aoc1* mRNA is rapidly degraded with a half-life of approximately one hour (figure 15a). Addition of sucrose to the culture medium increases *Aoc1* mRNA stability drastically beyond the measured timeframe. If extrapolated, *Aoc1* mRNA reaches a half-life of approximately 16 hours under hyperosmotic conditions, which corresponds to a 16-fold increase in stability. AOC1 protein is not detectable in cells transfected with the empty vector, even under hyperosmotic conditions. To evaluate if *Aoc1* mRNA stabilization results in elevated protein levels, M15 cells were either transfected with the empty pcDNA3 vector or with a pcDNA3 plasmid containing the *Aoc1* coding sequence (figure 15b). AOC1 is clearly present in cells transfected with the *Aoc1* expression construct, and further increases upon incubation in hyperosmotic medium (figure 15b). To verify that this is an *Aoc1*-specific effect, the pcDNA3 vector was transfected into M15 cells but this time with an eGFP ORF instead of *Aoc1*. As visible, hyperosmolarity does not change detectable eGFP levels.

3.9 The AOC1-205 signal peptide influences the subcellular localization of AOC1 protein and increases its secretion.

Hyperosmotic stress stimulates *Aoc1* expression. However, hyperosmolarity does not increase AOC1 protein in M15 cells despite an approximately 16-fold increase in *Aoc1* mRNA (figure 15a). This raises the possibility that the *Aoc1*-205 isoform that is enhanced by hyperosmolarity (figure 14a) is rapidly released from the cells. As a secreted molecule, AOC1 contains an N-terminal signal peptide (figure 16a). The *Aoc1*-205 isoform has an additional coding exon upstream of the sequence coding for the signal peptide. The AOC1 signal peptide consists of two N-terminal amino acids, followed by a 17 amino acids long hydrophobic core region and an 8 amino acids sequence next to the cleavage site (signal peptide C-terminus). With the additional protein coding exon, the AOC1-205 protein gains 22 extra amino acids N-terminal to its signal peptide (figure 16a). In the Ensembl database, the *Aoc1*-205 variant is not annotated completely and stops abruptly in the second exon without a stop-codon (figure 16b). Using specific primers located at the TSS and the 3' end of the coding sequence, the integrity of the complete coding sequence of *Aoc1*-205 was demonstrated by amplification via PCR (figure 16b).

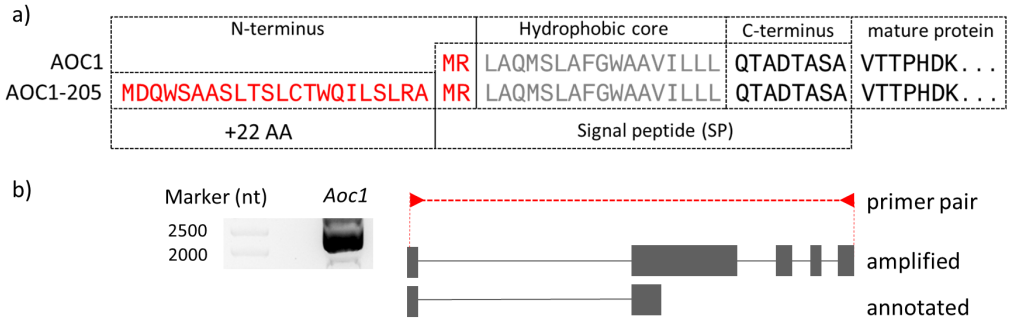

Figure 16: Description of AOC1 signal peptides and verification of the full length *Aoc1*-205 transcript.

a) Schematic drawing of the N-terminus of the AOC1 protein and the difference between AOC1 and of AOC1-205 (SP = signal peptide, AA = amino acids) isoforms. Annotation of functional regions according to SignalIP – 6.0 (https://services.healthtech.dtu.dk/service.php?SignalP-6.0). Adapted from Sieckmann *et al.* [161]. **b)** Annotated *Aoc1*-205 structure according to Ensembl database (Chr6: 48,849,830-48,886,122, GRCm39:CM000999.3) and the amplified regions using primers 5' ATGGATCAGTGGTCTGCTGC 3' and 5' TCACACAGGCTTGTAGGTCC 3' indicated by red arrowheads.

To assess the effect of the additional amino acids at the N-terminus of AOC1-205, the sequence corresponding to the AOC1 signal peptide with and without the 22 amino acids was cloned 5' in frame of the eGFP gene. eGFP without signal peptide has an ubiquitous cytoplasmic localization with a strong nuclear fluorescence (figure 17a). N-terminal addition of the AOC1 signal peptide, which is present in all AOC1 isoforms changes the intracellular distribution of eGFP (figure 17b). Here, the nuclear fluorescence is drastically weakened, the

cytoplasmic localization is slightly reduced and eGFP accumulates visibly in a perinuclear body (figure 17b'). With the N-terminal addition of the 22 amino acids present only in AOC1-205 to the signal peptide, eGFP shows less cytoplasmic localization (figure 17c). The additional 22 amino acids localize the eGFP fusion protein mostly perinuclear with no nuclear signal (figure 17c").

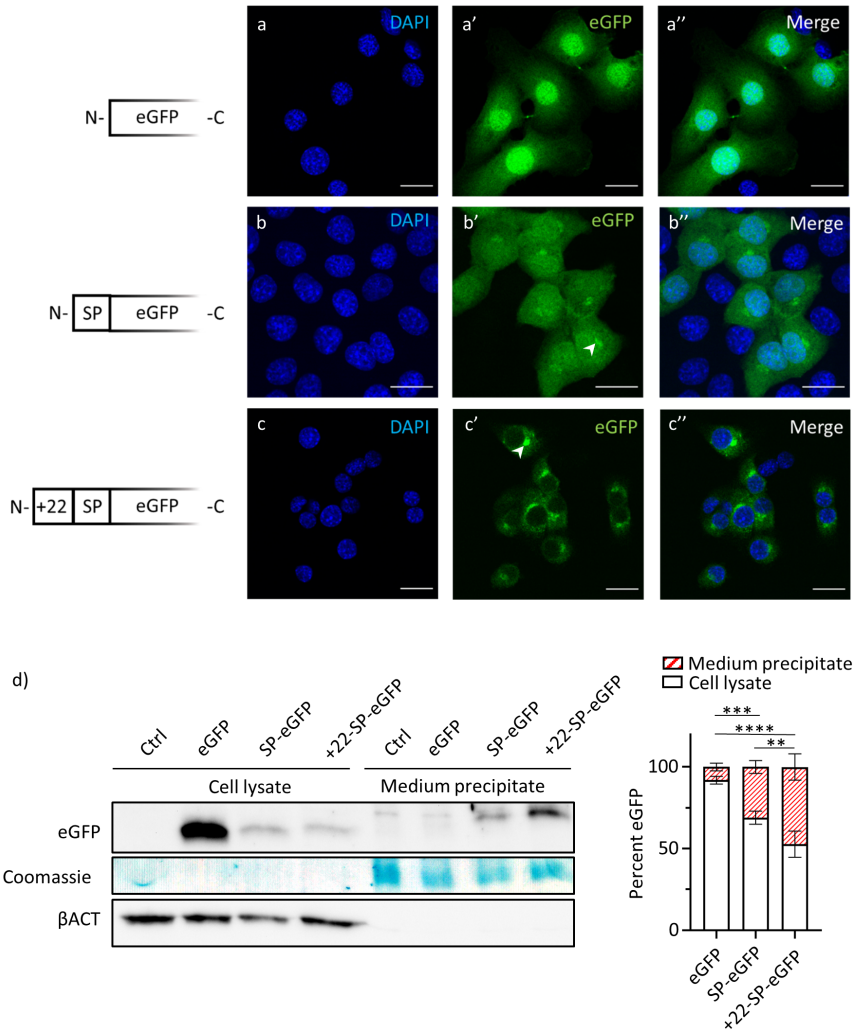

Figure 17: The additional 22 amino acids of AOC1-205 lead to increased secretion of the mature protein.

a-c) M15 cells transfected with eGFP-constructs with either no N-terminal addition (eGFP), N-terminal addition of AOC1 signal peptide (SP-eGFP) or addition of AOC1-205 N-terminal sequence (+22-SP-eGFP). Arrow heads point to perinuclear staining. Scale bars equal 20 µm. **d)** Immunoblotting of cell lysates and precipitated medium after 24 hours of cultivation of M15 cells transfected with eGFP-constructs with either no N-terminal addition (eGFP), N-terminal addition of AOC1 signal peptide (SP-eGFP) or addition of AOC1-205 N-terminal sequence (+22-SP-eGFP). Antibodies against eGFP and βACT were used. Coomassie staining of the membrane was performed as a loading control of the precipitated medium. Quantification of three experiments. Percentages were calculated by division of respective quantification by total quantifications from the supernatant and cell pellet. Significances were calculated using two-way ANOVA (*p<0.05; **p<0.01; ***p<0.001). Adapted from Sieckmann *et al.* [161].

The reduced cytoplasmic eGFP signal upon N-terminal inclusion of the 22 amino acids of AOC1-205 could be due to enhanced protein secretion. To test this hypothesis, the protein lysates of the transfected cells and the total protein precipitated from the culture medium were collected for immunoblotting (figure 17d). eGFP-transfected cells secrete only 8% of the eGFP into the medium as seen when comparing the amounts of eGFP in the cells with the medium of the transfected cells. Cells transfected with the SP-eGFP construct secrete 31% of the SP-eGFP fusion protein into the medium and cells transfected with the +22-SP-eGFP construct secrete 47%. The addition of the 22 amino acids of AOC1-205 leads therefore to increased secretion compared to the signal peptide alone.

3.10 *Aoc1* is required for normal proliferation of M15 cells

Various experimental approaches were taken to identify the biological processes targeted by *Aoc1* in response to tissue injury and during regeneration. One major challenge in regeneration of injured tissue is the replacement of dead cells, which requires proliferation of surviving cells. To gain insights into the possible role of *Aoc1* in cellular proliferation, *Aoc1* overexpression and *Aoc1* deletion by CRISPR/Cas9 were performed. Overexpression of *Aoc1* in mesonephric M15 cells does not stimulate cellular proliferation (figure 18a). Knockout of *Aoc1* does however reduces proliferation significantly. After three and four days of growth, the cells stop proliferating and start reaching a plateau at around 4.3 $*10^5$ cells per well.

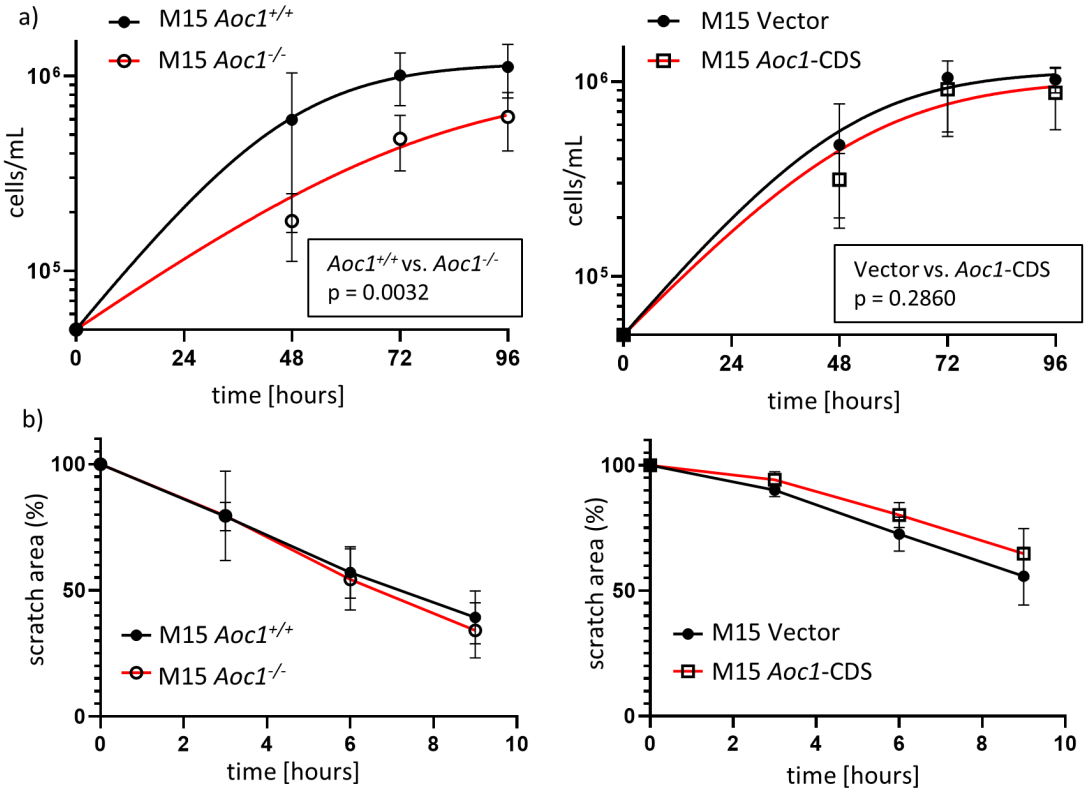

Figure 18: *Aoc1* overexpression alters cellular response to ER stress and autophagy.
a) Proliferation assay using M15 cells. Overexpression is designated as *Aoc1*-CDS, the vector control is pcDNA3. CRISPR/Cas9 mediated *Aoc1* knockout is designated as *Aoc1*$^{-/-}$, the vector control is pSpCas9(BB)-2A-GFP. Six experiments in total with two different clones each. **b)** Scratch assay using M15 cells. Total scratch area at start was set as 100%. Significances were calculated using the CGGC permutation test as described elsewhere [167].

Besides proliferation, cell migration is a prerequisite for wound healing. Here, migration was measured using a scratch assay. As shown in figure 18b, despite the reduced proliferation (figure 18a) *Aoc1* deletion does not lead to a decrease in migration. Furthermore, overexpression of *Aoc1* does not significantly change cell migration.

3.11 Phenotypic description of *Aoc1* knockout mice

To explore the role of *Aoc1* in renal injury, an ubiquitous *Aoc1* knockout mouse was established. The mice contain a genetic modification inserting a splice acceptor containing *lacZ* cassette within the *Aoc1* locus. The resulting AOC1 protein is therefore a fusion protein from *Aoc1*'s first exon and lacZ leading to a premature stop-codon (figure 19a).

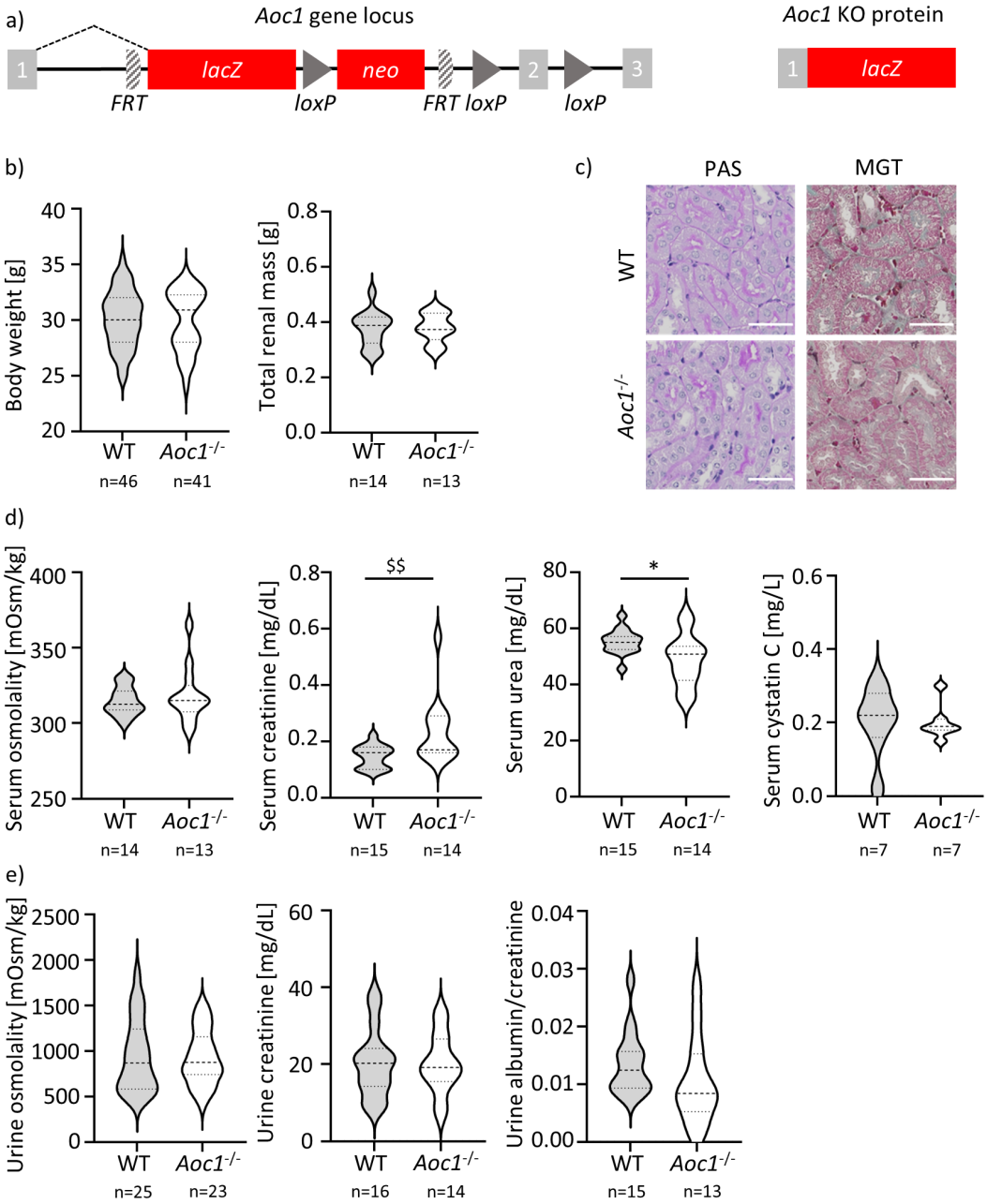

Figure 19: Genetic and phenotypic description of *Aoc1* knockout-first allele.

a) Schematic showing the design of the *Aoc1* knockout through a reporter knockout. The insertion of a splice acceptor containing β-galactosidase (*lacZ*) trapping cassette disrupts the gene function ubiquitously. Numbered, grey boxes indicate coding exons, solid line intronic sequences and dashed lines indicate splicing event. *FRT*: Flip recognition target; *loxP*: Locus of x(cross)-over in P1; *neo*: amino 3'-glycosyl phosphotransferase. **b)** Body weight and total renal mass of WT and *Aoc1*$^{-/-}$ mice. **c)** Periodic acid Schiff base (PAS) staining and Masson-Goldner Trichrome (MGT) staining of WT and *Aoc1*$^{-/-}$ kidneys. Scale bar indicates 50 µm. **d)** Measurement of osmolality, creatinine, urea, and cystatin C in serum of WT and *Aoc1*$^{-/-}$ mice. **e)** Measurement of osmolality, creatinine, and albumin in urine of WT and *Aoc1*$^{-/-}$ mice. Significances were calculated using unpaired t-test or Mann-Whitney test after testing for normal distribution using Shapiro-Wilk test. Significances for normal distributed data is indicated using asterisks (*p<0.05; **p<0.01; ***p<0.001) and for not normal distributed data by dollar signs ($^{\$}$p<0.05; $^{\$\$}$p<0.01). Adapted from Sieckmann *et al.* [161].

The mice show no differences in body weight and their total renal mass compared to wildtype animals (figure 17b). The renal histology is unremarkable with no detected changes in PAS and Masson Goldner trichrome staining (figure 19c). The renal excretory function was assessed by measuring serum osmolality, creatinine, urea, and cystatin C levels. While serum osmolality is unchanged, *Aoc1*$^{-/-}$ animals exhibit increased serum creatinine and decreased serum urea levels (figure 19d). As another marker of renal function, cystatin C shows unaltered levels (figure 17d). As measured in spot urine samples, *Aoc1*$^{-/-}$ mice exhibit no changes in osmolality, creatinine, or albumin (figure 19e). While the *Aoc1* knockout does not influence polyamine levels in kidney tissue or urine, serum putrescine levels are significantly elevated (figure 20).

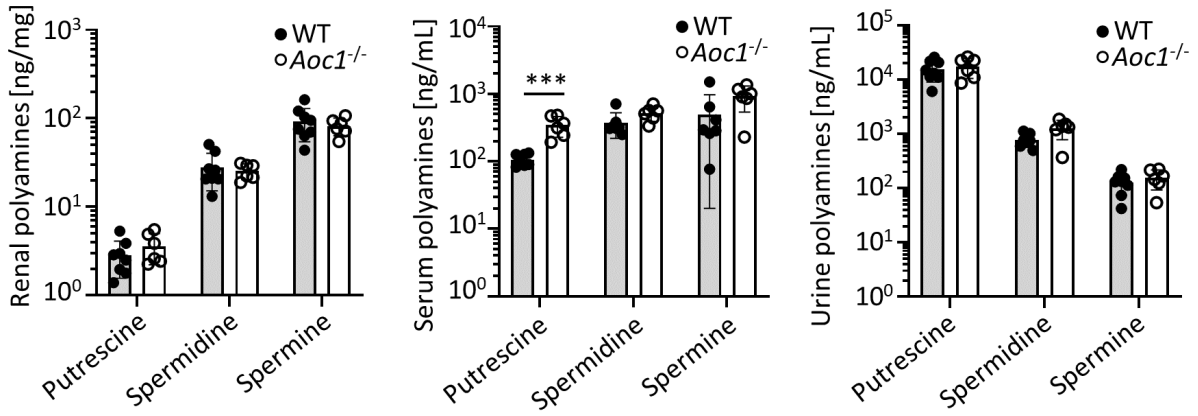

Figure 20: Polyamines in *Aoc1* WT and *Aoc1*$^{-/-}$ mice.
Measurement of polyamines in kidneys, serum, and urine of WT and Aoc1$^{-/-}$ mice. Significances were calculated using unpaired t-test after testing for normal distribution using Shapiro-Wilk test. Significances for normal distributed data is indicated using asterisks (*p<0.05; **p<0.01; ***p<0.001). Adapted from Sieckmann *et al.* [161].

While no histomorphologic changes were detected, expression of different transcripts was measured in *Aoc1* WT and *Aoc1*$^{-/-}$ kidneys. As shown in figure 21, no increase in markers for tubular injury was detected. However, markers for fibrosis (*Tgf*β and α*Sma*), the macrophage marker F4/80, anti-inflammatory phagocyte markers (*Mrc1* and *Arg1*), and the pro-inflammatory cytokine *Il1b* exhibit reduced expression. Within the polyamine system the transcripts of synthesizing *Odc1* and *Srm* are significantly reduced together with the disrupted *Aoc1*.

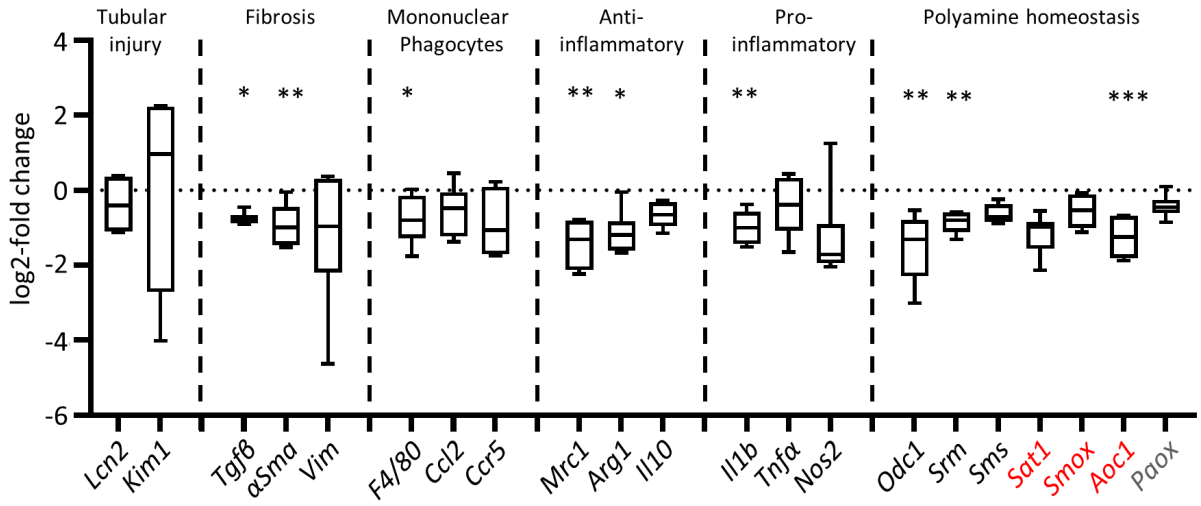

Figure 21: Expression changes of various genes in kidneys of *Aoc1*$^{-/-}$ mice.
Messenger RNA levels of various genes involved in renal pathophysiology and polyamine metabolism were measured in *Aoc1*$^{-/-}$ mice kidneys by qPCR (n=10). The values are shown as log2-fold change in relation to kidneys from WT animals, normalized to *Actb*. Significances were calculated using unpaired t-test after testing for normal distribution of data using the Shapiro-Wilk test (*p<0.05; **p<0.01; ***p<0.001). Error bars show minimum and maximum value. Adapted from Sieckmann *et al.* [161].

3.12 Influence of *Aoc1* on renal structure and function 21 days after renal unilateral IRI

Aoc1$^{-/-}$ and *Aoc1* WT mice underwent 25 min of renal unilateral IRI, followed by 21 days of reperfusion (figure 22a). While an increase in AOC1 protein is detectable in *Aoc1* WT mice after IRI, it is absent in the knockout animals (figure 22b). No differences in renal gross anatomy were detected after IRI between *Aoc1*$^{-/-}$ and *Aoc1* WT animals (figure 22c). No differences in renal excretory function were detected as measured in serum and urine besides an increase in measured osmolality of spot urine from *Aoc1*$^{-/-}$ mice (figure 22d,e). The renal histopathology is mainly unchanged with similar amounts of infiltrating mononuclear cells, apoptotic cells, and fibrosis (figure 22f). However, a decrease in cortical tubular casts was measured together with an increase in KIM1 positive tubules (figure 22f,g).

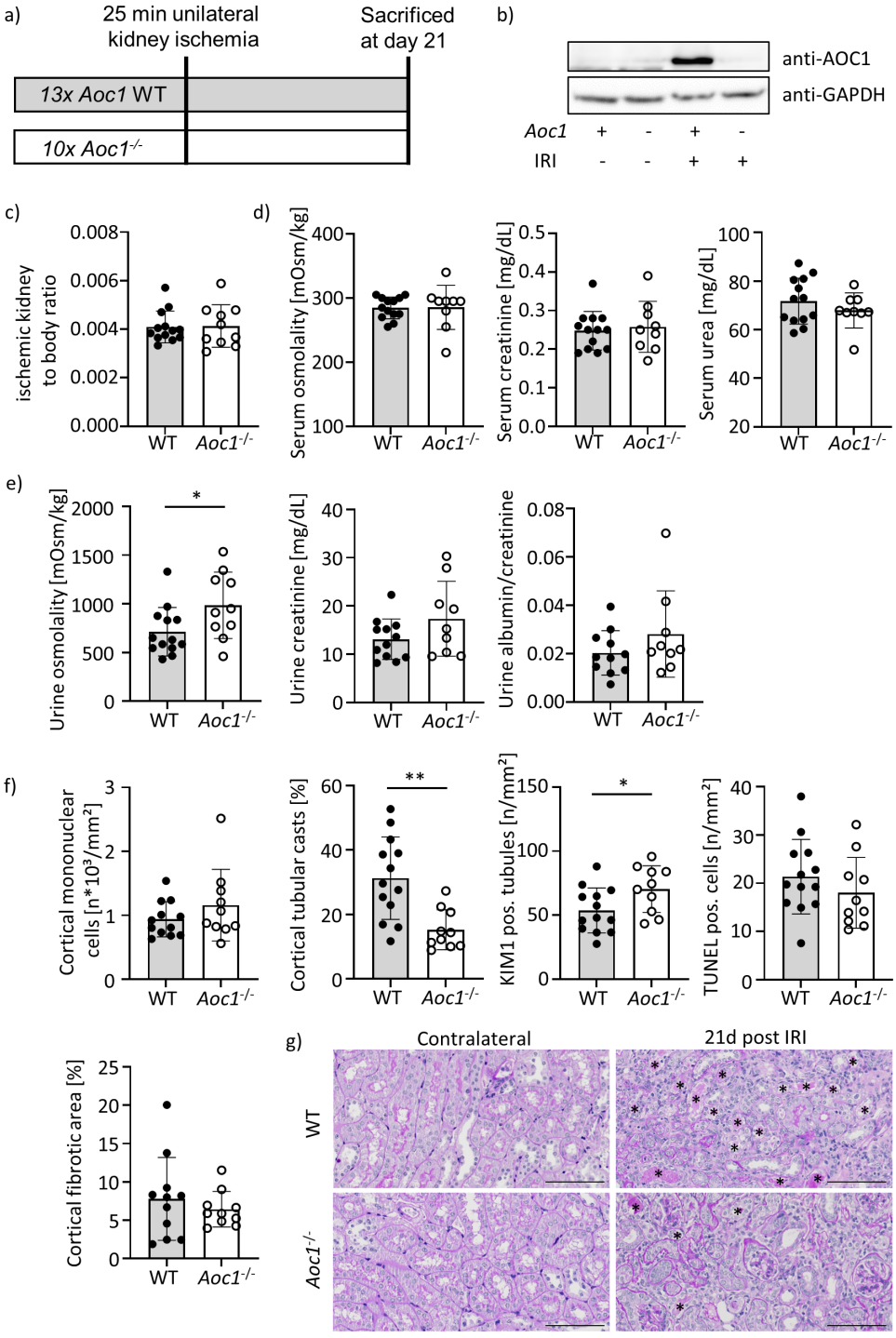

Figure 22: Changes in clinical parameters of renal function after unilateral IRI in WT and *Aoc1*$^{-/-}$ mice.

a) Schematic of the used study design. *Aoc1* WT and *Aoc1*$^{-/-}$ mice were subjected to 25 min unilateral renal ischemia followed by 21 days of reperfusion. **b)** Immunoblotting of AOC1 protein and GAPDH in contralateral control kidneys and kidneys that underwent IRI of *Aoc1* WT and *Aoc1*$^{-/-}$ mice. **c)** Weight of the ischemic kidney adjusted to the animals' body weight. **d)** Serum osmolality, creatinine, and urea 21 days after unilateral IRI. **e)** Urine osmolality, creatinine, and albumin 21 days after unilateral IRI. **f)** Histomorphologic changes in *Aoc1* WT and *Aoc1*$^{-/-}$ kidneys 21 days after IRI. Significances were calculated using unpaired t-test testing for normal distribution of data using the Shapiro-Wilk test (*p<0.05; **p<0.01) **g)** Representative images from the renal cortex of both genotypes contralateral and

ischemic kidneys 21 days after surgery. Asterisks indicate the presence of tubular casts. Scale bar represents 100 µm. Adapted from Sieckmann *et al.* [161].

To detect if certain processes involved in renal pathophysiology are influenced, selected transcripts were measured by qPCR. As demonstrated in figure 23, expression of *Lcn2*, *Tnfα* and *sXbp1* is significantly downregulated. For the mRNA levels of polyamine regulating enzymes, no difference is detectable with exception of the strong decrease in detected *Aoc1*.

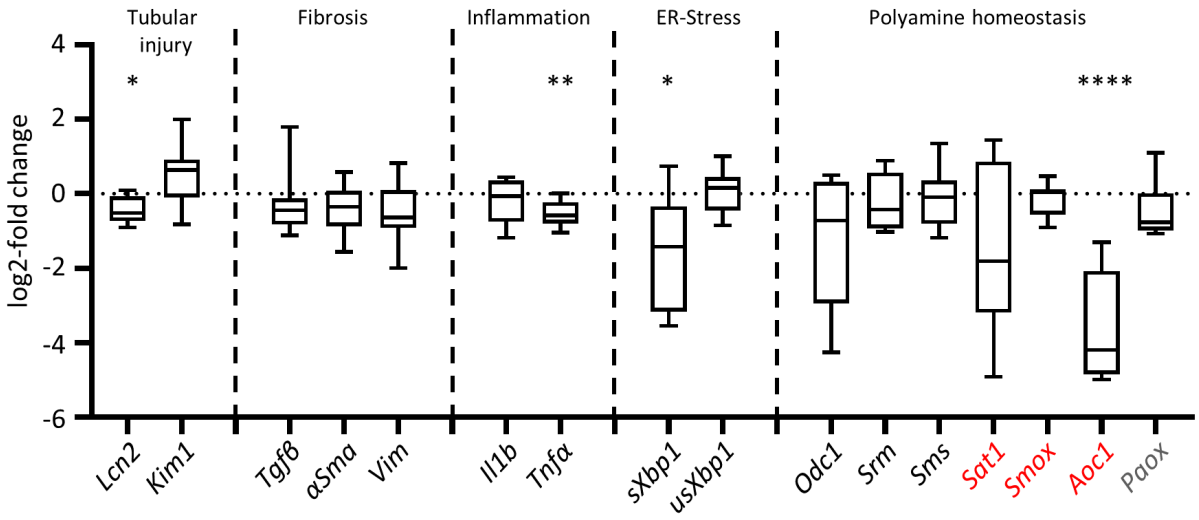

Figure 23: Changes in renal gene expression 21 days post IRI.
Renal gene expression changes of various genes involved in renal pathophysiology or polyamine metabolism in *Aoc1*$^{-/-}$ animals. Values are displayed as log2-fold change of indicated mRNAs relative to WT animals (n=9). Significances were calculated using unpaired t-test after testing for normal distribution of data using the Shapiro-Wilk test (*p<0.05; **p<0.01; ***p<0.001; ****p<0.0001). Error bars show minimum and maximum value. Adapted from Sieckmann *et al.* [161].

IRI leads to a decrease in renal putrescine and spermine levels while spermidine is elevated (figure 6). In figure 24a, kidneys from untreated control animals, the contralateral control kidney and kidneys 21 days after ischemia were used. This setup allows to compensate for possible extrarenal sources of polyamines as the post IRI kidneys can be compared to two separate controls. While the *Aoc1* knockout stabilizes renal putrescine levels, the increase in spermidine is unaffected. Spermine however exhibits no significant changes between the treatments and within one genotype. For serum polyamine levels (figure 24b) only an increase in putrescine is detectable. As polyamines are freely filtered, changes in serum polyamine levels can be compensated by altered polyamine excretion. As shown in figure 24b, *Aoc1*$^{-/-}$ mice excrete increased putrescine and spermidine amounts 21 days after IRI compared to *Aoc1* WT animals.

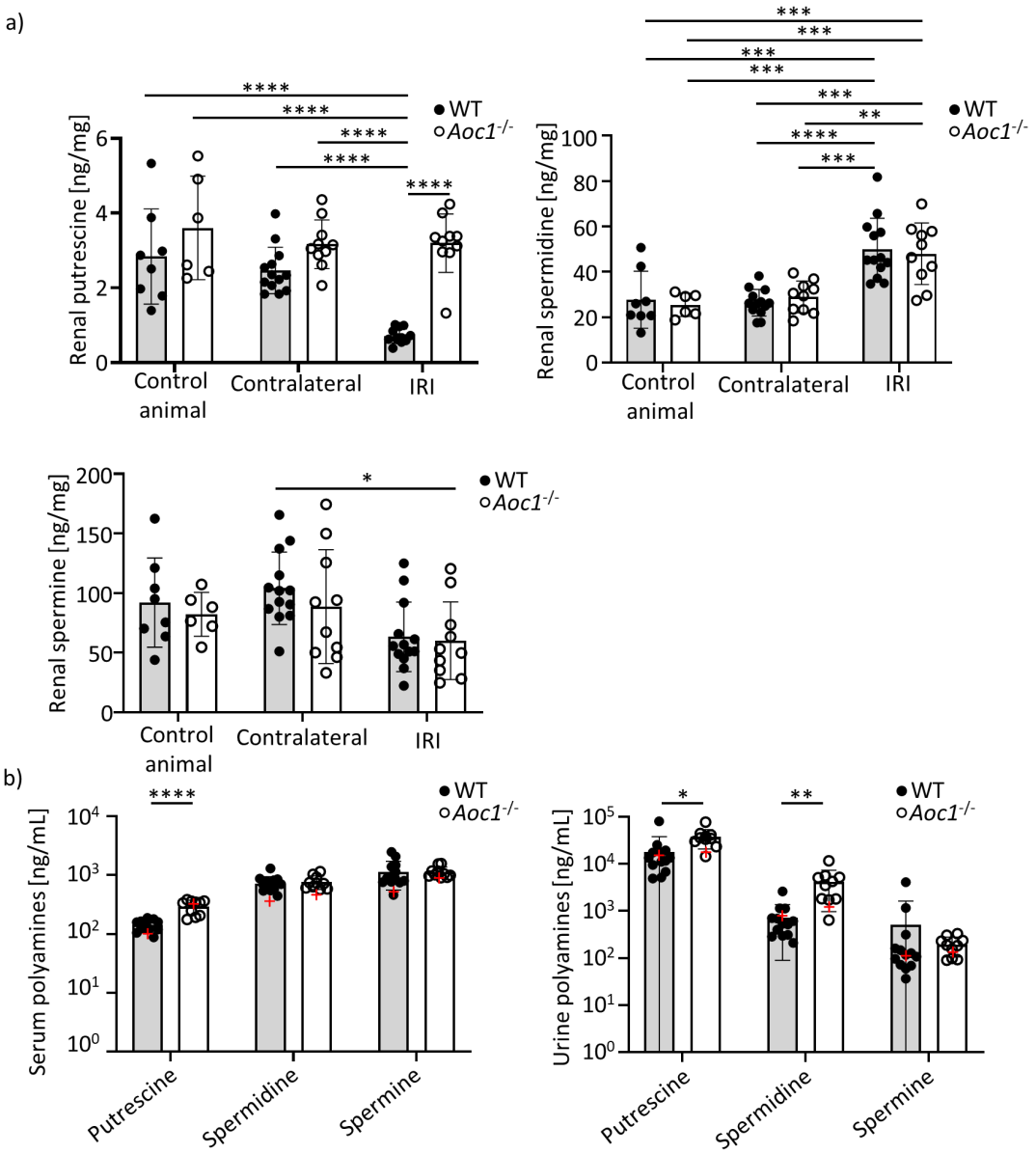

Figure 24: Changes in polyamine levels 21 days post IRI.

a) Changes in renal polyamine levels were determined in untreated control animals, the contralateral control kidney, and the ischemic kidney 21 days after IRI. Data of control animals is adapted from figure 20. **b)** Changes in serum and urinary polyamine levels of *Aoc1* WT and *Aoc1*$^{-/-}$ mice 21 days after unilateral IRI. The red plus-signs indicate the measured mean amount of each polyamine in untreated control animals (cf. figure 20), significances and tests for these comparisons are given within the text. Significances were calculated using unpaired t-test (for b) or by two-way ANOVA (for b) after testing for normal distribution of data using the Shapiro-Wilk test (*p<0.05; **p<0.01; ***p<0.001; ****p<0.0001). Data of polyamine levels from this experiment were used for visualizing figure 6. Adapted from Sieckmann *et al.* [161].

3.13 Influence of *Aoc1* on renal structure and function after 14 days of adenine feeding

To explore the role of *Aoc1* after kidney injury further, a second injury model was used. Here, tubulointerstitial nephritis was induced by feeding an adenine enriched diet for 14 days (figure 25a). Increased AOC1 protein is detectable in *Aoc1* WT animals after adenine feeding but not in *Aoc1*$^{-/-}$ mice (figure 25b). The two genotypes do not differ in their kidney weight (figure 25c), excretory kidney function (figure 25d,e), or in histomorphology (figure 25f).

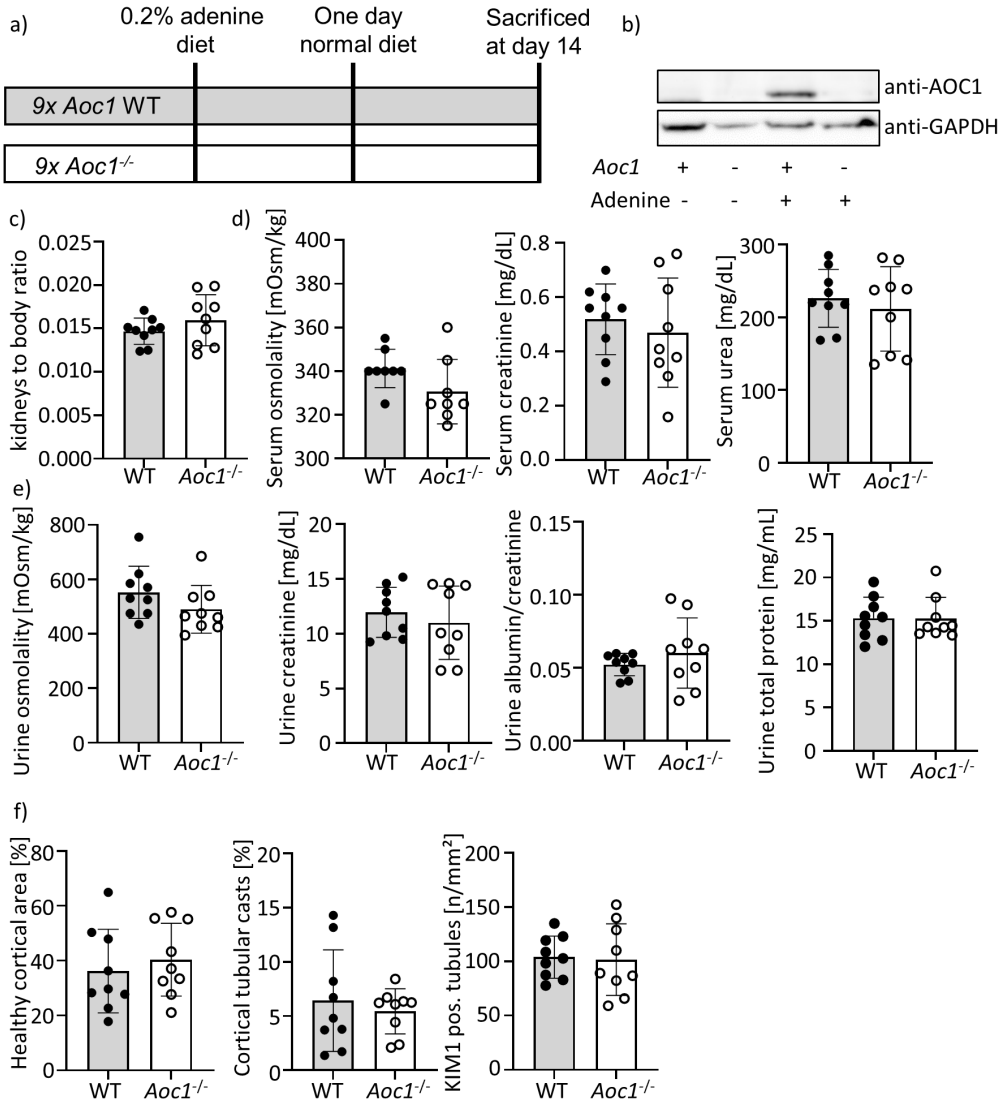

Figure 25: Changes in clinical parameters of renal function after 14 days of adenine feeding in *Aoc1* WT and *Aoc1*$^{-/-}$ mice.

a) Schematic of the used study design. *Aoc1* WT and *Aoc1*$^{-/-}$ mice were fed a synthetic diet containing 0.2% adenine. After 7 days, mice were able to return to a normal diet for one day before continuing the adenine enriched diet. **b)** Immunoblotting of AOC1 protein and GAPDH in kidneys of *Aoc1* WT and *Aoc1*$^{-/-}$ mice fed with normal chow or adenine enriched chow (0.2% adenine). **c)** Weight of both kidneys adjusted to the animals' body weight. **d)** Serum osmolality, creatinine, and urea after 14 days of adenine

feeding. **e)** Urine osmolality, creatinine, and albumin after 14 days of adenine feeding. **f)** Histomorphologic changes in *Aoc1* WT and *Aoc1*$^{-/-}$ kidneys after 14 days of adenine feeding. Significances were calculated using unpaired t-test after testing for normal distribution of data using the Shapiro-Wilk test (*p<0.05; **p<0.01; ***p<0.001; ****p<0.0001). Adapted from Sieckmann *et al.* [161].

Measurement of a panel of different genes involved in renal pathophysiology revealed reduced amounts of the pro-inflammatory cytokine *Il1b* (figure 26). Other investigated processes including tubular injury, fibrosis and other immunomodulatory genes exhibited no change. Within the polyamine homeostatic genes, only reduced expression of *Aoc1* is detected (figure 26).

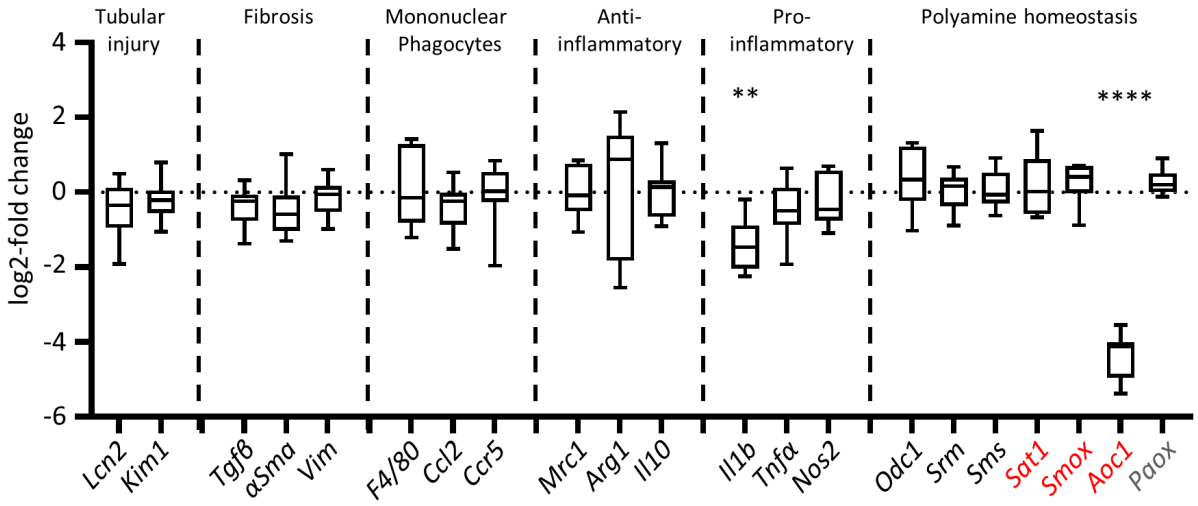

Figure 26: Gene expression changes in kidneys of mice after 14 days of adenine nephropathy. Gene expression of various genes involved in renal pathophysiology and polyamine metabolism were measured in *Aoc1*$^{-/-}$ mice kidneys by qPCR. The values are shown as log2-fold change of indicated mRNAs in relation to kidneys from WT animals, normalized to *Actb*. Significances were calculated using unpaired t-test after testing for normal distribution of data using the Shapiro-Wilk test (*p<0.05; **p<0.01; ***p<0.001; ****p<0.0001). Adapted from Sieckmann *et al.* [161].

While renal function, histology and gene expression remain mainly unchanged, polyamine levels exhibit large differences. As shown in figure 27a, renal putrescine is elevated in *Aoc1*$^{-/-}$ animals compared to *Aoc1* WT animals and untreated animals. Interestingly, the interindividual differences in renal putrescine content are very large. While renal spermidine levels remain unchanged, a decrease in spermine is detectable for both genotypes (figure 27a). For serum and urinary polyamines, putrescine levels are significantly elevated in *Aoc1*$^{-/-}$ animals compared to *Aoc1* WT while elevated spermidine is only detected in urine (figure 27a). Substantially, serum and urine putrescine content is significantly (p<0.0001; two-way ANOVA) higher in KO animals after adenine feeding compared to untreated controls (red plus signs in figure 27). *Aoc1* WT and *Aoc1*$^{-/-}$ animals show elevated serum spermidine levels (p<0.01; two-way ANOVA) but only knockout mice excrete increased spermidine via urine (p<0.01; two-way ANOVA) compared to the untreated control animals.

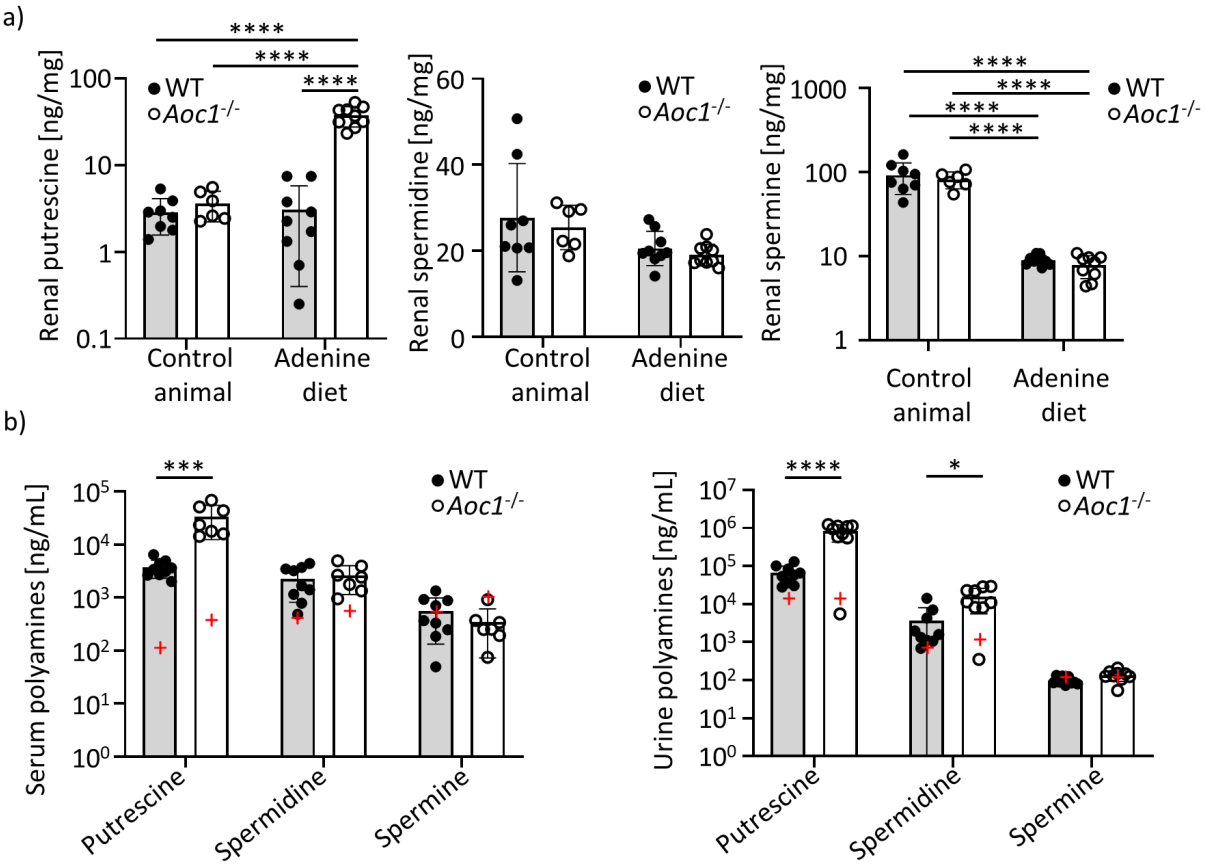

Figure 27: Changes in polyamine levels in renal tissue, serum, and urine of WT and *Aoc1*$^{-/-}$ mice with adenine nephropathy.

a) Changes in renal polyamine levels were determined in untreated control animals and mice after 14 days of adenine feeding. Data from control animals is adapted from figure 20. Significances were calculated using two-way ANOVA (*p<0.05; **p<0.01; ***p<0.001; ****p<0.0001). **b)** Changes in serum and urinary polyamine levels of *Aoc1* WT and *Aoc1*$^{-/-}$ mice after 14 days of adenine feeding. The red plus-signs indicate the measured mean amount of each polyamine from untreated control animals (cf. figure 20), significances and tests for these comparisons are given within the text. Significances were calculated using unpaired t-test after testing for normal distribution of data using the Shapiro-Wilk test (*p<0.05; **p<0.01; ***p<0.001; ****p<0.0001). Adapted from Sieckmann *et al.* [161].

4 Discussion

4.1 The polyamine system in kidney injury

This study demonstrates that the polyamine system undergoes uniform changes after kidney injury following a conserved scheme (figure 3 and 4). It is shown that the genes involved in polyamine synthesis (*Odc1*, *Srm*, and *Sms*) are negatively correlated, while the catabolic gene *Aoc1* is positively correlated with different markers of tubular injury and repair (figure 4). Little is known about the polyamine synthesizing enzymes in kidney injury so far. Two studies reported a decrease of renal ODC1 in kidney injury by streptozotocin induced diabetes and IRI [132, 168]. Here, downregulation of *Odc1* expression was present in all models of kidney injury tested (figure 3). Data from this study support the hypothesis that enzymes involved in polyamine catabolism are commonly upregulated after kidney injury. Previous studies in models of kidney injury reported an increased expression of polyamine catabolic enzymes, such as *Sat1*, after bilateral IRI and increased SAT1 enzyme activity after kidney injury induced by folic acid and type 1 diabetes [104, 132, 169]. Following cisplatin-induced AKI, increased renal SAT1 and SMOX levels were also observed [124]. Upregulation of *Aoc1* is most frequently observed (figure 3). There have been few reports on the induction of *Aoc1* after renal injury, though the data presented in this study are consistent with hints found in previous studies. Increased *Aoc1* mRNA during the kidney repair phase was detected using microarray data after IRI [143]. In another transcriptomic study, increased *Aoc1* expression was detected after transplantation [170]. Furthermore, increased AOC1 activity was detected in CKD patients with undisclosed etiologies undergoing dialysis [171]. This indicates, that the results of this study might also have implications in patients with kidney disease. The increase in *Sat1* expression observed in this study (figure 3) is most prominent in the early stages of kidney injury, as seen in kidney samples harvested after 24 hours after rhabdomyolysis and 6 hours after IRI. This is consistent with previous reports of increased SAT1 after bilateral IRI and kidney injury induced by folic acid, which peaked at 12 hours and declined thereafter [104, 120]. These findings suggest that the dysregulation of the polyamine system may be regulated spatiotemporally. It is possible that polyamine catabolism is upregulated in a biphasic manner, with *Sat1* expression being an early response to injury followed by increased *Aoc1* expression during regeneration. The localization of the injury may also be important, as the increase of *Smox* in hypertension or diabetic nephropathy models (figure 3) may be due to vascular or glomerular injury, respectively, leading to the absence of *Aoc1* expression. Further research, including longitudinal measurement of these genes after injury and determination of polyamine levels, is needed to fully understand these dynamics.

The genes encoding polyamine synthesizing enzymes were most prominently downregulated and *Aoc1* as a catabolic enzyme shows a strong negative correlation to *Odc1* and *Sms* (figure 4). It is noteworthy that this inverse regulation is additive and may result in an overall

shutdown of the polyamine system. Interestingly, a strong decrease of putrescine levels was observed after IRI (figure 6a and 24a) which was abrogated in the *Aoc1* knockout mice (figure 24a). After adenine nephropathy, renal putrescine levels in WT mice remained equal to untreated control animals (figure 27a). Consistent with the IRI model, renal putrescine levels increased in *Aoc1* knockout mice after adenine feeding compared to *Aoc1* WT mice (figure 27a). This demonstrates that the upregulation of AOC1 is the major regulating factor for the renal putrescine levels after kidney injury. Still, differences between both models were observed. Besides the different mechanisms of injury, the timepoints of analysis were different. It is possible that an early rise in putrescine levels is compensated by later increase in AOC1. This is in line with earlier reports showing increasing renal putrescine levels 6, 12 and 24 hours after IRI [104, 172]. Another possibility is that increased renal putrescine levels result from the drastic increase in serum and urine putrescine levels observed after adenine treatment (figure 27b), but not after IRI (figure 24b). In this study, the kidneys were not perfused prior to measurement of tissue polyamines. It is therefore possible that remaining blood and urine within the kidney increases the measured tissue putrescine levels.

Within the serum, *Aoc1*$^{-/-}$ mice exhibit increased putrescine levels in comparison to *Aoc1* WT mice (figure 24b and 27b). And elevated serum putrescine and spermidine levels are detected in *Aoc1* WT mice after IRI and adenine feeding (figure 6b and 27b). Elevated serum spermine is only detected after IRI (figure 6b). The observation of increasing serum putrescine, is consistent with reports of increased serum putrescine in CKD patients [115,116]. The detected elevation in serum spermidine and spermine however is contradictory to the reported decrease in CKD patients [115,116]. For the unilateral IRI model the reason for these discrepancies may be that the contralateral kidney can compensate the resorptive capacity of the injured kidney, thus elevating serum spermidine and spermine levels. As elevated serum spermidine levels are also detected in adenine nephropathy (figure 27b), it could also be that the assessed timepoints are not comparable to the progression of CKD in patients.

Interestingly, the renal polyamine system exhibits and maintains a strong spatial separation between synthesis and catabolism. The most prominent changes observed after kidney IRI were the reduction in cortical *Odc1* expression and the strong induction of cortical *Aoc1* expression (figure 7 and 8a). Previous research has identified *Odc1* in the proximal tubules of healthy rats and mice [169, 173, 174], and the finding of the present study of tubular *Odc1* expression (figure 7) is consistent with this. As ornithine reabsorption, which is necessary for the synthesis of putrescine, occurs primarily in the proximal tubules [175], the reduction in *Odc1* expression may be due to reduced ornithine availability resulting from damage to these tubules. Within the healthy kidney, *Aoc1* was not expressed in the cortex but rather in the medulla (figure 8a). This is supported by qPCR data, indicating the highest levels of *Aoc1* expression in the inner stripe of the outer medulla and inner medulla [176]. Additionally, the expression of other genes regulating the polyamine system was generally downregulated throughout the entire kidney (figure 7). In accordance with the RNAScope data, cortical expression of *Srm*

and *Sms* (figure 7) has been described before [176]. The weaker expression of *Srm* and *Sms* in comparison to *Odc1* may highlight the role of *Odc1* as the "gatekeeper" of the polyamine system. The strong cortical tubular *Sat1* expression (figure 7) is also in line with previous reports [174, 176]. The expression of the interconverting enzyme *Paox* was relatively weak but exclusive to cortical tubules (figure 7), as previously reported in the proximal tubules within the cortex and outer stripe of the medulla [176, 177]. The limited presence of *Paox*, compared to *Sat1*, may lead to decreased putrescine pools, as *Paox* is necessary for back-conversion. Interestingly, it is known that the different polyamines are unevenly distributed across the kidney [178]. Localizing the different polyamines before and after injury could provide valuable insights into their possible roles. Finally, the presented data is only based on expression and further experiments should be dedicated to localizing the corresponding proteins.

4.2 Increasing polyamine catabolism as a reaction to injury

Across all evaluated models, a shift in the expression of the renal polyamine system towards degradation is evident (figure 3). This shift is independent of the underlying etiology, as almost all studied models exhibit decreased *Odc1* expression and increased expression of *Aoc1*, *Sat1*, or *Smox*. As this dysregulation was observed in eleven murine models of kidney injury with different etiologies, a potentially conserved mode of action is suggested. *Odc1* exhibits the strongest negative correlation and *Aoc1* the strongest positive correlation with *Lcn2* expression (figure 4 and 5). Other tested markers for processes like fibrosis (α*Sma*, *Vim*, *Tgf*β), inflammation (*Il1*β, *Tnf*α) also correlate with downregulation of *Odc1* and increase in *Aoc1*, however the correlation is weaker. As most detected injury markers correlate with each other, a categorization of a dysregulated polyamine system to a certain mechanism is hard to establish. This indicates that changes in the expression of polyamine regulating enzymes correlate with the severity of injury rather than with a specific type of damage. All the models in this study showed increased *Lcn2* mRNA levels (figure 3). *Lcn2* has been shown to rapidly increase in mRNA levels after kidney injury, with increases detectable three hours after IRI [30]. *Lcn2* is not only a marker of tubular injury, it has been proposed as a biomarker for the transition from AKI to CKD [143, 165] highlighting its role in recovery and adaptation.

It is known that in pathologies of other organs than the kidney, changes in the polyamine system occur. Tissue damage often results in similar alterations of polyamine levels. In rats with lesioned brains and mice with IRI of the bladder, an early increase in tissue ODC1 activity with increased putrescine levels was detected, while spermidine and spermine remained unchanged [179, 180]. Similarly, tissue putrescine and spermidine levels are increased compared to spermine in rats after partial hepatectomy and in a mouse colitis model [181, 182]. Here, the question arises - is the response of the polyamine system different in injured kidneys compared to other organs? As in the model of kidney IRI a reduction of renal putrescine was observed (figure 6a) and all analyzed models of kidney injury showed a downregulation of *Odc1* expression (figure 3). Increased expression of polyamine catabolic

enzymes as observed in this study (figure 3) is a common feature of various pathologies. Enhanced polyamine catabolism and *Sat1* expression have been detected after traumatic brain injury and cerebral IRI [183–185], increased SAT1 was also detected in the myocardium after IRI [186], and enhanced SAT1 and PAOX in early response of the liver to IRI [172]. The importance of this back-conversion is highlighted by the findings that SAT1 deficient mice show reduced putrescine levels after renal and hepatic IRI compared to wildtype animals [127] and that brain putrescine levels drop by 70% after inhibition of PAOX [187]. The polyamine back-conversion pathway has been observed to be upregulated in the early stages after injury in various models, with peak levels occurring between 6- and 12-hours post-injury [104, 120, 172, 186]. However, later, this pathway is downregulated and there is an increase in AOC1 expression. After IRI and transplantation [143, 170], in wounded guinea pig skin [188] and after 70% small intestine resection [189] an increase in *Aoc1* is detectable, often occurring after the initial injury and within the phase of highest proliferation and regeneration. This proposition of a biphasic response of polyamine metabolism is strengthened by the observation of a late reduction in renal putrescine levels (figure 6a and 24a). While early SAT1 activity may be responsible for the build-up of increased renal putrescine levels [127], AOC1 is responsible for the degradation of it (figure 24a and 27a).

These findings suggest a conserved dysregulation of the polyamine system across various injuries and organs. Further investigation, such as testing IRI on different organs at different time points, could provide insight into the regulation and potential functions of the polyamine system in various tissues.

4.3 The role of the putrescine degrading enzyme AOC1 in kidney injury

Analyzing the histological localization of AOC1 expression after IRI indicated, that regenerating tubular cells are the main source for AOC1 protein in the injured kidney (figure 11). AOC1 has been described as a secreted glycoprotein [190]. Nevertheless, a substantial amount of AOC1 protein accumulates in the tubular epithelium, where it is produced (figure 9d). Further studies are needed to clarify, to what extend AOC1 is secreted from the tubular epithelium into the circulation. Expression of *Aoc1* mRNA is exclusive to the proximal tubule and thin descending limb of Henle's loop (figure 10), and colocalizes with KIM1, a marker for regenerating tubular epithelial cells [191]. This raises the question if AOC1 expression is restricted locally to certain segments or functionally to specific cells. The restricted expression within the proximal tubule may be due to initial injury, as it is generally acknowledged that renal IRI damages primarily the S3 segment of the proximal tubule [192]. The shown correlation of *Aoc1* to the severity of renal injury (figure 5) and the localization within damaged cells (figure 11) hint to a role for *Aoc1* in tissue regeneration. However, it is unclear how *Aoc1* contributes to regeneration. Expression of AOC1 leads to depletion of putrescine, which might counteract proliferation [173]. Furthermore, it has been shown, that inhibition of AOC1 improves healing in rat models of facial nerve

injury [193] and small bowel transection resection [194]. Contrary, however *Aoc1* expression is required for normal proliferation in M15 cells (figure 18). There is also low overlap between apoptotic, necrotic, or proliferating cells and *Aoc1*-expressing cells (figure 11a), suggesting a role for *Aoc1* in the terminal phase of regeneration. In future studies, *Aoc1* expression should be studied in more diverse injury models. It would be interesting to see, if upregulation of *Aoc1* is a conserved mechanism that is not cell type specific. Injury models that specifically damage the glomerulus or exhibit more distal damage patterns could answer this question. The role of *Aoc1* within regeneration should be addressed in more detail.

4.4 Hyperosmolarity as a stimulus of *Aoc1* expression

The new finding of AOC1 upregulation after kidney injury (figure 3) leads to the question, which factors regulate the expression of AOC1 in kidney injury. Hypoxia and hyperosmolarity were identified as noxae that resulted in a similar dysregulation of the polyamine system (figure 12), evident by the downregulation of *Odc1* and upregulation of *Aoc1*. The relationship between hypoxia and an altered polyamine system is controversial, as some studies have shown that hypoxia leads to increased polyamine synthesis and ODC1 levels in cancer cell lines [195] and in fetal rat brain [196]. Others have shown, that hypoxia leads to decreased ODC1 activity in rat lung [197] and increased SMOX levels in retinal glial cells [198], thus favoring catabolism. Interestingly, elevated AOC1 levels under hypoxia have been only described in plants as in fava beans or soy beans, leading to increased GABA production [199, 200]. These discrepancies in different reports could be based on the type of tissue that was assessed or based on the time point. In fact, ODC1 activity is first increased and later decreased in hypoxic cardiomyoblasts [201]. The hypothesis, that the type of tissue determines changes in the polyamine system under hypoxia, is strengthened by the observations, that *Aoc1* expression is only induced in embryonic kidneys under hypoxia but not in adult primary proximal tubules or cell lines (figure 13a). In contrast, hyperosmolarity was further confirmed as a stimulus of *Aoc1* expression in cell lines and primary proximal tubule (figure 13a). Furthermore, renal *Aoc1* expression was detected in the medulla of healthy kidneys *i.e.*, the tissue with the highest osmolality (figure 8). Consistent with this, elevated *Aoc1* mRNA levels were detected in embryonic kidneys, primary proximal tubules, and cell lines upon cultivation under hyperosmotic conditions (figure 13a). However, little is known about the effects of tonicity on the mammalian polyamine system. Previous studies have reported increased *Odc1* activity in hypotonic conditions in mouse leukemia cells, which confers protective effects [202, 203]. Consistently, hyperosmotic stress leads to a reduction of putrescine in HeLa cells [204]. These findings align with the shown positive correlation between increasing osmolality and *Aoc1* expression (figure 13d). Interestingly, bacteria also reduce putrescine content with increasing tonicity [205, 206], while plants exhibit increased putrescine biosynthesis under hyperosmotic stress [207]. These differences might resemble the structural specificities of these cells. While plant cells have a cell wall that is capable of sustaining large turgor pressure [208], mammalian and bacterial cells need to rapidly adapt to changes in external tonicity. Here,

osmoregulatory processes are initialized by cell volume regulation and organic osmolyte accumulation. Polyamines can block different channels such as porins in bacteria [209, 210], inward rectifier K^+ channels and TRP channels in mammalian cells [211, 212]. As such, increased polyamine catabolism may reduce the blocking of these channels and allow for a compensatory influx of ions and osmolytes to counteract external tonicity.

Interestingly, upregulation of *Aoc1* under stress conditions might be restricted to epithelial cells. *Aoc1* is elevated only in epithelial cells after IRI (figure 11) and in epithelial cell lines under hyperosmotic stress (figure 13d). Also in the embryonic kidney explant culture, AOC1 appears in the epithelial cells in hypertonic conditions (figure 13c). Epithelial and mesenchymal cells can respond differently to hyperosmotic stress [213]. Therefore, it would be interesting to test how different epithelial and mesenchymal cell lines react to exposure to hyperosmotic stress and if they increase *Aoc1* mRNA. Additionally, the influence of *Aoc1* and polyamines onto mammalian osmoregulation should be assessed. Here, measuring the volume of *Aoc1* overexpressing or *Aoc1* deficient cells exposed to increasing tonicity could give some new insights.

The mechanisms by which hyperosmolarity is increasing *Aoc1* mRNA are transcriptional induction by NFAT5 and mRNA stabilization (figure 14 and 15). Hyperosmolarity is known to activate NFAT5 [214] which regulates downstream targets for osmoprotection [215, 216]. Hyperosmotic conditions can damage cells through various mechanisms, including the production of reactive oxygen species [217,218], the inhibition of replication [219], transcription and translation [220], and depolarization of mitochondrial membranes [221]. After renal IRI, cortical NFAT5 expression can be detected in damaged proximal tubules [222, 223]. In agreement, *Aoc1* expression is induced via direct influence on an upstream NFAT5 binding site *in vitro* (figure 14b,c). However, it remains unclear if NFAT5 is the common factor driving *Aoc1* activation in both the osmoadaptive response and renal injury. The increased mRNA stability is another regulatory mechanism contributing to the elevated *Aoc1* mRNA levels under high tonicity (figure 15). While a clear increase in stability is observed, the exact mechanism behind this increase has not been determined. Cells overexpressing *Aoc1* under control of a CMV promoter show elevated AOC1 protein levels, when exposed to hypertonicity. This may be due to increased mRNA stability or other processes, such as increased translation or protein stabilization. Hyperosmolarity is well known to influence mRNA stability [224], translation efficiency [225] and protein stability [226]. Future studies using chromatin immunoprecipitation of DNA from injured kidneys could reveal if NFAT5 activates *Aoc1* transcription *in vivo*. The characterization of the molecular processes leading to increased *Aoc1* mRNA levels and protein could place *Aoc1* correctly within its regulatory network. This way the function of AOC1 after renal injury and hyperosmotic stress could be better understood.

4.5 Subcellular localization of the different AOC1 isoforms

Aoc1 has several transcripts, which have not been further characterized. Hyperosmolarity induced *Aoc1* promoter activity by NFAT5, binding upstream of the *Aoc1*-205 isoform (figure 14a). Elevated *Aoc1*-205 mRNA levels were detected under hyperosmolarity and after kidney injury [161]. This suggests a potential link between the response to hyperosmotic stress and renal injury, with *Aoc1*-205 expression possibly playing a role in both situations. *Aoc1*-205 is the only *Aoc1* isoform containing an additional coding exon. This exon corresponds to 22 additional amino acids N-terminally before the AOC1 signal peptide. The presence of the full-length proteinogenic transcript was confirmed through PCR (figure 16b). *In silico* analysis of the N-terminus of Aoc1-205 revealed that the amino acid sequence is still recognized as a signal peptide (figure 16a). Within the constructed signal peptide-eGFP fusion constructs, a strong influence on the subcellular localization and secretion of the protein was observed (figure 17). Specifically, the addition of the +22AA signal peptide led to increased secretion into the medium. AOC1 is known to be a secreted glycoprotein [190, 227], but the influence of the alternative first exon has never been described before. Various stimuli have been linked to increased secretion of AOC1, including heparin and other glycosaminoglycans [190, 228, 229] triglycerides and fatty acids [230], fat absorption [231], intestinal ischemia [232], and pregnancy related secretion from the placenta [233]. The N-terminal addition of the AOC1-205 signal peptide further increases the secretion (figure 17d). Signal peptides are generally heterogeneous and variable in length [234, 235]. Despite this heterogeneity, their composition is relatively conserved as they consist of a positively charged N-terminus, a hydrophobic core region and a polar C-terminus containing the cleavage site. The N-terminus is usually short consisting of 4-5 residues [236] but variations exist. While the exact amino acid sequence does not affect secretion [237] its net positive charge is required [238]. Therefore, it is possible that the elongation or alteration of charge of the AOC1-205 signal peptide leads to increased secretion. To identify the structures in which AOC1 is translocated could give further insight into the secretion mechanism. Using immunohistochemistry to localize AOC1 along with markers of different organelles could be informative. Additionally, studying protein-signal peptide interactions to identify potential binding proteins may help to understand how the elongated signal peptide facilitates secretion.

Within the kidney, AOC1 is localized in renal tubules in vesicles along the plasma membrane [239] where it is found in microsomes [240]. This is in line with the localization of the *Aoc1* signaling peptide within extranuclear bodies (figure 17b',c') and after renal injury, AOC1 protein is localized perinuclear (figure 9a'). It is generally thought that AOC1 is readily stored in vesicles within the kidney and intestine and released upon stimulation, with release from the small intestine occurring upon heparin stimulation into the venous effluent [147]. Here, it can be bound in vasculature [241, 242], possibly regulating circulating histamine and polyamine levels. This is in line with the observation that serum putrescine levels are significantly upregulated in *Aoc1*$^{-/-}$ animals (figure 20). However, it is unclear whether the renal tubules secrete AOC1 into

the tubular lumen or basolateral into the circulation. Quantification of AOC1 in urine and blood could determine whether regenerating tubules are secreting AOC1 basolaterally or luminally.

4.6 The Influence of AOC1 on cellular processes

The function of AOC1 is clearly described as a histamine and putrescine degrading enzyme. Nevertheless, the consequences of this enzymatic activity on the diverse cellular processes are poorly understood. The increase of *Aoc1* expression in kidney injury and hyperosmolarity may be detrimental or required for normal repair. To address this question, the influence of AOC1 on different aspects of regeneration was tested. Regeneration of biological structures requires significant changes within the damaged tissue, including proliferation and migration to replace necrotic cells. Polyamines and their ability to activate eIF5A are crucial for proliferation [72] and migration [243,244], so increasing AOC1 levels could deplete polyamine pools and reduce proliferation and migration. Reduced proliferation through AOC1 was demonstrated in prostate cancer cells [245], fibroblasts [173], and lymphocytes [246]. Consistently, suppression of AOC1 leads to increased proliferation after ileal resection [194]. However *Aoc1* is necessary for normal proliferation but not for migration in M15 cells (figure 18a,b). Overexpression of AOC1 does not influence neither proliferation nor migration (figure 18a,b). Consistently, it was shown that AOC1 is required for normal kidney organogenesis and AOC1 inhibition disrupts tubular branching [247]. Elevated AOC1 levels have been linked to increased proliferation and migration in various cancer cell lines including gastric cancer cells [149], colorectal cancer cells [248] and in hepatocellular carcinoma cells [150]. In gastric cancer cells and hepatocellular carcinoma cells, AOC1 influenced proliferation and migration by modulating various pathways, including AKT and JAK/STAT3 [149,150], with reduced AOC1 levels leading to a decrease in tumor growth [149]. It is possible that the effect of AOC1 on proliferation depends on the specific cell type and its effect on polyamine pools or modulation of signaling pathways.

To further understand the role of AOC1 in proliferation, several key questions need to be answered. To reveal the mechanism of AOC1's involvement, intracellular and extracellular polyamine levels should be quantified. Additionally, it will be necessary to test whether the absence of AOC1 changes known signaling pathways that influence proliferation.

4.7 The role of AOC1 in renal physiology and polyamine metabolism

The renal polyamine system has been described incomplete so far. While *Aoc1* exhibits only a weak renal expression within the medulla, its germline deletion could cause pathologic changes within the kidney. As shown, *Aoc1*$^{-/-}$ mice are viable and show only little changes in renal function (figure 19). While it was shown that AOC1 is needed for normal branching

morphogenesis during embryonic development [247], adult *Aoc1*$^{-/-}$ mice show no visible changes in total renal mass or renal histology. Serum creatinine is elevated in some animals, however cystatin C levels are unchanged (figure 19d). This increase of only a single marker of decreased kidney function could be the result of the ubiquitous *Aoc1* knockout. As creatine synthesis and polyamine synthesis are linked through arginase activity, changes in the polyamine system could influence creatine biosynthesis. In *Aoc1*$^{-/-}$ mice, *Arg1* mRNA is reduced, hinting to changes in arginase availability (figure 21). Consistently, it was shown that some patients with arginase 1 deficiency exhibit increased plasma creatine levels [249]. The reduced serum urea may be based on reduced hepatic urea production. As putrescine builds up, it is possible that arginase activity is diminished as a compensatory mechanism leading to reduced ornithine and urea production. This is partly strengthened by the observation of reduced *Arg1* mRNA in kidneys of *Aoc1*$^{-/-}$ mice (figure 21). To clarify if both creatinine and urea synthesis are influenced by arginase activity through deletion of *Aoc1*, arginase enzyme activity should be quantified together with arginine and ornithine levels. These mice further show reduced levels of different transcripts involved in immunomodulatory functions (figure 21). In line with these observations, it is known that putrescine levels can modulate macrophage activation [250] and differentiation of dendritic cells [251]. Expression of polyamine synthesizing enzymes is also reduced in *Aoc1*$^{-/-}$ mice compared to *Aoc1* WT mice (figure 21). Here, it is likely that the lack of putrescine degradation is compensated by reduction of *Odc1* and *Srm* expression. This compensatory mechanism and the relative low expression levels of *Aoc1* within the kidney (figure 7) may explain the unchanged renal polyamine levels of *Aoc1*$^{-/-}$ mice (figure 20). Elevated serum putrescine in the *Aoc1*$^{-/-}$ mice might be a result of the ubiquitous *Aoc1* deletion, including the gut. AOC1 degrades putrescine in the small intestine and inhibition of AOC1 leads to elevated putrescine uptake [252]. In future studies, it would be beneficial to use a kidney specific *Aoc1* deletion to dismiss influences arising from ablation of *Aoc1* in distant organs.

4.8 Influence of *Aoc1* on the outcome of kidney injury models

Both serum putrescine and renal putrescine levels are elevated in *Aoc1*$^{-/-}$ animals compared to *Aoc1* WT after IRI and adenine feeding (figure 24a,b and 27a,b). Furthermore, in both injury models, *Aoc1*$^{-/-}$ animals excrete more putrescine and spermidine via the urine (figure 24a,b and 27a,b). These changes in polyamine levels had only limited effect on the outcome after IRI or adenine nephropathy. While major descriptors of renal excretory function are unchanged between *Aoc1* WT and *Aoc1*$^{-/-}$ mice (figure 22d,e and 25d,e), *Aoc1*$^{-/-}$ animals exhibit reduced tubular cast formation (figure 22f,g). The formation of intratubular casts by detached epithelial cells and cellular debris is as common process after IRI. A reduction of tubular casts can therefore hint to either reduced shedding of cells or improved clearing of the tubular lumen. Consistently, administration of putrescine in acute liver injury exhibited anti-apoptotic effects [253]. While there was no detected difference in TUNEL positive cells 21 days after IRI, this could be explained by the late timepoint with most apoptosis occurring seven days

after unilateral IRI and subsequent normalization thereafter [36]. Other protective effects could include the increase in KIM1 as seen in more KIM1 positive tubules (figure 22f). Here, KIM1 is involved in mediating phagocytic processes, thus reducing renal injury [254]. The reduced *Tnfα* expression in *Aoc1*$^{-/-}$ mice after IRI (figure 23) could be another antiapoptotic factor as it was demonstrated that tubular apoptosis after IRI is induced by TNFα [255]. Consistently, *Aoc1*$^{-/-}$ mice exhibit decreased *Lcn2* expression as well as decreased spliced *Xbp1*, a marker for endoplasmatic reticulum stress [256].

As demonstrated, *Aoc1*$^{-/-}$ animals exhibit increased renal putrescine levels compared to *Aoc1* WT animals after kidney injury (figure 24a and 27a). Eventhough renal putrescine levels are elevated in both models, only a mild influence on the outcome is detectable. Earlier studies described renoprotective effects of *Sat1* ablation and reduction of renal putrescine levels [127]. Consistently it was shown that excess putrescine levels decrease cell viability in hepatocytes [172] likely through inhibition of eIF5a formation and increased apoptosis [257, 258]. However, next to toxic effects mediated by the increased putrescine levels, it is also possible that catabolism of putrescine itself is damaging through resulting products like hydrogen peroxide or acrolein. The combination of increased putrescine levels which could be damaging, together with reduced catabolism through *Aoc1* deletion could therefore result in effects being reciprocally neutralized.

Overall, *Aoc1*$^{-/-}$ mice exhibit a mild improvement in outcome after kidney injury by IRI. Due to the redundancy within the polyamine system and the shown compensatory counter-regulation upon *Aoc1* knockout, it is likely that more factors than a single enzyme must be changed to achieve a therapeutic effect. Here, two strategies could be interesting to test. First, the genetic deletion of ODC1 antizymes in *Aoc1*$^{-/-}$ animals, thus stabilizing ODC1 expression, leading to a further increase in putrescine levels. And second, a double germline deletion of *Aoc1* and *Sat1*, inhibiting the major polyamine degrading enzymes.

4.9 Translational aspects

Within this work, the suppression of polyamine synthesis and activation of polyamine catabolism is presented as a common process in various types of kidney injury. Both, the downregulation of *Odc1* and therefore putrescine synthesis and upregulation of polyamine catabolism through *de novo* expression of *Aoc1* are common to most renal injuries. Within different models, renal polyamine levels are disturbed after kidney injury with *Aoc1* being the major regulating factor of renal putrescine levels after injury. These data are from rodent models only and need therefore to be extended to clinics involving AKI and CKD patients. Here, biopsies of AKI and CKD patients could be used for determination of polyamine levels and expression of polyamine homeostatic genes.

Expression of *Aoc1* is regulated by the transcription factor NFAT5 upon hyperosmotic stress in

vitro and by stabilization of *Aoc1* mRNA. Identification of factors regulating AOC1 expression could serve as a foundation for new pharmacologic treatment options. After injury, one specific isoform is strongly expressed, exhibiting increased secretory ability. Here, the specific detection of *Aoc1*-205 in blood and urine could answer the question if AOC1 is secreted basolaterally or luminally.

Germline deletion of *Aoc1* increases the renal putrescine level after injury but offers only mild improvement in renal function. While the deletion of *Aoc1* may be compensated by decreasing expression of polyamine synthesizing genes, an acute reduction of *Aoc1* after injury could be beneficial. Here inhibition of AOC1 activity by administration of aminoguanidine could overcome the compensatory mechanisms and lead to improvements. Furthermore, adjustments of the polyamine system by combined therapies could alleviate the consequences of renal injury. Here, inhibitors of different enzymes of the polyamine system are available and could be used for influencing renal polyamine levels. Overall, thorough investigation of the dysregulated polyamine system could be an entry point for development of new therapeutics or diagnostic approaches.

5 Bibliography

[1] J. R. Pappenheimer, “Passage of molecules through capillary walls,” *Physiological Reviews*, vol. 33, no. 3, pp. 387–423, 1953.

[2] A. Verniory, R. Du Bois, P. Decoodt, J. Gassee, and P. Lambert, “Measurement of the permeability of biological membranes application to the glomerular wall,” *The Journal of general physiology*, vol. 62, no. 4, pp. 489–507, 1973.

[3] E. Verney and E. H. Starling, “On secretion by the isolated kidney,” *The Journal of Physiology*, vol. 56, no. 5, p. 353, 1922.

[4] S. Semple and H. De Wardener, “Effect of increased renal venous pressure on circulatory "autoregulation" of isolated dog kidneys,” *Circulation Research*, vol. 7, no. 4, pp. 643–648, 1959.

[5] M. N. Levy, “Effect of variations of blood flow on renal oxygen extraction,” *American Journal of Physiology-Legacy Content*, vol. 199, no. 1, pp. 13–18, 1960.

[6] P. Persson, H. Ehmke, H. Kirchheim, B. Janssen, J. Baumann, A. Just, and B. Nafz, “Autoregulation and non-homeostatic behaviour of renal blood flow in conscious dogs,” *The Journal of Physiology*, vol. 462, no. 1, pp. 261–273, 1993.

[7] L. Young, M. Regan, M. Barry, J. Geraghty, and J. Fitzpatrick, “Methods of renal blood flow measurement,” *Urological Research*, vol. 24, pp. 149–160, 1996.

[8] A. Chonko, R. Osgood, A. Nickel, T. Ferris, and J. Stein, “The measurement of nephron filtration rate and absolute reabsorption in the proximal tubule of the rabbit kidney,” *The Journal of Clinical Investigation*, vol. 56, no. 1, pp. 232–235, 1975.

[9] B. Corman, N. Roinel, and C. De Rouffignac, “Water reabsorption capacity of the proximal convoluted tubule: a microperfusion study on rat kidney,” *The Journal of physiology*, vol. 316, no. 1, pp. 379–392, 1981.

[10] O. W. Moe, P. A. Preisig, and R. J. Alpern, “Cellular model of proximal tubule NaCl and $NaHCO_3$ absorption,” *Kidney international*, vol. 38, no. 4, pp. 605–611, 1990.

[11] KDIGO Work Group. , “KDIGO clinical practice guideline for acute kidney injury,” *Kidney Int Suppl*, vol. 2, no. 1, pp. 1–138, 2012.

[12] A. Levin, P. E. Stevens, R. W. Bilous, J. Coresh, A. L. De Francisco, P. E. De Jong, K. E. Griffith, B. R. Hemmelgarn, K. Iseki, and E. J. Lamb, “Kidney disease: Improving global outcomes (KDIGO) CKD Work Group. KDIGO 2012 clinical practice guideline for the evaluation and management of chronic kidney disease,” *Kidney international supplements*, vol. 3, no. 1, pp. 1–150, 2013.

[13] N. R. Hill, S. T. Fatoba, J. L. Oke, J. A. Hirst, C. A. O'Callaghan, D. S. Lasserson, and F. R. Hobbs, "Global prevalence of chronic kidney disease–a systematic review and meta-analysis," *PloS one*, vol. 11, no. 7, p. e0158765, 2016.

[14] J. Cerdá, A. Bagga, V. Kher, and R. M. Chakravarthi, "The contrasting characteristics of acute kidney injury in developed and developing countries," *Nature clinical practice Nephrology*, vol. 4, no. 3, pp. 138–153, 2008.

[15] P. Susantitaphong, D. N. Cruz, J. Cerda, M. Abulfaraj, F. Alqahtani, I. Koulouridis, and B. L. Jaber, "World incidence of AKI: a meta-analysis," *Clinical Journal of the American Society of Nephrology*, vol. 8, no. 9, pp. 1482–1493, 2013.

[16] S. G. Coca, S. Singanamala, and C. R. Parikh, "Chronic kidney disease after acute kidney injury: a systematic review and meta-analysis," *Kidney international*, vol. 81, no. 5, pp. 442–448, 2012.

[17] R. L. Mehta, E. A. Burdmann, J. Cerdá, J. Feehally, F. Finkelstein, G. García-García, M. Godin, V. Jha, N. H. Lameire, and N. W. Levin, "Recognition and management of acute kidney injury in the international society of nephrology 0by25 global snapshot: a multinational cross-sectional study," *The Lancet*, vol. 387, no. 10032, pp. 2017–2025, 2016.

[18] Z. Zhong, G. E. Arteel, H. D. Connor, M. Yin, M. V. Frankenberg, R. F. Stachlewitz, J. A. Raleigh, R. P. Mason, and R. G. Thurman, "Cyclosporin A increases hypoxia and free radical production in rat kidneys: prevention by dietary glycine," *American Journal of Physiology-Renal Physiology*, vol. 275, no. 4, pp. F595–F604, 1998.

[19] M. Ranucci, F. Romitti, G. Isgrò, M. Cotza, S. Brozzi, A. Boncilli, and A. Ditta, "Oxygen delivery during cardiopulmonary bypass and acute renal failure after coronary operations," *The Annals of thoracic surgery*, vol. 80, no. 6, pp. 2213–2220, 2005.

[20] M. Oostendorp, E. E. de Vries, J. M. Slenter, C. J. Peutz-Kootstra, M. G. Snoeijs, M. J. Post, L. E. van Heurn, and W. H. Backes, "MRI of renal oxygenation and function after normothermic ischemia-reperfusion injury," *NMR in Biomedicine*, vol. 24, no. 2, pp. 194–200, 2011.

[21] R. Zager, M. S. Jurkowitz, and A. Merola, "Responses of the normal rat kidney to sequential ischemic events," *American Journal of Physiology-Renal Physiology*, vol. 249, no. 1, pp. F148–F159, 1985.

[22] B. Molitoris, R. Dahl, and A. Geerdes, "Cytoskeleton disruption and apical redistribution of proximal tubule Na(+)-K(+)-ATPase during ischemia," *American Journal of Physiology-Renal Physiology*, vol. 263, no. 3, pp. F488–F495, 1992.

[23] D. J. Pagliarini, S. E. Calvo, B. Chang, S. A. Sheth, S. B. Vafai, S.-E. Ong, G. A. Walford, C. Sugiana, A. Boneh, and W. K. Chen, "A mitochondrial protein compendium elucidates complex I disease biology," *Cell*, vol. 134, no. 1, pp. 112–123, 2008.

[24] M. S. Paller, “Hemoglobin-and myoglobin-induced acute renal failure in rats: role of iron in nephrotoxicity,” *American Journal of Physiology-Renal Physiology*, vol. 255, no. 3, pp. F539–F544, 1988.

[25] P. Shanley, M. Rosen, M. Brezis, P. Silva, F. Epstein, and S. Rosen, “Topography of focal proximal tubular necrosis after ischemia with reflow in the rat kidney,” *The American journal of pathology*, vol. 122, no. 3, p. 462, 1986.

[26] N. S. Shin, A. Marlier, L. Xu, T. Lam, L. G. Cantley, and J.-K. Guo, “Characterization of temporospatial distribution of renal tubular casts by nephron tracking after ischemia-reperfusion injury,” *American Journal of Physiology-Renal Physiology*, vol. 322, no. 3, pp. F322–F334, 2022.

[27] R. Beeri, Z. Symon, M. Brezis, S. A. Ben-Sasson, P. H. Baehr, S. Rosen, and R. A. Zager, “Rapid DNA fragmentation from hypoxia along the thick ascending limb of rat kidneys,” *Kidney international*, vol. 47, no. 6, pp. 1806–1810, 1995.

[28] A. Linkermann, J. H. Bräsen, M. Darding, M. K. Jin, A. B. Sanz, J.-O. Heller, F. De Zen, R. Weinlich, A. Ortiz, and H. Walczak, “Two independent pathways of regulated necrosis mediate ischemia–reperfusion injury,” *Proceedings of the National Academy of Sciences*, vol. 110, no. 29, pp. 12024–12029, 2013.

[29] T. Yoshida, A. Shimizu, Y. Masuda, A. Mii, E. Fujita, K. Yoshizaki, S. Higo, G. Kanzaki, Y. Kajimoto, and H. Takano, “Caspase-3-independent internucleosomal DNA fragmentation in ischemic acute kidney injury,” *Nephron Experimental Nephrology*, vol. 120, no. 3, pp. e103–e113, 2012.

[30] J. Mishra, Q. Ma, A. Prada, M. Mitsnefes, K. Zahedi, J. Yang, J. Barasch, and P. Devarajan, “Identification of neutrophil gelatinase-associated lipocalin as a novel early urinary biomarker for ischemic renal injury,” *Journal of the American Society of Nephrology*, vol. 14, no. 10, pp. 2534–2543, 2003.

[31] K. Mori, H. T. Lee, D. Rapoport, I. R. Drexler, K. Foster, J. Yang, K. M. Schmidt-Ott, X. Chen, J. Y. Li, and S. Weiss, “Endocytic delivery of lipocalin-siderophore-iron complex rescues the kidney from ischemia-reperfusion injury,” *The Journal of clinical investigation*, vol. 115, no. 3, pp. 610–621, 2005.

[32] Y. Kirita, H. Wu, K. Uchimura, P. C. Wilson, and B. D. Humphreys, “Cell profiling of mouse acute kidney injury reveals conserved cellular responses to injury,” *Proceedings of the National Academy of Sciences*, vol. 117, no. 27, pp. 15874–15883, 2020.

[33] P. S. Kellerman, R. Clark, C. A. Hoilien, S. L. Linas, and B. A. Molitoris, “Role of microfilaments in maintenance of proximal tubule structural and functional integrity,” *American Journal of Physiology-Renal Physiology*, vol. 259, no. 2, pp. F279–F285, 1990.

[34] R. Witzgall, D. Brown, C. Schwarz, and J. V. Bonventre, “Localization of proliferating cell nuclear antigen, vimentin, c-fos, and clusterin in the postischemic kidney. evidence for a heterogenous genetic response among nephron segments, and a large pool of mitotically active and dedifferentiated cells,” *The Journal of clinical investigation*, vol. 93, no. 5, pp. 2175–2188, 1994.

[35] Z. Zhang and C. X. Cai, “Kidney injury molecule-1 (KIM-1) mediates renal epithelial cell repair via ERK MAPK signaling pathway,” *Molecular and cellular biochemistry*, vol. 416, no. 1, pp. 109–116, 2016.

[36] L. Yang, T. Y. Besschetnova, C. R. Brooks, J. V. Shah, and J. V. Bonventre, “Epithelial cell cycle arrest in G2/M mediates kidney fibrosis after injury,” *Nature medicine*, vol. 16, no. 5, pp. 535–543, 2010.

[37] B. D. Humphreys, S.-L. Lin, A. Kobayashi, T. E. Hudson, B. T. Nowlin, J. V. Bonventre, M. T. Valerius, A. P. McMahon, and J. S. Duffield, “Fate tracing reveals the pericyte and not epithelial origin of myofibroblasts in kidney fibrosis,” *The American journal of pathology*, vol. 176, no. 1, pp. 85–97, 2010.

[38] O. Skalli, P. Ropraz, A. Trzeciak, G. Benzonana, D. Gillessen, and G. Gabbiani, “A monoclonal antibody against alpha-smooth muscle actin: a new probe for smooth muscle differentiation,” *The Journal of cell biology*, vol. 103, no. 6, pp. 2787–2796, 1986.

[39] Y. Ikezumi, R. C. Atkins, and D. J. Nikolic-Paterson, “Interferon-γ augments acute macrophage-mediated renal injury via a glucocorticoid-sensitive mechanism,” *Journal of the American Society of Nephrology*, vol. 14, no. 4, pp. 888–898, 2003.

[40] S.-K. Jo, S.-A. Sung, W.-Y. Cho, K.-J. Go, and H.-K. Kim, “Macrophages contribute to the initiation of ischaemic acute renal failure in rats,” *Nephrology Dialysis Transplantation*, vol. 21, no. 5, pp. 1231–1239, 2006.

[41] A. Sola, A. Weigert, M. Jung, E. Vinuesa, K. Brecht, N. Weis, B. Brüne, N. Borregaard, and G. Hotter, “Sphingosine-1-phosphate signalling induces the production of Lcn-2 by macrophages to promote kidney regeneration,” *The Journal of pathology*, vol. 225, no. 4, pp. 597–608, 2011.

[42] S. Lee, S. Huen, H. Nishio, S. Nishio, H. K. Lee, B.-S. Choi, C. Ruhrberg, and L. G. Cantley, “Distinct macrophage phenotypes contribute to kidney injury and repair,” *Journal of the American Society of Nephrology*, vol. 22, no. 2, pp. 317–326, 2011.

[43] M. Jung, A. Sola, J. Hughes, D. C. Kluth, E. Vinuesa, J. L. Viñas, A. Pérez-Ladaga, and G. Hotter, “Infusion of IL-10-expressing cells protects against renal ischemia through induction of lipocalin-2,” *Kidney international*, vol. 81, no. 10, pp. 969–982, 2012.

[44] Z. Ma, Q. Wei, G. Dong, Y. Huo, and Z. Dong, “DNA damage response in renal ischemia–reperfusion and ATP-depletion injury of renal tubular cells,” *Biochimica et*

Biophysica Acta (BBA)-Molecular Basis of Disease, vol. 1842, no. 7, pp. 1088–1096, 2014.

[45] A. Abdelkader, J. Ho, C. P. Ow, G. A. Eppel, N. W. Rajapakse, M. P. Schlaich, and R. G. Evans, "Renal oxygenation in acute renal ischemia-reperfusion injury," *American Journal of Physiology-Renal Physiology*, vol. 306, no. 9, pp. F1026–F1038, 2014.

[46] U. H. Beier, E. A. Hartung, S. Concors, P. T. Hernandez, Z. Wang, C. Perry, J. A. Baur, M. R. Denburg, W. W. Hancock, and T. P. Gade, "Tissue metabolic profiling shows that saccharopine accumulates during renal ischemic-reperfusion injury, while kynurenine and itaconate accumulate in renal allograft rejection," *Metabolomics*, vol. 16, no. 5, pp. 1–6, 2020.

[47] J. A. Ardura, R. Berruguete, D. Rámila, M. V. Alvarez-Arroyo, and P. Esbrit, "Parathyroid hormone-related protein interacts with vascular endothelial growth factor to promote fibrogenesis in the obstructed mouse kidney," *American Journal of Physiology-Renal Physiology*, vol. 295, no. 2, pp. F415–F425, 2008.

[48] J. Lutz, R. Lu, M. Strobl, H. Huang, M. Deng, M. Wang, N. Ouyang, and U. Heemann, "ICOS/B7RP-1 interference in mouse kidney transplantation," *Transplantation*, vol. 84, no. 2, pp. 223–230, 2007.

[49] S.-S. Lv, G. Liu, J.-P. Wang, W.-W. Wang, J. Cheng, A.-L. Sun, H.-Y. Liu, H.-B. Nie, M.-R. Su, and G.-J. Guan, "Mesenchymal stem cells transplantation ameliorates glomerular injury in streptozotocin-induced diabetic nephropathy in rats via inhibiting macrophage infiltration," *International immunopharmacology*, vol. 17, no. 2, pp. 275–282, 2013.

[50] C. Zheng, L. Huang, W. Luo, W. Yu, X. Hu, X. Guan, Y. Cai, C. Zou, H. Yin, and Z. Xu, "Inhibition of STAT3 in tubular epithelial cells prevents kidney fibrosis and nephropathy in STZ-induced diabetic mice," *Cell death & disease*, vol. 10, no. 11, pp. 1–14, 2019.

[51] A. A. Alhaider, H. M. Korashy, M. M. Sayed-Ahmed, M. Mobark, H. Kfoury, and M. A. Mansour, "Metformin attenuates streptozotocin-induced diabetic nephropathy in rats through modulation of oxidative stress genes expression," *Chemico-biological interactions*, vol. 192, no. 3, pp. 233–242, 2011.

[52] R. Zager, "Studies of mechanisms and protective maneuvers in myoglobinuric acute renal injury," *Laboratory investigation; a journal of technical methods and pathology*, vol. 60, no. 5, pp. 619–629, 1989.

[53] M. Fähling, S. Mathia, A. Paliege, R. Koesters, R. Mrowka, H. Peters, P. B. Persson, H.-H. Neumayer, S. Bachmann, and C. Rosenberger, "Tubular von Hippel-Lindau knockout protects against rhabdomyolysis-induced AKI," *Journal of the American Society of Nephrology*, vol. 24, no. 11, pp. 1806–1819, 2013.

[54] F. Knauf, J. R. Asplin, I. Granja, I. M. Schmidt, G. W. Moeckel, R. J. David, R. A. Flavell, and P. S. Aronson, “NALP3-mediated inflammation is a principal cause of progressive renal failure in oxalate nephropathy,” *Kidney international*, vol. 84, no. 5, pp. 895–901, 2013.

[55] T. Yokozawa, P. D. Zheng, and H. Oura, “Biochemical features induced by adenine feeding in rats. Polyuria, electrolyte disorders, and 2, 8-dihydroxyadenine deposits,” *Journal of nutritional science and vitaminology*, vol. 30, no. 3, pp. 245–254, 1984.

[56] S. D. Ricardo, G. Ding, M. Eufemio, and J. R. Diamond, “Antioxidant expression in experimental hydronephrosis: role of mechanical stretch and growth factors,” *American Journal of Physiology-Renal Physiology*, vol. 272, no. 6, pp. F789–F798, 1997.

[57] R. Nagle, R. Bulger, R. Cutler, H. Jervis, and E. Benditt, “Unilateral obstructive nephropathy in the rabbit. I. Early morphologic, physiologic, and histochemical changes,” *Laboratory investigation*, vol. 28, no. 4, pp. 456–467, 1973.

[58] J. R. Diamond, D. Kees-Folts, S. D. Ricardo, A. Pruznak, and M. Eufemio, “Early and persistent up-regulated expression of renal cortical osteopontin in experimental hydronephrosis,” *The American journal of pathology*, vol. 146, no. 6, p. 1455, 1995.

[59] C. Zoumas-Morse, C. L. Rock, E. L. Quintana, M. L. Neuhouser, E. W. Gerner, and F. L. Meyskens Jr, “Development of a polyamine database for assessing dietary intake,” *Journal of the American Dietetic Association*, vol. 107, no. 6, pp. 1024–1027, 2007.

[60] M. Matsumoto and Y. Benno, “The relationship between microbiota and polyamine concentration in the human intestine: a pilot study,” *Microbiology and immunology*, vol. 51, no. 1, pp. 25–35, 2007.

[61] A. Pegg, R. Wechter, R. Pakala, and R. Bergeron, “Effect of N1, N12-bis (ethyl) spermine and related compounds on growth and polyamine acetylation, content, and excretion in human colon tumor cells,” *Journal of Biological Chemistry*, vol. 264, no. 20, pp. 11744–11749, 1989.

[62] K. Igarashi, I. Sakamoto, N. Goto, K. Kashiwagi, R. Honma, and S. Hirose, “Interaction between polyamines and nucleic acids or phospholipids,” *Archives of biochemistry and biophysics*, vol. 219, no. 2, pp. 438–443, 1982.

[63] R. Hasan, M. K. Alam, and R. Ali, “Polyamine induced Z-conformation of native calf thymus DNA,” *FEBS letters*, vol. 368, no. 1, pp. 27–30, 1995.

[64] R. D. Snyder, “Polyamine depletion is associated with altered chromatin structure in HeLa cells,” *Biochemical Journal*, vol. 260, no. 3, pp. 697–704, 1989.

[65] D. Esposito, P. Del Vecchio, and G. Barone, “Interactions with natural polyamines and thermal stability of DNA. A DSC study and a theoretical reconsideration,” *Journal of the American Chemical Society*, vol. 119, no. 11, pp. 2606–2613, 1997.

[66] M. A. Xaplanteri, A. D. Petropoulos, G. P. Dinos, and D. L. Kalpaxis, “Localization of spermine binding sites in 23S rRNA by photoaffinity labeling: parsing the spermine contribution to ribosomal 50S subunit functions,” *Nucleic acids research*, vol. 33, no. 9, pp. 2792–2805, 2005.

[67] I. P. Ivanov, B.-S. Shin, G. Loughran, I. Tzani, S. K. Young-Baird, C. Cao, J. F. Atkins, and T. E. Dever, “Polyamine control of translation elongation regulates start site selection on antizyme inhibitor mRNA via ribosome queuing,” *Molecular cell*, vol. 70, no. 2, pp. 254–264. e6, 2018.

[68] K. Igarashi and K. Kashiwagi, “Effects of polyamines on protein synthesis and growth of escherichia coli,” *Journal of Biological Chemistry*, vol. 293, no. 48, pp. 18702–18709, 2018.

[69] K. Alm, P. S. Berntsson, D. L. Kramer, C. W. Porter, and S. M. Oredsson, “Treatment of cells with the polyamine analog N1, N11-diethylnorspermine retards S phase progression within one cell cycle,” *European Journal of Biochemistry*, vol. 267, no. 13, pp. 4157–4164, 2000.

[70] T. Maeda, T. Wakasawa, Y. Shima, I. Tsuboi, S. Aizawa, and I. Tamai, “Role of polyamines derived from arginine in differentiation and proliferation of human blood cells,” *Biological and Pharmaceutical Bulletin*, vol. 29, no. 2, pp. 234–239, 2006.

[71] L. Han, C. Xu, C. Jiang, H. Li, W. Zhang, Y. Zhao, L. Zhang, Y. Zhang, W. Zhao, and B. Yang, “Effects of polyamines on apoptosis induced by simulated ischemia/reperfusion injury in cultured neonatal rat cardiomyocytes,” *Cell biology international*, vol. 31, no. 11, pp. 1345–1352, 2007.

[72] K. Nishimura, K. Murozumi, A. Shirahata, M. H. Park, K. Kashiwagi, and K. Igarashi, “Independent roles of eIF5A and polyamines in cell proliferation,” *Biochemical Journal*, vol. 385, no. 3, pp. 779–785, 2005.

[73] H. Hanauske-Abel, M.-H. Park, A.-R. Hanauske, A. Popowicz, M. Lalande, and J. Folk, “Inhibition of the G1-S transition of the cell cycle by inhibitors of deoxyhypusine hydroxylation,” *Biochimica et Biophysica Acta (BBA)-Molecular Cell Research*, vol. 1221, no. 2, pp. 115–124, 1994.

[74] D.-L. T. Koomoa, L. P. Yco, T. Borsics, C. J. Wallick, and A. S. Bachmann, “Ornithine decarboxylase inhibition by α-difluoromethylornithine activates opposing signaling pathways via phosphorylation of both Akt/protein kinase B and p27Kip1 in neuroblastoma,” *Cancer research*, vol. 68, no. 23, pp. 9825–9831, 2008.

[75] T. Zou, L. Liu, J. N. Rao, B. S. Marasa, J. Chen, L. Xiao, H. Zhou, M. Gorospe, and J.-Y. Wang, “Polyamines modulate the subcellular localization of RNA-binding protein HuR through AMP-activated protein kinase-regulated phosphorylation and acetylation of importin α1,” *Biochemical Journal*, vol. 409, no. 2, pp. 389–398, 2008.

[76] J. Chen, J. N. Rao, T. Zou, L. Liu, B. S. Marasa, L. Xiao, X. Zeng, D. J. Turner, and J.-Y. Wang, "Polyamines are required for expression of toll-like receptor 2 modulating intestinal epithelial barrier integrity," *American Journal of Physiology-Gastrointestinal and Liver Physiology*, vol. 293, no. 3, pp. G568–G576, 2007.

[77] L. Liu, X. Guo, J. N. Rao, T. Zou, L. Xiao, T. Yu, J. A. Timmons, D. J. Turner, and J.-Y. Wang, "Polyamines regulate E-cadherin transcription through c-Myc modulating intestinal epithelial barrier function," *American Journal of Physiology-Cell Physiology*, vol. 296, no. 4, pp. C801–C810, 2009.

[78] B. Fakler, U. Brändle, E. Glowatzki, S. Weidemann, H.-P. Zenner, and J. Ruppersberg, "Strong voltage-dependent inward rectification of inward rectifier K^+ channels is caused by intracellular spermine," *Cell*, vol. 80, no. 1, pp. 149–154, 1995.

[79] L. Catacuzzeno, D. A. Pisconti, A. A. Harper, A. Petris, and F. Franciolini, "Characterization of the large-conductance Ca-activated K channel in myocytes of rat saphenous artery," *Pflügers Archiv*, vol. 441, no. 2, pp. 208–218, 2000.

[80] B. Nilius, J. Prenen, T. Voets, and G. Droogmans, "Intracellular nucleotides and polyamines inhibit the Ca^{2+}-activated cation channel TRPM4b," *Pflügers Archiv*, vol. 448, no. 1, pp. 70–75, 2004.

[81] G. P. Ahern, X. Wang, and R. L. Miyares, "Polyamines are potent ligands for the capsaicin receptor TRPV1," *Journal of Biological Chemistry*, vol. 281, no. 13, pp. 8991–8995, 2006.

[82] B.-C. Suh and B. Hille, "Electrostatic interaction of internal Mg/textsuperscript2+ with membrane PIP2 Seen with KCNQ K^+ channels," *The Journal of general physiology*, vol. 130, no. 3, pp. 241–256, 2007.

[83] C. Lopez-Garcia, A. J. Lopez-Contreras, A. Cremades, M. T. Castells, F. Marin, F. Schreiber, and R. Penafiel, "Molecular and morphological changes in placenta and embryo development associated with the inhibition of polyamine synthesis during midpregnancy in mice," *Endocrinology*, vol. 149, no. 10, pp. 5012–5023, 2008.

[84] T. Slotkin, W. Whitmore, L. Lerea, R. Slepetis, S. Weigel, P. Trepanier, and F. Seidler, "Role of ornithine decarboxylase and the polyamines in nervous system development: Short-term postnatal administration of α-difluoromethylornithine, an irreversible inhibitor of ornithine decarboxylase," *International Journal of Developmental Neuroscience*, vol. 1, no. 1, pp. 7–16, 1983.

[85] X. Guo, J. N. Rao, L. Liu, T. Zou, K. M. Keledjian, D. Boneva, B. S. Marasa, and J.-Y. Wang, "Polyamines are necessary for synthesis and stability of occludin protein in intestinal epithelial cells," *American journal of physiology-Gastrointestinal and liver physiology*, vol. 288, no. 6, pp. G1159–G1169, 2005.

[86] M. Takigawa, Y. Nishida, F. Suzuki, J.-i. Kishi, K. Yamashita, and T. Hayakawa, “Induction of angiogenesis in chick yolk-sac membrane by polyamines and its inhibition by tissue inhibitors of metalloproteinases (TIMP and TIMP-2),” *Biochemical and biophysical research communications*, vol. 171, no. 3, pp. 1264–1271, 1990.

[87] X. Wang, Y. Ikeguchi, D. E. McCloskey, P. Nelson, and A. E. Pegg, “Spermine synthesis is required for normal viability, growth, and fertility in the mouse,” *Journal of Biological Chemistry*, vol. 279, no. 49, pp. 51370–51375, 2004.

[88] F. J. Perez-Cano, A. Gonzalez-Castro, C. Castellote, A. Franch, and M. Castell, “Influence of breast milk polyamines on suckling rat immune system maturation,” *Developmental & Comparative Immunology*, vol. 34, no. 2, pp. 210–218, 2010.

[89] M. Matsumoto, S. Kurihara, R. Kibe, H. Ashida, and Y. Benno, “Longevity in mice is promoted by probiotic-induced suppression of colonic senescence dependent on upregulation of gut bacterial polyamine production,” *PloS one*, vol. 6, no. 8, p. e23652, 2011.

[90] S. Okumura, T. Teratani, Y. Fujimoto, X. Zhao, T. Tsuruyama, Y. Masano, N. Kasahara, T. Iida, S. Yagi, and T. Uemura, “Oral administration of polyamines ameliorates liver ischemia/reperfusion injury and promotes liver regeneration in rats,” *Liver Transplantation*, vol. 22, no. 9, pp. 1231–1244, 2016.

[91] D. J. Puleston, F. Baixauli, D. E. Sanin, J. Edwards-Hicks, M. Villa, A. M. Kabat, M. M. Kamiński, M. Stanckzak, H. J. Weiss, and K. M. Grzes, “Polyamine metabolism is a central determinant of helper T cell lineage fidelity,” *Cell*, vol. 184, no. 16, pp. 4186–4202. e20, 2021.

[92] D. J. Puleston, M. D. Buck, R. I. K. Geltink, R. L. Kyle, G. Caputa, D. O’Sullivan, A. M. Cameron, A. Castoldi, Y. Musa, and A. M. Kabat, “Polyamines and eIF5A hypusination modulate mitochondrial respiration and macrophage activation,” *Cell metabolism*, vol. 30, no. 2, pp. 352–363. e8, 2019.

[93] C. W. Tabor and S. M. Rosenthal, “Pharmacology of spermine and spermidine. some effects on animals and bacteria,” *Journal of Pharmacology and Experimental Therapeutics*, vol. 116, no. 2, pp. 139–155, 1956.

[94] T. Sakurada, K. Onodera, T. Tadano, and K. Kisara, “Effects of polyamines on the central nervous system,” *The Japanese Journal of Pharmacology*, vol. 25, no. 6, pp. 653–661, 1975.

[95] H. Pendeville, N. Carpino, J.-C. Marine, Y. Takahashi, M. Muller, J. A. Martial, and J. L. Cleveland, “The ornithine decarboxylase gene is essential for cell survival during early murine development,” *Molecular and cellular biology*, vol. 21, no. 19, pp. 6549–6558, 2001.

[96] R. Starks, P. Kirby, M. Ciliberto, and M. Hefti, “Snyder-Robinson syndrome,” *Autopsy & case reports*, vol. 8, no. 3, 2018.

[97] L. D. Morrison and S. J. Kish, “Brain polyamine levels are altered in alzheimer’s disease,” *Neuroscience letters*, vol. 197, no. 1, pp. 5–8, 1995.

[98] U. V. Mahajan, V. R. Varma, M. E. Griswold, C. T. Blackshear, Y. An, A. M. Oommen, S. Varma, J. C. Troncoso, O. Pletnikova, and R. O’Brien, “Dysregulation of multiple metabolic networks related to brain transmethylation and polyamine pathways in alzheimer disease: A targeted metabolomic and transcriptomic study,” *PLoS medicine*, vol. 17, no. 1, p. e1003012, 2020.

[99] G. G. Chen, L. M. Fiori, L. Moquin, A. Gratton, O. Mamer, N. Mechawar, and G. Turecki, “Evidence of altered polyamine concentrations in cerebral cortex of suicide completers,” *Neuropsychopharmacology*, vol. 35, no. 7, pp. 1477–1484, 2010.

[100] N. Ahmad, A. C. Gilliam, S. K. Katiyar, T. G. O’Brien, and H. Mukhtar, “A definitive role of ornithine decarboxylase in photocarcinogenesis,” *The American journal of pathology*, vol. 159, no. 3, pp. 885–892, 2001.

[101] J. P. Marsh and B. T. Mossman, “Role of asbestos and active oxygen species in activation and expression of ornithine decarboxylase in hamster tracheal epithelial cells,” *Cancer research*, vol. 51, no. 1, pp. 167–173, 1991.

[102] R. R. Mohan, A. Challa, S. Gupta, D. G. Bostwick, N. Ahmad, R. Agarwal, S. R. Marengo, S. B. Amini, F. Paras, and G. T. MacLennan, “Overexpression of ornithine decarboxylase in prostate cancer and prostatic fluid in humans,” *Clinical Cancer Research*, vol. 5, no. 1, pp. 143–147, 1999.

[103] A. Mizutani, H. Inoue, and Y. Takeda, “Changes in polyamine metabolism during wound healing in rat skin,” *Biochimica et Biophysica Acta (BBA)-General Subjects*, vol. 338, no. 1, pp. 183–190, 1974.

[104] K. Zahedi, Z. Wang, S. Barone, A. E. Prada, C. N. Kelly, R. A. Casero, N. Yokota, C. W. Porter, H. Rabb, and M. Soleimani, “Expression of SSAT, a novel biomarker of tubular cell damage, increases in kidney ischemia-reperfusion injury,” *American journal of physiology-renal physiology*, vol. 284, no. 5, pp. F1046–F1055, 2003.

[105] Y.-J. Zhao, C.-Q. Xu, W.-H. Zhang, L. Zhang, S.-L. Bian, Q. Huang, H.-L. Sun, Q.-F. Li, Y.-Q. Zhang, and Y. Tian, “Role of polyamines in myocardial ischemia/reperfusion injury and their interactions with nitric oxide,” *European journal of pharmacology*, vol. 562, no. 3, pp. 236–246, 2007.

[106] R. M. Adibhatla, J. F. Hatcher, K. Sailor, and R. J. Dempsey, “Polyamines and central nervous system injury: spermine and spermidine decrease following transient focal cerebral ischemia in spontaneously hypertensive rats,” *Brain research*, vol. 938, no. 1-2, pp. 81–86, 2002.

[107] M. Terakura, I. Higaki, I. Matsui-Yuasa, H. Kinoshita, and S. Otani, “Polyamine metabolism in the rat liver after orthotopic liver transplantation,” *Biochimica et Biophysica Acta (BBA)-General Subjects*, vol. 1245, no. 2, pp. 207–214, 1995.

[108] H. Xu, R. Liu, B. He, C. W. Bi, K. Bi, and Q. Li, “Polyamine metabolites profiling for characterization of lung and liver cancer using an LC-tandem MS method with multiple statistical data mining strategies: Discovering potential cancer biomarkers in human plasma and urine,” *Molecules*, vol. 21, no. 8, p. 1040, 2016.

[109] R. Liu, P. Li, C. W. Bi, R. Ma, Y. Yin, K. Bi, and Q. Li, “Plasma N-acetylputrescine, cadaverine and 1, 3-diaminopropane: potential biomarkers of lung cancer used to evaluate the efficacy of anticancer drugs,” *Oncotarget*, vol. 8, no. 51, p. 88575, 2017.

[110] R. J. Niemi, A. N. Roine, M. R. Häkkinen, P. S. Kumpulainen, T. A. Keinänen, J. J. Vepsäläinen, T. Lehtimäki, N. K. Oksala, and J. U. Mäenpää, “Urinary polyamines as biomarkers for ovarian cancer,” *International Journal of Gynecologic Cancer*, vol. 27, no. 7, 2017.

[111] S. Saiki, Y. Sasazawa, M. Fujimaki, K. Kamagata, N. Kaga, H. Taka, Y. Li, S. Souma, T. Hatano, and Y. Imamichi, “A metabolic profile of polyamines in parkinson disease: A promising biomarker,” *Annals of neurology*, vol. 86, no. 2, pp. 251–263, 2019.

[112] H. Kim, H. Lee, T. Shin, J. Jung, W. Baek, H. Park, G. Lee, M. Paik, and C. Suh, “Polyamine patterns in plasma of patients with systemic lupus erythematosus and fever,” *Lupus*, vol. 27, no. 6, pp. 930–938, 2018.

[113] C. Van Den Berg, A. Koudijs, L. Ritsma, and T. Rabelink, “In vivo assessment of size-selevtive glomerular sieving in transplanted human induced pluripotent stem cell-derived kidney organoids,” *Journal of the American Society of Nephrology*, vol. 31, no. 5, pp. 921–929, 2020.

[114] M. E. Brosnan, S. Ray, B. Walters, and D. Pink, “How does the kidney handle plasma polyamines?,” *Contributions to nephrology*, vol. 121, pp. 129–135, 1997.

[115] K. Sakata, K. Kashiwagi, S. Sharmin, S. Ueda, Y. Irie, N. Murotani, and K. Igarashi, “Increase in putrescine, amine oxidase, and acrolein in plasma of renal failure patients,” *Biochemical and biophysical research communications*, vol. 305, no. 1, pp. 143–149, 2003.

[116] K. Igarashi, S. Ueda, K. Yoshida, and K. Kashiwagi, “Polyamines in renal failure,” *Amino acids*, vol. 31, no. 4, pp. 477–483, 2006.

[117] M. Martin-Lorenzo, A. Ramos-Barron, P. Gutierrez-Garcia, A. Martin-Blazquez, A. Santiago-Hernandez, E. Rodrigo Calabia, C. Gomez-Alamillo, and G. Alvarez-Llamas, “Urinary spermidine predicts and associates with in-hospital acute kidney injury after cardiac surgery,” *Antioxidants*, vol. 10, no. 6, p. 896, 2021.

[118] K. J. Boudonck, M. W. Mitchell, L. Német, L. Keresztes, A. Nyska, D. Shinar, and M. Rosenstock, “Discovery of metabolomics biomarkers for early detection of nephrotoxicity,” *Toxicologic pathology*, vol. 37, no. 3, pp. 280–292, 2009.

[119] O.-N. Goek, C. Prehn, P. Sekula, W. Römisch-Margl, A. Döring, C. Gieger, M. Heier, W. Koenig, R. Wang-Sattler, and T. Illig, “Metabolites associate with kidney function decline and incident chronic kidney disease in the general population,” *Nephrology Dialysis Transplantation*, vol. 28, no. 8, pp. 2131–2138, 2013.

[120] I. Matsui and A. E. Pegg, “Induction of spermidine N1-acetyltransferase in rat kidney by treatment with folic acid,” *FEBS letters*, vol. 139, no. 2, pp. 205–208, 1982.

[121] K. Zahedi, S. Barone, C. Destefano-Shields, M. Brooks, T. Murray-Stewart, M. Dunworth, W. Li, J. R. Doherty, M. A. Hall, and R. D. Smith, “Activation of endoplasmic reticulum stress response by enhanced polyamine catabolism is important in the mediation of cisplatin-induced acute kidney injury,” *PloS one*, vol. 12, no. 9, p. e0184570, 2017.

[122] P. R. Gajjala, H. Bruck, H. Noels, G. Heinze, F. Ceccarelli, A. Kribben, J. Saez-Rodriguez, N. Marx, W. Zidek, and J. Jankowski, “Novel plasma peptide markers involved in the pathology of CKD identified using mass spectrometric approach,” *Journal of Molecular Medicine*, vol. 97, no. 10, pp. 1451–1463, 2019.

[123] N. Babbar and R. A. Casero Jr, “Tumor necrosis factor-α increases reactive oxygen species by inducing spermine oxidase in human lung epithelial cells: a potential mechanism for inflammation-induced carcinogenesis,” *Cancer research*, vol. 66, no. 23, pp. 11125–11130, 2006.

[124] K. Zahedi, S. Barone, Y. Wang, T. Murray-Stewart, P. Roy-Chaudhury, R. D. Smith, R. A. Casero Jr, and M. Soleimani, “Proximal tubule epithelial cell specific ablation of the spermidine/spermine N1-acetyltransferase gene reduces the severity of renal ischemia/reperfusion injury,” *PLoS One*, vol. 9, no. 11, p. e110161, 2014.

[125] K. Zahedi, J. J. Bissler, Z. Wang, A. Josyula, L. Lu, P. Diegelman, N. Kisiel, C. W. Porter, and M. Soleimani, “Spermidine/spermine N1-acetyltransferase overexpression in kidney epithelial cells disrupts polyamine homeostasis, leads to dna damage, and causes G2 arrest,” *American Journal of Physiology-Cell Physiology*, vol. 292, no. 3, pp. C1204–C1215, 2007.

[126] S. Mandal, A. Mandal, and M. H. Park, “Depletion of the polyamines spermidine and spermine by overexpression of spermidine/spermine N 1-acetyltransferase 1 (SAT1) leads to mitochondria-mediated apoptosis in mammalian cells,” *Biochemical Journal*, vol. 468, no. 3, pp. 435–447, 2015.

[127] K. Zahedi, A. B. Lentsch, T. Okaya, S. Barone, N. Sakai, D. P. Witte, L. J. Arend, L. Alhonen, J. Jell, and J. Janne, “Spermidine/spermine-N1-acetyltransferase ablation protects against liver and kidney ischemia-reperfusion injury in mice,” *American Journal*

of Physiology-Gastrointestinal and Liver Physiology, vol. 296, no. 4, pp. G899–G909, 2009.

[128] J. Kim, "Spermidine rescues proximal tubular cells from oxidative stress and necrosis after ischemic acute kidney injury," *Archives of pharmacal research*, vol. 40, no. 10, pp. 1197–1208, 2017.

[129] J. Kim, "Spermidine is protective against kidney ischemia and reperfusion injury through inhibiting DNA nitration and PARP1 activation," *Anatomy & cell biology*, vol. 50, no. 3, pp. 200–206, 2017.

[130] W. Liang, K. Yamahara, C. Hernando-Erhard, S. Lagies, N. Wanner, H. Liang, C. Schell, B. Kammerer, T. B. Huber, and T. Bork, "A reciprocal regulation of spermidine and autophagy in podocytes maintains the filtration barrier," *Kidney international*, vol. 98, no. 6, pp. 1434–1448, 2020.

[131] B. Yan, S.-J. Min, B. Xu, C. Zhang, J. Pei, W. Zhang, and G.-H. Luo, "The protective effects of exogenous spermine on renal ischemia-reperfusion injury in rats," *Translational Andrology and Urology*, vol. 10, no. 5, p. 2051, 2021.

[132] X. Zhang, L. Zhang, Z. Chen, S. Li, B. Che, N. Wang, J. Chen, C. Xu, and C. Wei, "Exogenous spermine attenuates diabetic kidney injury in rats by inhibiting AMPK/mTOR signaling pathway," *International Journal of Molecular Medicine*, vol. 47, no. 3, pp. 1–1, 2021.

[133] B. O. Elmore, J. A. Bollinger, and D. M. Dooley, "Human kidney diamine oxidase: heterologous expression, purification, and characterization," *JBIC Journal of Biological Inorganic Chemistry*, vol. 7, no. 6, pp. 565–579, 2002.

[134] G. Manzotti, D. Breda, M. Di Gioacchino, and S. Burastero, "Serum diamine oxidase activity in patients with histamine intolerance," *International journal of immunopathology and pharmacology*, vol. 29, no. 1, pp. 105–111, 2016.

[135] R. Heatley, J. Denburg, N. Bayer, and J. Bienenstock, "Increased plasma histamine levels in migraine patients," *Clinical & Experimental Allergy*, vol. 12, no. 2, pp. 145–149, 1982.

[136] E. García-Martín, C. Martínez, M. Serrador, H. Alonso-Navarro, P. Ayuso, F. Navacerrada, J. A. Agúndez, and F. J. Jiménez-Jiménez, "Diamine oxidase rs10156191 and rs2052129 variants are associated with the risk for migraine," *Headache: The Journal of Head and Face Pain*, vol. 55, no. 2, pp. 276–286, 2015.

[137] J. Izquierdo-Casas, O. Comas-Basté, M. L. Latorre-Moratalla, M. Lorente-Gascón, A. Duelo, M. C. Vidal-Carou, and L. Soler-Singla, "Low serum diamine oxidase (DAO) activity levels in patients with migraine," *Journal of physiology and biochemistry*, vol. 74, no. 1, pp. 93–99, 2018.

[138] J. Izquierdo-Casas, O. Comas-Basté, M. L. Latorre-Moratalla, M. Lorente-Gascón, A. Duelo, L. Soler-Singla, and M. C. Vidal-Carou, "Diamine oxidase (DAO) supplement reduces headache in episodic migraine patients with DAO deficiency: A randomized double-blind trial," *Clinical Nutrition*, vol. 38, no. 1, pp. 152–158, 2019.

[139] W. J. Schnedl, M. Schenk, S. Lackner, D. Enko, H. Mangge, and F. Forster, "Diamine oxidase supplementation improves symptoms in patients with histamine intolerance," *Food science and biotechnology*, vol. 28, no. 6, pp. 1779–1784, 2019.

[140] W. Schmidt, J. Sattler, R. Hesterberg, H. Röher, T. Zoedler, H. Sitter, and W. Lorenz, "Human intestinal diamine oxidase (DAO) activity in Crohn's disease: a new marker for disease assessment?," *Agents and Actions*, vol. 30, no. 1, pp. 267–270, 1990.

[141] G. D. Luk, T. M. Bayless, and S. B. Baylin, "Plasma postheparin diamine oxidase. sensitive provocative test for quantitating length of acute intestinal mucosal injury in the rat," *The Journal of Clinical Investigation*, vol. 71, no. 5, pp. 1308–1315, 1983.

[142] G. Bounous, V. Echavé, S. J. Vobecky, H. Navert, and A. Wollin, "Acute necrosis of the intestinal mucosa with high serum levels of diamine oxidase," *Digestive diseases and sciences*, vol. 29, no. 9, pp. 872–874, 1984.

[143] G. J. Ko, D. N. Grigoryev, D. Linfert, H. R. Jang, T. Watkins, C. Cheadle, L. Racusen, and H. Rabb, "Transcriptional analysis of kidneys during repair from AKI reveals possible roles for NGAL and KIM-1 as biomarkers of AKI-to-CKD transition," *American Journal of Physiology-Renal Physiology*, 2010.

[144] N. Tsunooka, K. Maeyama, H. Nakagawa, T. Doi, A. Horiuchi, K. Miyauchi, Y. Watanabe, H. Imagawa, and K. Kawachi, "Localization and changes of diamine oxidase during cardiopulmonary bypass in rabbits," *Journal of Surgical Research*, vol. 131, no. 1, pp. 58–63, 2006.

[145] A. L. Southren, Y. Kobayashi, D. H. Sherman, L. Levine, G. Gordon, and A. B. Weingold, "Diamine oxidase in human pregnancy: plasma diamine oxidase in nonpregnant and normal pregnant patients," *American Journal of Obstetrics and Gynecology*, vol. 89, no. 2, pp. 199–203, 1964.

[146] S. B. Baylin, M. D. Abeloff, K. C. Wieman, J. W. Tomford, and D. S. Ettinger, "Elevated histaminase (diamine oxidase) activity in small-cell carcinoma of the lung," *New England Journal of Medicine*, vol. 293, no. 25, pp. 1286–1290, 1975.

[147] K. M. Shakir, S. Margolis, and S. B. Baylin, "Localization of histaminase (diamine oxidase) in rat small intestinal mucosa: site of release by heparin," *Biochemical pharmacology*, vol. 26, no. 24, pp. 2343–2347, 1977.

[148] R. Chanda and A. Ganguly, "Diamine-oxidase activity and tissue di-and poly-amine contents of human ovarian, cervical and endometrial carcinoma," *Cancer letters*, vol. 89, no. 1, pp. 23–28, 1995.

[149] F. Xu, Y. Xu, J.-H. Xiong, J.-H. Zhang, J. Wu, J. Luo, and J.-P. Xiong, “AOC1 contributes to tumor progression by promoting the AKT and EMT pathways in gastric cancer,” *Cancer Management and Research*, vol. 12, p. 1789, 2020.

[150] Q. Ding, D. Lin, Y. Zhou, F. Li, J. Lai, J. Duan, J. Chen, and C. Jiang, “Downregulation of amine oxidase copper containing 1 inhibits tumor progression by suppressing IL-6/JAK/STAT3 pathway activation in hepatocellular carcinoma,” *Oncology Letters*, vol. 22, no. 6, pp. 1–9, 2021.

[151] E. Vigolo, L. Markó, C. Hinze, D. N. Müller, R. Schmidt-Ullrich, and K. M. Schmidt-Ott, “Canonical BMP signaling in tubular cells mediates recovery after acute kidney injury,” *Kidney international*, vol. 95, no. 1, pp. 108–122, 2019.

[152] M. Ashraf, H. Schwelberger, K. Brendel, J. Feurle, J. Andrassy, K. Kotsch, H. Regele, J. Pratschke, H. Maier, and F. Aigner, “Exogenous lipocalin 2 ameliorates acute rejection in a mouse model of renal transplantation,” *American Journal of Transplantation*, vol. 16, no. 3, pp. 808–820, 2016.

[153] M. Fähling, S. Mathia, J. Scheidl, R. Abramovitch, Z. Milman, A. Paliege, H. Peters, P. Persson, S. Heyman, and C. Rosenberger, “Cyclosporin A induces renal episodic hypoxia,” *Acta Physiologica*, vol. 219, no. 3, pp. 627–641, 2017.

[154] A. Hartner, N. Cordasic, C. Menendez-Castro, G. Volkert, J. M. Yabu, M. Kupraszewicz-Hutzler, W. Rascher, and K. F. Hilgers, “Lack of α8-integrin aggravates podocyte injury in experimental diabetic nephropathy,” *American Journal of Physiology-Renal Physiology*, vol. 299, no. 5, pp. F1151–F1157, 2010.

[155] B. Knier, N. Cordasic, B. Klanke, J. Heusinger-Ribeiro, C. Daniel, R. Veelken, A. Hartner, and K. F. Hilgers, “Effect of the plasminogen-plasmin system on hypertensive renal and cardiac damage,” *Journal of hypertension*, vol. 29, no. 8, pp. 1602–1612, 2011.

[156] A. Hartner, L. Jagusch, N. Cordasic, K. Amann, R. Veelken, J. Jacobi, and K. F. Hilgers, “Impaired neovascularization and reduced capillary supply in the malignant vs. non-malignant course of experimental renovascular hypertension,” *Frontiers in physiology*, vol. 7, p. 370, 2016.

[157] L. I. Neumeier, R. B. Thomson, M. Reichel, K.-U. Eckardt, P. S. Aronson, and F. Knauf, “Enteric oxalate secretion mediated by Slc26a6 defends against hyperoxalemia in murine models of chronic kidney disease,” *Journal of the American Society of Nephrology*, vol. 31, no. 9, pp. 1987–1995, 2020.

[158] J. Kalucka, G. Schley, A. Georgescu, B. Klanke, S. Rössler, J. Baumgartl, J. Velden, K. Amann, C. Willam, and R. S. Johnson, “Kidney injury is independent of endothelial HIF-1α,” *Journal of Molecular Medicine*, vol. 93, no. 8, pp. 891–904, 2015.

[159] T. Breiderhoff, N. Himmerkus, M. Stuiver, K. Mutig, C. Will, I. C. Meij, S. Bachmann, M. Bleich, T. E. Willnow, and D. Müller, "Deletion of claudin-10 (Cldn10) in the thick ascending limb impairs paracellular sodium permeability and leads to hypermagnesemia and nephrocalcinosis," *Proceedings of the National Academy of Sciences*, vol. 109, no. 35, pp. 14241–14246, 2012.

[160] C. Magnes, A. Fauland, E. Gander, S. Narath, M. Ratzer, T. Eisenberg, F. Madeo, T. Pieber, and F. Sinner, "Polyamines in biological samples: Rapid and robust quantification by solid-phase extraction online-coupled to liquid chromatography–tandem mass spectrometry," *Journal of chromatography A*, vol. 1331, pp. 44–51, 2014.

[161] T. Sieckmann, G. Schley, N. Ögel, S. Kelterborn, F. Boivin, M. Fähling, M. Ashraf, M. Reichel, E. Vigolo, A. Hartner, F. Lichtenberger, T. Breiderhoff, F. Knauf, C. Rosenberger, F. Aigner, K. Schmidt-Ott, H. Scholz, and K. Kirschner, "Strikingly conserved gene expression changes of polyamine regulating enzymes among various forms of acute and chronic kidney injury," *Kidney International*, In Press.

[162] S. H. Larsson, J.-P. Charlieu, K. Miyagawa, D. Engelkamp, M. Rassoulzadegan, A. Ross, F. Cuzin, V. van Heyningen, and N. D. Hastie, "Subnuclear localization of WT1 in splicing or transcription factor domains is regulated by alternative splicing," *Cell*, vol. 81, no. 3, pp. 391–401, 1995.

[163] F. Ran, P. D. Hsu, J. Wright, V. Agarwala, D. A. Scott, and F. Zhang, "Genome engineering using the CRISPR-Cas9 system," *Nature protocols*, vol. 8, no. 11, pp. 2281–2308, 2013.

[164] O. Warburg, "Isolation and crystallization of enolase," *Biochemische Zeitschrift*, vol. 310, pp. 384–421, 1942.

[165] A. Viau, K. El Karoui, D. Laouari, M. Burtin, C. Nguyen, K. Mori, E. Pillebout, T. Berger, T. W. Mak, and B. Knebelmann, "Lipocalin 2 is essential for chronic kidney disease progression in mice and humans," *The Journal of clinical investigation*, vol. 120, no. 11, pp. 4065–4076, 2010.

[166] C. López-Rodríguez, J. Aramburu, A. S. Rakeman, and A. Rao, "NFAT5, a constitutively nuclear NFAT protein that does not cooperate with Fos and Jun," *Proceedings of the National Academy of Sciences*, vol. 96, no. 13, pp. 7214–7219, 1999.

[167] C. Elso, L. Roberts, G. Smyth, R. Thomson, T. Baldwin, S. Foote, and E. Handman, "Leishmaniasis host response loci (lmr1–3) modify disease severity through a Th1/Th2-independent pathway," *Genes & Immunity*, vol. 5, no. 2, pp. 93–100, 2004.

[168] J. Johnson and F. Grillo, "Thyroid hormone induction of ornithine decarboxylase in ischemic acute renal failure," *Renal failure*, vol. 16, no. 4, pp. 435–444, 1994.

[169] O. Levillain, J.-J. Diaz, I. Reymond, and D. Soulet, "Ornithine metabolism along the female mouse nephron: localization of ornithine decarboxylase and ornithine aminotransferase," *Pflügers Archiv*, vol. 440, no. 5, pp. 761–769, 2000.

[170] K. Famulski, G. Broderick, G. Einecke, K. Hay, J. Cruz, B. Sis, M. Mengel, and P. Halloran, “Transcriptome analysis reveals heterogeneity in the injury response of kidney transplants,” *American Journal of Transplantation*, vol. 7, no. 11, pp. 2483–2495, 2007.

[171] R. A. DiSilvestro, A. A. Jones, D. Smith, and R. Wildman, “Plasma diamine oxidase activities in renal dialysis patients, a human with spontaneous copper deficiency and marginally copper deficient rats,” *Clinical biochemistry*, vol. 30, no. 7, pp. 559–563, 1997.

[172] S. Barone, T. Okaya, S. Rudich, S. Petrovic, K. Tenrani, Z. Wang, K. Zahedi, R. A. Casero, A. B. Lentsch, and M. Soleimani, “Distinct and sequential upregulation of genes regulating cell growth and cell cycle progression during hepatic ischemia-reperfusion injury,” *American Journal of Physiology-Cell Physiology*, vol. 289, no. 4, pp. C826–C835, 2005.

[173] J. Gaugas and D. Dewey, “Hog kidney diamine oxidase conversion of biogenic diamines to inhibitors of cell proliferation,” *The Journal of Pathology*, vol. 134, no. 3, pp. 243–252, 1981.

[174] S. Bettuzzi, P. Strocchi, P. Davalli, M. Marinelli, L. Furci, and A. Corti, “Androgen responsiveness and intrarenal localization of transcripts coding for the enzymes of polyamine metabolism in the mouse,” *Biochemistry and Cell Biology*, vol. 79, no. 2, pp. 133–140, 2001.

[175] J. Brown, A. Samiy, and R. Pitts, “Localization of amino-nitrogen reabsorption in the nephron of the dog,” *American Journal of Physiology-Legacy Content*, vol. 200, no. 2, pp. 370–372, 1961.

[176] O. Levillain, B. Ramos-Molina, F. Forcheron, and R. Penafiel, “Expression and distribution of genes encoding for polyamine-metabolizing enzymes in the different zones of male and female mouse kidneys,” *Amino Acids*, vol. 43, no. 5, pp. 2153–2163, 2012.

[177] R. Van den Munckhof, M. Denyn, W. Tigchelaar-Gutter, R. G. Schipper, A. Verhofstad, C. Van Noorden, and W. M. Frederiks, “In situ substrate specificity and ultrastructural localization of polyamine oxidase activity in unfixed rat tissues,” *Journal of Histochemistry & Cytochemistry*, vol. 43, no. 11, pp. 1155–1162, 1995.

[178] O. Levillain, R. Havouis, and J.-P. Moulinoux, “Polyamines are unevenly distributed within the rat and rabbit kidney,” *Amino Acids*, vol. 18, no. 2, pp. 129–137, 2000.

[179] M. A. Desiderio, I. Zini, P. Davalli, M. Zoli, A. Corti, K. Fuxe, and L. F. Agnati, “Polyamines, ornithine decarboxylase, and diamine oxidase in the substantia nigra and striatum of the male rat after hemitransection,” *Journal of neurochemistry*, vol. 51, no. 1, pp. 25–31, 1988.

[180] K. Kawano, H. Masuda, M. Yano, K. Kihara, A. Sugimoto, and H. Azuma, “Altered nitric oxide synthase, arginase and ornithine decarboxylase activities, and polyamine synthesis in response to ischemia of the rabbit detrusor,” *The Journal of urology*, vol. 176, no. 1, pp. 387–393, 2006.

[181] D. H. Russell, V. J. Medina, and S. H. Snyder, “The dynamics of synthesis and degradation of polyamines in normal and regenerating rat liver and brain,” *Journal of Biological Chemistry*, vol. 245, no. 24, pp. 6732–6738, 1970.

[182] A. P. Gobert, N. T. Al-Greene, K. Singh, L. A. Coburn, J. C. Sierra, T. G. Verriere, P. B. Luis, C. Schneider, M. Asim, and M. M. Allaman, “Distinct immunomodulatory effects of spermine oxidase in colitis induced by epithelial injury or infection,” *Frontiers in immunology*, vol. 9, p. 1242, 2018.

[183] A. M. Rao, J. F. Hatcher, A. Dogan, and R. J. Dempsey, “Elevated N1-acetylspermidine levels in gerbil and rat brains after CNS injury,” *Journal of neurochemistry*, vol. 74, no. 3, pp. 1106–1111, 2000.

[184] G. N. Babu, K. A. Sailor, D. Sun, and R. J. Dempsey, “Spermidine/spermine N1-acetyl transferase activity in rat brain following transient focal cerebral ischemia and reperfusion,” *Neuroscience letters*, vol. 300, no. 1, pp. 17–20, 2001.

[185] K. Zahedi, F. Huttinger, R. Morrison, T. Murray-Stewart, R. A. Casero Jr, and K. I. Strauss, “Polyamine catabolism is enhanced after traumatic brain injury,” *Journal of neurotrauma*, vol. 27, no. 3, pp. 515–525, 2010.

[186] J.-H. Ryu, Y.-S. Cho, Y.-S. Chun, and J.-W. Park, “Myocardial SSAT induction via AMPK signaling and its implication for ischemic injury,” *Biochemical and biophysical research communications*, vol. 366, no. 2, pp. 438–444, 2008.

[187] N. Seiler and F. N. Bolkenius, “Polyamine reutilization and turnover in brain,” *Neurochemical research*, vol. 10, no. 4, pp. 529–544, 1985.

[188] J. Woźniak, T. Biegański, and C. Maśliński, “Diamine oxidase activity during wound healing in guinea pig skin,” *Agents and Actions*, vol. 9, no. 1, pp. 45–47, 1979.

[189] R. Mennigen, T. Bieganski, A. Elbers, and J. Kusche, “The histamine-diamine oxidase system and mucosal proliferation under the influence of aminoguanidine and seventy percent resection of the rat small intestine,” *Agents and Actions*, vol. 27, no. 1, pp. 221–223, 1989.

[190] B. Daniele and A. Quaroni, “Polarized secretion of diamine oxidase by intestinal epithelial cells and its stimulation by heparin,” *Gastroenterology*, vol. 99, no. 6, pp. 1675–1687, 1990.

[191] T. Ichimura, J. V. Bonventre, V. Bailly, H. Wei, C. A. Hession, R. L. Cate, and M. Sanicola, “Kidney injury molecule-1 (KIM-1), a putative epithelial cell adhesion molecule containing

a novel immunoglobulin domain, is up-regulated in renal cells after injury," *Journal of Biological Chemistry*, vol. 273, no. 7, pp. 4135–4142, 1998.

[192] M. A. Venkatachalam, D. B. Bernard, J. F. Donohoe, and N. G. Levinsky, "Ischemic damage and repair in the rat proximal tubule: differences among the S1, S2, and S3 segments," *Kidney international*, vol. 14, no. 1, pp. 31–49, 1978.

[193] V. H. Gilad, W. G. Tetzlaff, J. M. Rabey, and G. M. Gilad, "Accelerated recovery following polyamines and aminoguanidine treatment after facial nerve injury in rats," *Brain research*, vol. 724, no. 1, pp. 141–144, 1996.

[194] S. H. Erdman, J. H. Park, J. S. Thompson, C. J. Grandjean, M. H. Hart, and J. A. Vanderhoof, "Suppression of diamine oxidase activity enhances postresection ileal proliferation in the rat," *Gastroenterology*, vol. 96, no. 6, pp. 1533–1538, 1989.

[195] K. J. Svensson, J. E. Welch, P. Kucharzewska, P. Bengtson, M. Bjurberg, S. Påhlman, G. B. Ten Dam, L. Persson, and M. Belting, "Hypoxia-mediated induction of the polyamine system provides opportunities for tumor growth inhibition by combined targeting of vascular endothelial growth factor and ornithine decarboxylase," *Cancer research*, vol. 68, no. 22, pp. 9291–9301, 2008.

[196] L. D. Longo, S. Packianathan, J. A. McQueary, R. B. Stagg, C. V. Byus, and C. D. Cain, "Acute hypoxia increases ornithine decarboxylase activity and polyamine concentrations in fetal rat brain," *Proceedings of the National Academy of Sciences*, vol. 90, no. 2, pp. 692–696, 1993.

[197] P. Babal, M. Ruchko, K. Ault-Ziel, L. Cronenberg, J. W. Olson, and M. N. Gillespie, "Regulation of ornithine decarboxylase and polyamine import by hypoxia in pulmonary artery endothelial cells," *American Journal of Physiology-Lung Cellular and Molecular Physiology*, vol. 282, no. 4, pp. L840–L846, 2002.

[198] D. Wu, K. Noda, M. Murata, Y. Liu, A. Kanda, and S. Ishida, "Regulation of spermine oxidase through hypoxia-inducible factor-1α signaling in retinal glial cells under hypoxic conditions," *Investigative ophthalmology & visual science*, vol. 61, no. 6, pp. 52–52, 2020.

[199] R. Yang, Q. Guo, and Z. Gu, "GABA shunt and polyamine degradation pathway on γ-aminobutyric acid accumulation in germinating fava bean (Vicia faba l.) under hypoxia," *Food chemistry*, vol. 136, no. 1, pp. 152–159, 2013.

[200] Y. Guo, R. Yang, H. Chen, Y. Song, and Z. Gu, "Accumulation of γ-aminobutyric acid in germinated soybean (Glycine max l.) in relation to glutamate decarboxylase and diamine oxidase activity induced by additives under hypoxia," *European Food Research and Technology*, vol. 234, no. 4, pp. 679–687, 2012.

[201] B. Tantini, E. Fiumana, S. Cetrullo, C. Pignatti, F. Bonavita, L. M. Shantz, E. Giordano, C. Muscari, F. Flamigni, and C. Guarnieri, "Involvement of polyamines in apoptosis of

cardiac myoblasts in a model of simulated ischemia," *Journal of molecular and cellular cardiology*, vol. 40, no. 6, pp. 775–782, 2006.

[202] R. Poulin, R. Wechter, and A. Pegg, "An early enlargement of the putrescine pool is required for growth in L1210 mouse leukemia cells under hypoosmotic stress," *Journal of Biological Chemistry*, vol. 266, no. 10, pp. 6142–6151, 1991.

[203] E. Lövkvist-Wallström, L. Stjernborg-Ulvsbäck, I. E. Scheffler, and L. Persson, "Regulation of mammalian ornithine decarboxylase: Studies on the induction of the enzyme by hypotonic stress," *European journal of biochemistry*, vol. 231, no. 1, pp. 40–44, 1995.

[204] G. F. Munro, R. A. Miller, C. A. Bell, and E. L. Verderber, "Effects of external osmolality on polyamine metabolism in HeLa cells," *Biochimica et Biophysica Acta (BBA)-General Subjects*, vol. 411, no. 2, pp. 263–281, 1975.

[205] G. F. Munro, K. Hercules, J. Morgan, and W. Sauerbier, "Dependence of the putrescine content of Escherichia coli on the osmotic strength of the medium," *Journal of Biological Chemistry*, vol. 247, no. 4, pp. 1272–1280, 1972.

[206] D. Schiller, D. Kruse, H. Kneifel, R. Krämer, and A. Burkovski, "Polyamine transport and role of potE in response to osmotic stress in Escherichia coli," *Journal of Bacteriology*, vol. 182, no. 21, pp. 6247–6249, 2000.

[207] H. E. Flores and A. W. Galston, "Polyamines and plant stress: activation of putrescine biosynthesis by osmotic shock," *Science*, vol. 217, no. 4566, pp. 1259–1261, 1982.

[208] U. Zimmermann and E. Steudle, "Effects of potassium concentration and osmotic pressure of sea water on the cell-turgor pressure of chaetomorpha linum," *Marine Biology*, vol. 11, no. 2, pp. 132–137, 1971.

[209] R. Iyer and A. H. Delcour, "Complex inhibition of ompf and ompc bacterial porins by polyamines," *Journal of Biological Chemistry*, vol. 272, no. 30, pp. 18595–18601, 1997.

[210] H. Samartzidou and A. H. Delcour, "Distinct sensitivities of ompf and phoe porins to charged modulators," *FEBS letters*, vol. 444, no. 1, pp. 65–70, 1999.

[211] E. Ficker, M. Taglialatela, B. A. Wible, C. M. Henley, and A. M. Brown, "Spermine and spermidine as gating molecules for inward rectifier K^+ channels," *Science*, vol. 266, no. 5187, pp. 1068–1072, 1994.

[212] H. H. Kerschbaum, J. A. Kozak, and M. D. Cahalan, "Polyvalent cations as permeant probes of MIC and TRPM7 pores," *Biophysical journal*, vol. 84, no. 4, pp. 2293–2305, 2003.

[213] R. A. Oeckler, W.-Y. Lee, M.-G. Park, O. Kofler, D. L. Rasmussen, H.-B. Lee, H. Belete, B. J. Walters, R. W. Stroetz, and R. D. Hubmayr, "Determinants of plasma membrane

wounding by deforming stress," *American Journal of Physiology-Lung Cellular and Molecular Physiology*, vol. 299, no. 6, pp. L826–L833, 2010.

[214] H. Miyakawa, S. K. Woo, S. C. Dahl, J. S. Handler, and H. M. Kwon, "Tonicity-responsive enhancer binding protein, a rel-like protein that stimulates transcription in response to hypertonicity," *Proceedings of the National Academy of Sciences*, vol. 96, no. 5, pp. 2538–2542, 1999.

[215] T. Kino, H. Takatori, I. Manoli, Y. Wang, A. Tiulpakov, M. R. Blackman, Y. A. Su, G. P. Chrousos, A. H. DeCherney, and J. H. Segars, "Brx mediates the response of lymphocytes to osmotic stress through the activation of NFAT5," *Science signaling*, vol. 2, no. 57, pp. ra5–ra5, 2009.

[216] S. Libert, F. Willermain, C. Weber, A. Bryla, D. Salik, F. Gregoire, N. Bolaky, L. Caspers, J. Perret, and C. Delporte, "Involvement of TonEBP/NFAT5 in osmoadaptative response of human retinal pigmented epithelial cells to hyperosmolar stress," *Molecular vision*, vol. 22, p. 100, 2016.

[217] T. Yang, A. Zhang, M. Honeggar, D. E. Kohan, D. Mizel, K. Sanders, J. R. Hoidal, J. P. Briggs, and J. B. Schnermann, "Hypertonic induction of COX-2 in collecting duct cells by reactive oxygen species of mitochondrial origin," *Journal of Biological Chemistry*, vol. 280, no. 41, pp. 34966–34973, 2005.

[218] X. Zhou, J. D. Ferraris, Q. Cai, A. Agarwal, and M. B. Burg, "Increased reactive oxygen species contribute to high NaCl-induced activation of the osmoregulatory transcription factor TonEBP/OREBP," *American Journal of Physiology-Renal Physiology*, vol. 289, no. 2, pp. F377–F385, 2005.

[219] L. Michea, D. Ferguson, E. Peters, P. Andrews, M. Kirby, and M. Burg, "Cell cycle delay and apoptosis are induced by high salt and urea in renal medullary cells," *American Journal of Physiology-Renal Physiology*, vol. 278, no. 2, pp. F209–F218, 2000.

[220] E. Robbins, T. Pederson, and P. Klein, "Comparison of mitotic phenomena and effects induced by hypertonic solutions in HeLa cells," *The Journal of cell biology*, vol. 44, no. 2, pp. 400–416, 1970.

[221] L. Michea, C. Combs, P. Andrews, N. Dmitrieva, and M. B. Burg, "Mitochondrial dysfunction is an early event in high-NaCl-induced apoptosis of mIMCD3 cells," *American Journal of Physiology-Renal Physiology*, vol. 282, no. 6, pp. F981–F990, 2002.

[222] S. Villanueva, C. Suazo, D. Santapau, F. Perez, M. Quiroz, J. E. Carreño, S. Illanes, S. Lavandero, L. Michea, and C. E. Irarrazabal, "NFAT5 is activated by hypoxia: role in ischemia and reperfusion in the rat kidney," *PloS one*, vol. 7, no. 7, p. e39665, 2012.

[223] L. M. Gerhardt, J. Liu, K. Koppitch, P. E. Cippà, and A. P. McMahon, "Single-nuclear transcriptomics reveals diversity of proximal tubule cell states in a dynamic response to

acute kidney injury," *Proceedings of the National Academy of Sciences*, vol. 118, no. 27, p. e2026684118, 2021.

[224] Q. Cai, J. D. Ferraris, and M. B. Burg, "High NaCl increases TonEBP/OREBP mRNA and protein by stabilizing its mRNA," *American Journal of Physiology-Renal Physiology*, vol. 289, no. 4, pp. F803–F807, 2005.

[225] M. Brigotti, P. G. Petronini, D. Carnicelli, R. R. Alfieri, M. A. Bonelli, A. F. Borghetti, and K. P. Wheeler, "Effects of osmolarity, ions and compatible osmolytes on cell-free protein synthesis," *Biochemical Journal*, vol. 369, no. 2, pp. 369–374, 2003.

[226] F. Umenishi, T. Narikiyo, and R. W. Schrier, "Effect on stability, degradation, expression, and targeting of aquaporin-2 water channel by hyperosmolality in renal epithelial cells," *Biochemical and biophysical research communications*, vol. 338, no. 3, pp. 1593–1599, 2005.

[227] E. Gludovacz, D. Maresch, L. L. de Carvalho, V. Puxbaum, L. J. Baier, L. Sützl, G. Guédez, C. Grünwald-Gruber, B. Ulm, and S. Pils, "Oligomannosidic glycans at Asn-110 are essential for secretion of human diamine oxidase," *Journal of Biological Chemistry*, vol. 293, no. 3, pp. 1070–1087, 2018.

[228] Y. Kobayashi, J. Kupelian, and D. V. Maudsley, "Release of diamine oxidase by heparin in the rat," *Biochemical Pharmacology*, vol. 18, no. 7, pp. 1585–1591, 1969.

[229] L. D'Agostino, S. Pignata, B. Daniele, R. Ventriglia, G. Ferrari, C. Ferraro, S. Spagnuolo, P. Lucchelli, and G. Mazzacca, "Release of diamine oxidase into plasma by glycosaminoglycans in rats," *Biochimica et Biophysica Acta (BBA)-General Subjects*, vol. 993, no. 2-3, pp. 228–232, 1989.

[230] A. Wollin, X. Wang, and P. Tso, "Nutrients regulate diamine oxidase release from intestinal mucosa," *American Journal of Physiology-Regulatory, Integrative and Comparative Physiology*, vol. 275, no. 4, pp. R969–R975, 1998.

[231] Y. Ji, Y. Sakata, X. Li, C. Zhang, Q. Yang, M. Xu, A. Wollin, W. Langhans, and P. Tso, "Lymphatic diamine oxidase secretion stimulated by fat absorption is linked with histamine release," *American Journal of Physiology-Gastrointestinal and Liver Physiology*, vol. 304, no. 8, pp. G732–G740, 2013.

[232] A. Wollin, H. Navert, and G. Bounous, "Effect of intestinal ischemia on diamine oxidase activity in rat intestinal tissue and blood," *Gastroenterology*, vol. 80, no. 2, pp. 349–355, 1981.

[233] P. Velicky, K. Windsperger, K. Petroczi, S. Pils, B. Reiter, T. Weiss, S. Vondra, R. Ristl, S. Dekan, and C. Fiala, "Pregnancy-associated diamine oxidase originates from extravillous trophoblasts and is decreased in early-onset preeclampsia," *Scientific reports*, vol. 8, no. 1, pp. 1–11, 2018.

[234] J. D. Bendtsen, H. Nielsen, G. Von Heijne, and S. Brunak, “Improved prediction of signal peptides: Signalp 3.0,” *Journal of molecular biology*, vol. 340, no. 4, pp. 783–795, 2004.

[235] J. A. Hiss and G. Schneider, “Architecture, function and prediction of long signal peptides,” *Briefings in bioinformatics*, vol. 10, no. 5, pp. 569–578, 2009.

[236] G. Von Heijne and L. Abrahmsèn, “Species-specific variation in signal peptide design implications for protein secretion in foreign hosts,” *FEBS letters*, vol. 244, no. 2, pp. 439–446, 1989.

[237] P. A. Brown, H. O. Halvorson, P. Raney, and D. Perlman, “Conformational alterations in the proximal portion of the yeast invertase signal peptide do not block secretion,” *Molecular and General Genetics MGG*, vol. 197, no. 3, pp. 351–357, 1984.

[238] R. Green, R. Kramer, and D. Shields, “Misplacement of the amino-terminal positive charge in the prepro-α-factor signal peptide disrupts membrane translocation in vivo,” *Journal of Biological Chemistry*, vol. 264, no. 5, pp. 2963–2968, 1989.

[239] H. Schwelberger, A. Hittmair, and S. Kohlwein, “Analysis of tissue and subcellular localization of mammalian diamine oxidase by confocal laser scanning fluorescence microscopy,” *Inflammation research: official journal of the European Histamine Research Society...[et al.]*, vol. 47, pp. S60–S61, 1998.

[240] C. Sartori, A. M. Bargagli, and M. P. Argento-Cerù, “Subcellular localization of diamine oxidase in rabbit kidney cortex,” *Biochimica et Biophysica Acta (BBA)-General Subjects*, vol. 758, no. 1, pp. 58–69, 1983.

[241] A. Robinson-White, S. B. Baylin, T. Olivecrona, and M. A. Beaven, “Binding of diamine oxidase activity to rat and guinea pig microvascular endothelial cells. comparisons with lipoprotein lipase binding,” *The Journal of clinical investigation*, vol. 76, no. 1, pp. 93–100, 1985.

[242] N. L. Baenziger, P. Mack, Y. Jong, L. R. Dalemar, N. Perez, C. Lindberg, B. Wilhelm, and R. C. Haddock, “An environmentally regulated receptor for diamine oxidase modulates human endothelial cell/fibroblast histamine degradative uptake,” *Journal of Biological Chemistry*, vol. 269, no. 21, pp. 14892–14898, 1994.

[243] S. A. McCormack, M. J. Viar, and L. R. Johnson, “Polyamines are necessary for cell migration by a small intestinal crypt cell line,” *American Journal of Physiology-Gastrointestinal and Liver Physiology*, vol. 264, no. 2, pp. G367–G374, 1993.

[244] R. M. Ray, S. A. McCormack, C. Covington, M. J. Viar, Y. Zheng, and L. R. Johnson, “The requirement for polyamines for intestinal epithelial cell migration is mediated through rac1,” *Journal of Biological Chemistry*, vol. 278, no. 15, pp. 13039–13046, 2003.

[245] Y. Ding, Y. Feng, Z. Huang, Y. Zhang, X. Li, R. Liu, H. Li, T. Wang, Y. Ding, and Z. Jia, "SOX15 transcriptionally increases the function of AOC1 to modulate ferroptosis and progression in prostate cancer," *Cell Death & Disease*, vol. 13, no. 8, pp. 1–13, 2022.

[246] T. Metaye, M. Baudry, and P. Lalegerie, "Enhancement of mitogen-induced lymphocyte proliferation by some inhibitors of alkaline phosphatase and diamine oxidase," *International journal of immunopharmacology*, vol. 11, no. 6, pp. 629–636, 1989.

[247] K. M. Kirschner, J. F. Braun, C. L. Jacobi, L. J. Rudigier, A. B. Persson, and H. Scholz, "Amine oxidase copper-containing 1 (AOC1) is a downstream target gene of the Wilms tumor protein, WT1, during kidney development," *Journal of Biological Chemistry*, vol. 289, no. 35, pp. 24452–24462, 2014.

[248] F. Liu, W. Ou, W. Tang, Z. Huang, Z. Zhu, W. Ding, J. Fu, Y. Zhu, C. Liu, and W. Xu, "Increased AOC1 expression promotes cancer progression in colorectal cancer," *Frontiers in Oncology*, vol. 11, p. 657210, 2021.

[249] F. Ingoglia, J.-L. Chong, M. Pasquali, and N. Longo, "Creatine metabolism in patients with urea cycle disorders," *Molecular Genetics and Metabolism Reports*, vol. 29, p. 100791, 2021.

[250] D. M. Hardbower, M. Asim, P. B. Luis, K. Singh, D. P. Barry, C. Yang, M. A. Steeves, J. L. Cleveland, C. Schneider, and M. B. Piazuelo, "Ornithine decarboxylase regulates M1 macrophage activation and mucosal inflammation via histone modifications," *Proceedings of the National Academy of Sciences*, vol. 114, no. 5, pp. E751–E760, 2017.

[251] P. Huang, M. Wang, Z. Lu, S. Shi, X. Wei, C. Bi, G. Wang, H. Liu, T. Hu, and B. Wang, "Putrescine accelerates the differentiation of bone marrow derived dendritic cells via inhibiting phosphorylation of STAT3 at Tyr705," *International Immunopharmacology*, vol. 116, p. 109739, 2023.

[252] S. Bardocz, G. Grant, D. S. Brown, and A. Pusztai, "Putrescine as a source of instant energy in the small intestine of the rat," *Gut*, vol. 42, no. 1, pp. 24–28, 1998.

[253] K. N. Tzirogiannis, G. I. Panoutsopoulos, M. D. Demonakou, G. K. Papadimas, V. G. Kondyli, K. T. Kourentzi, R. I. Hereti, and M. G. Mykoniatis, "The hepatoprotective effect of putrescine against cadmium-induced acute liver injury," *Archives of toxicology*, vol. 78, pp. 321–329, 2004.

[254] L. Yang, C. R. Brooks, S. Xiao, V. Sabbisetti, M. Y. Yeung, L.-L. Hsiao, T. Ichimura, V. Kuchroo, and J. V. Bonventre, "KIM-1–mediated phagocytosis reduces acute injury to the kidney," *The Journal of clinical investigation*, vol. 125, no. 4, pp. 1620–1636, 2015.

[255] T. Adachi, N. Sugiyama, H. Yagita, and T. Yokoyama, "Renal atrophy after ischemia–reperfusion injury depends on massive tubular apoptosis induced by TNFα in the later phase," *Medical molecular morphology*, vol. 47, pp. 213–223, 2014.

[256] M. Hirota, M. Kitagaki, H. Itagaki, and S. Aiba, “Quantitative measurement of spliced XBP1 mRNA as an indicator of endoplasmic reticulum stress,” *The Journal of toxicological sciences*, vol. 31, no. 2, pp. 149–156, 2006.

[257] E. M. Tome, M. S. Fiser, M. C. Payne, and W. E. Gerner, “Excess putrescine accumulation inhibits the formation of modified eukaryotic initiation factor 5A (eIF-5A) and induces apoptosis,” *Biochemical Journal*, vol. 328, no. 3, pp. 847–854, 1997.

[258] X. Xie, M. E. Tome, and E. W. Gerner, “Loss of intracellular putrescine pool-size regulation induces apoptosis,” *Experimental cell research*, vol. 230, no. 2, pp. 386–392, 1997.

6 Appendix

6.1 Makros

Makro for scratch closure calculation:

```
1  run("Duplicate...", "duplicate");
2  run("Find Edges", "stack");
3  run("Gaussian Blur...", "sigma=4 stack");
4  run("Auto Threshold", "method=Intermodes white stack");
5  run("Invert", "stack");
6  run("Analyze Particles...", "size=50000-Infinity display summarize add stack");
```